Alma Mater Studiorum - Università di Bologna

DOTTORATO DI RICERCA IN:

MODELLISTICA FISICA PER LA PROTEZIONE DELL'AMBIENTE

Ciclo XXIV

Settore concorsuale di afferenza: 08/A1

Settore scientifico-disciplinare: ICAR/02

Development of parallelizable flood inundation models for large scale analysis

Presentata da: Francesco Dottori

Coordinatore Dottorato:
Prof. Rolando Rizzi

Relatore:
Prof. Ezio Todini

Esame finale anno 2012

Alla mia famiglia

Ringraziamenti - Acknowledgements

Questa tesi è il risultato di tre anni di ricerca resi possibili dalla borsa di studio fornita dal Ministero dell'Istruzione della Repubblica Italiana.

Il mio primo ringraziamento va al prof. Ezio Todini, che ha proposto e indirizzato l'argomento di ricerca e le attivit descritte in questa tesi.

Un ringraziamento speciale a Mario Martina, Gabriele Coccia e ai compagni di corso per il loro supporto e i loro utilissimi suggerimenti.

I would like also to thank Giuliano di Baldassarre, Leonardo Alfonso and all the collegues and friends of the UNESCO-IHE Institute for Water Education.

Infine, vorrei ringraziare le tante persone che con un consiglio, un suggerimento o un parere mi hanno aiutato a completare questa tesi.

Abstract

Flood disasters are a major cause of fatalities and economic losses, and several studies indicate that global flood risk is currently increasing. In order to reduce and mitigate the impact of river flood disasters, the current trend is to integrate existing structural defences with non structural measures. This calls for a wider application of advanced hydraulic models for flood hazard and risk mapping, engineering design, and flood forecasting systems.

Within this framework, two different hydraulic models for large scale analysis of flood events have been developed. The two models, named CA2D and IFD-GGA, adopt an integrated approach based on the diffusive shallow water equations and a simplified finite volume scheme. The models are also designed for massive code parallelization, which has a key importance in reducing run times in large scale and high-detail applications.

The two models were first applied to several numerical cases, to test the reliability and accuracy of different model versions. Then, the most effective versions were applied to different real flood events and flood scenarios.

The IFD-GGA model showed serious problems that prevented further applications. On the contrary, the CA2D model proved to be fast and robust, and able to reproduce 1D and 2D flow processes in terms of water depth and velocity. In most applications the accuracy of model results was good and adequate to large scale analysis. Where complex flow processes occurred local errors were observed, due to the model approximations. However, they did not compromise the correct representation of overall flow processes.

In conclusion, the CA model can be a valuable tool for the simulation of a wide range of flood event types, including lowland and flash flood events.

Contents

Chapter 1

INTRODUCTION

1.1 Motivation of the thesis

...essentially, all models are wrong, but some are useful.
George E.P. Box

Flood disasters are recognized as one of the greatest causes of fatalities, economic losses, and infrastructure damage (Commission EC, 2007; Kalyanapu et al., 2011). According to the Emergency Events Database (EM-DAT, 2011), in 2010 floods were responsible for the loss of more than 8000 human lives and affected about 180 million people.

Floodplains along rivers, lakes and coastal areas have always been a favourable place for human settlements, despite being prone to frequent and sometimes catastrophic flood events. However, in the 20th century global changing demographics lead to a dramatic increase of industrial development, urban expansion and infrastructure construction in floodprone areas. As a consequence, flood risk has been increasing and is likely to grow further because of additional factors, such as land use changes, climate variability and change, and technological and socio-economic conditions (UN-ISDR Scientific and Technical Committee, 2009; Di Baldassarre and Ulhenbrook, 2012)

In European countries, the traditional approach for defending urban and industrial settlements from flood risk have consisted of developing structural measures, such as dyke systems. Despite these huge efforts flood risk could not be completely prevented, as demonstrated by recent ratastrophic events, such as the Central European flooding in 2002, the UK floods in 2000 and 2007, and the floods in Italy in 2011. Actually, flood defences can increase the overall vulnerability of urban and industrial settlements: protection from regular flooding reduces perception of risk and encourages inappropriate development, which is vulnerable to high-consequence and low-probability events (Castellarin et al., 2011). In addition, river and coastal embankments can increase the magnitude of flood events, thus increasing damage if a failure occurs (Di Baldassarre et al., 2009a).

Therefore, the current trend is to shift from traditional flood defence approach to an integrated flood management approach. The objective is to minimize the human, economic and ecological losses from extreme floods while at the same time maximising the social,

economic and ecological benefits of ordinary floods (Di Baldassarre and Ulhenbrook, 2012). This "living with floods" approach requires the development and integration of several non structural measures, including land use planning, flood hazard and risk mapping, flood forecasting systems, building of population awareness and preparedness (Di Baldassarre et al., 2010a; Kalyanapu et al., 2011).

Economically and socially sustainable measures are also urgently needed to mitigate flood risk in developing countries and in countries in transition. In these countries, socio-economic conditions and the limitations in (or even the absence of) effective planning measures result in intensive and unplanned human settlements in flood prone areas, that appear to be playing a major role in increasing flood risk (Di Baldassarre et al., 2010a). As a consequence, flood fatalities in Africa have increased by more than an order of magnitude in the last 60 years (EM-DAT, 2011). In this framework, the introduction of flood forecasting and early warning systems, the building of population awareness and preparedness, effective urban planning including discouragement of human settlements in flood prone areas, along with the development of local institutional capacities, are actions that should be pursued (Di Baldassarre et al., 2010a).

Given this global framework, the socio-economic relevance of river flood studies is constantly increasing, and reliable methodologies for simulating the hydraulic behaviour of river systems are nowadays required both by public institutions and private companies. For instance, the European Flood Directive 60/2007 (Commission EC, 2007) prescribes the definition of flood hazard maps and flood risk maps, and the development of flood management plans, in all the European river basins. On the other hand, different countries (e.g. United Kingdom) are developing flood insurance programs that require reliable flood hazard and flood vulnerability assessment tools. The fullfillment of such requirements calls for a wider application of existing flood modelling tools and the development of new ones. Flood modeling can be extremely useful in different key management activities including flood hazard and risk mapping, engineering design, and flood forecasting systems (Kalyanapu et al., 2011; Di Baldassarre and Ulhenbrook, 2012) .

The use of hydraulic models for the analysis of flood events dates to the 60s (Zanobetti et al., 1970; Xanthopoulos and Koutitas, 1976), but, until the last decade, practical applications were limited by the scarcity of detailed topographic data and the high demand of computation resources required by more complex hydraulic models (Bates et al., 2004). Such a situation radically changed in recent years thanks to the advances in computational resources and the availability of new topographic data sources, such as laser altimetry (e.g. LiDAR) (Bates et al., 2006; Hunter et al., 2008; Schubert et al., 2008), aerial photogrammetry (Gallegos et al., 2009), and aerial ans satellate SAR (synthetic aperture radar) interferometry (Bates et al., 2006; Horritt et al., 2007; Di Baldassarre et al., 2010b). As such, there has been a proliferation of scientific studies applying flood inundation models (Hunter et al., 2007).

A wide number of different modelling approaches are currently applied nowadays. These approaches can broadly be classified according to the complexity of equations that reproduce flow dynamics. As such, flood models go from simple methods based on GIS-based

relationships (e.g. interpolation of exisiting flood depths) to complex 3D hydraulic models. A more detailed review of existing modelling approaches is presented in Chapter 2.

Despite the large number of modelling tools available nowadays, there is still a considerable gap between research modelling tools and the models currently applied for flood risk assessment and prevention at large scales. In Italy, for instance, most of the existing flood maps developed by river basin Authorities are based either on simple GIS-based interpolations or 1D approaches (ISPRA, 2009). Although these methods may provide good results (Chapter 2), in many cases more advanced hydraulic models should be used.

As already mentioned, this gap is mainly due to past limitations in computation power and data availability, that prevented the application of complex models exept for specific data-rich events. Although these constraints are gradually being removed, the application of complex hydraulic models is often not straigthforward and requires relevant skills and training. While such skills are diffused nowadays in universities and research centres, this is not the case of public institutions in many countries, where personnel is generally trained to use more established and simple modelling tools.

Therefore, one of the current needs is to promote the use of advanced modeling tools, in order to improve flood risk assessment and flood prevention measures. These models should have limited requirements in terms of input data, and they should be able to reproduce flow processes at large scale with an adequate level of detail; computation times should also be as much reduced as possible, to allow the reproduction of flood events involving wide areas.The development of such modeling tools is the overall aim of the present thesis.

1.2 Overview of the research work

The present research can be considered a practical application of the framework described in the previous section. The starting point has been the requirement of modeling tools to simulate large scale flood risk scenarios, coming from the Civil Protection of the Emilia-Romagna district.

After a comprehensive literature review on the current state of the art in flood modeling, it was decided to develop two complementary, reduced complexity models, each one offering a different level of compromise between accuracy and computational speed. The reasons behind the choice of these modeling approaches are presented in Chapter 3.

Starting from the initial idea, during the thesis period the two research lines have been modified and updated, according to the results and findings coming from the research work and the latest literature.

Besides the development of model codes, the effectiveness of the chosen modeling approaches needs to be evaluated. As a matter of fact, the field of application of reduced complexity models have dramatically increased in the last decade, following the already mentioned development of high performance computers and topographic survey techniques. While past applications were limited to flood events in rural areas, often using very coarse resolution grids, current applications regard both rural and urban flood events, and usually involve the use of very high resolution grids.

Despite this widespread use, so far only few research works carried out a comprehensive analysis of the ability of reduced complexity models to deal with specific flow conditions. For instance, localized processes such as hydraulic jumps, supercritical flow conditions, flow over steep slopes, are relevant in many flood events, however little is known about the ability of reduced complexity models to reproduce them. Therefore this research work is partly devoted to investigate these issues.

A further objective of this research is to develop the model codes suitable for a massive parallelization on multicore processors or GPU (Graphical processing Unit) processors. As it will be described in Section, parallelization allows for a dramatic increase of computational speed, which has a key importance for large scale or high-detail applications.

1.3 Thesis composition

The thesis has the following structure. Chapter 2 presents an overview of the existing approaches to model inundation processes, and includes an exhaustive literature review. In Chapter 3, the two developed models are described, including the different versions developed along the thesis research period. Chapter 4 presents the application of the two models to several numerical cases, that were used to test the reliability and accuracy of the models. This section includes a comprehensive discussion about the advantages and drawbacks of each model version. Chapter 5 describes the applications of the most effective model versions to different flood events and flood scenarios. Finally, Chapter 6 reports the conclusions of the research work and some perspectives about future research lines.

Chapter 2

RESEARCH FRAMEWORK

2.1 Overview of flood inundation models

Nowadays, a large number of modelling tools for the analysis and simulation of flood events are available in literature. Existing models can be classified according to the number of dimensions in which they represent the spatial domain and flow processes (Hunter et al., 2007). Their range goes from simple GIS-based methods, usually called 0D models, to 1D, 2D and complete 3D mathematical descriptions of flow, including various combinations and intermediate classes, e.g. 1D2D models and quasi 2D models. Each modelling approach has advantages and drawbacks, which define its range of application: depending on the specific problem to be studied, a one-, two- or even three-dimensional model may be most appropriate (see Section 2.8). Due to the huge number of flood inundation models that can be found in literature, in the present section only some established or significant models are mentioned. The selection includes both commercial and reseach softwares. The section dedicated to 2D models is obviously more detailed, since this is the main topic of the research work. Finally, the present classification should be intended as a proposal, although based on a generally accepted literature convention; in other works, some definitions here applied can be used for different category of models, or can be identified with other names.

2.2 0D models

Rather than proper hydraulic models, this category includes all the methods to compute flood extent and water depths through simple geometric or topographic interpolation, without expliticly reproducing flow processes. For instance, a number of observed water marks or flood shorelines can be interpolated to obtain water surface. These methods are generally easy to apply in a GIS environment, given that only topographic information and observed flood data are required. Results from hydraulic models can be also used (see Section 2.3). However, caution should be used in applying interpolation methods: since flow processes are not simulated, the range of application should be limited to flood events where depression filling is predominant, or where observed data are enough to infer overall water surface. In

other conditions their accuracy can be extremely low and physically based models would be more recommendable. In addition, no information about flow velocity and time evolution of flood event can be obtained from these methods, unless enough data at different times are available.

2.3 1D models

Traditionally, one dimensional models have been extensively used as inundation models, despite being mainly designed to simulate flow inside natural or artificial channels. In the past, suh a choice was generally driven by data scarcity and computational power constraints, that did not enable the application of more complex models (Chapter 1). More recent applications (Horritt and Bates, 2002; Werner et al., 2005; Di Baldassarre et al., 2009b) demonstrated that 1D models have still some advantages in respect to 2D models. In particular, 1D models are less demanding both in terms of data and computational resources: only information about river cross sections and upstream - downstream boundary conditions are required to run a simulation and run times are generally much more reduced. The latter is a key element in a number of practical applications, such as realtime flood inundation forecasting, simulations over wide areas (Di Baldassarre et al., 2009b) and analyses involving multiple simulations, e.g. in a Monte Carlo framework (Aronica et al., 1998; Horritt and Bates, 2002).

However, drawbacks of 1D models are significant and should always be considered. Results are provided only at specific cross sections along the river reach, thus they have to be interpolated over the site topography to obtain spatialized information (see Section 2.2). Moreover, 1D models can provide good results in flood events essentially dominated by 1D flow, for instance in rivers with confined, narrow flood plains (Horritt and Bates, 2002; Werner et al., 2005), whereas their accuracy decreases significantly where flow becomes two dimensional (Di Baldassarre et al., 2009b; Castellarin et al., 2011; Prestininzi et al., 2011). In order to represent flow out of river banks, the 1D grid can be either linked with a grid of interconnected storage cells, to form a quasi 2D model (see Section 2.4), or it can be coupled with a 2D model (see Section 2.6).

The one dimensional models used for flood inundation analysis are generally based on the fully dynamic continuity and momentum equations, or 1D De Saint Venant equations. HEC-RAS (HEC, 2001), SOBEK 1D (Werner et al. (2005); *www.deltaressystems.com/hydro*), MIKE11 (*www.dhigroup.com*), are examples of 1D models which have beeen used for flood inundation analysis (Horritt and Bates, 2002; Werner et al., 2005). On the contrary, 1D models bases on the diffusive or kinematic approximations are generally not used as flood models.

2.4 quasi 2D models

In literature, the definition "quasi 2D models" is used to identify hydraulic modes which reproduce two-dimensional flow dynamics without using the complete set of 2D governing

equations (that is, momentum and continuity equations). These model are typically based on a storage cell approach and the use of simplified equations; flux between adjacent cells can be computed either with the Manning equation (Neelz and Pender, 2010), the weir equation (Castellarin et al., 2011) or other simplified formulations which replace the momentum equation. Volumes are updated with the continuity equation, using geometric relationships to determine the storage for each storge cell. Therefore, a partially physically-based approximation of 2D flow dynamics is obtained. Example of quasi 2D models are Dynamic RSFM, Flood Risk Mapper and Flowroute (Neelz and Pender, 2010). As mentioned in Section 2.3, quasi 2D models can also be linked to 1D models, to simulate flow out of river banks (Castellarin et al., 2011). The main advantage of these models is the code simplicity: the resulting small computation burden allows for applications to wide areas. However, it must be remembered that quasi 2D models do not perform a truly 2D reproduction of flow processes. Although they can simulate the time evolution of flow, the simplifying assumptions can introduce errors in time integration, and only approximate information about flow velocity can be obtained (Neelz and Pender, 2010). In addition, the reliability of results is likely to depend on site topography, thus these models are suitable only for a limited range of applications.

2.5 2D models

In literature, the definition "2D models" is generally used to identify hydraulic modes based on the 2D depth-averaged governing equations of flow, usually called Shallow Water Equations (SWE; see Section 3.1 for a detailed description).

2D models can be further classified in dynamic, gravity, diffusion or kinematic wave models, according to the formulation adopted for the SWE; in addition, models based on the fully dynamic SWE can include shock-capturing schemes and different turbulence closure methods. Dynamic wave models retain all the terms of the momentum equation, whereas gravity wave models neglect the effects of bed slope and viscous energy loss and describe flows dominated by inertia. When the acceleration terms in the SWE are neglected, the diffusive wave model, or zero inertia model is obtained (see Section 3.1). Finally, the further omission of the water depth gradient terms brings to the kinematic wave equation (Aricó et al., 2011). 2D flood inundation models are generally based either on the diffusive or fully dynamic SWE. JFLOW (Bradbrook et al., 2004) is based on the diffusive equations, while CCHE2D (Jia and Wang, 2001), ISIS2D (Lin et al., 2006), MIKE Flood (*www.deltaressystems.com/hydro*), TELEMAC 2D (Hervouet and Van Haren (1996); *www.opentelemac.org*) and TUFLOW (Syme, 2001) are examples of 2D models based on fully dynamic SW equations. In Hunter et al. (2008) and Neelz and Pender (2010), an extended list of research and commercial models can be found.

A second classification criterium is given by the numerical scheme used for integrating and solving the governing equations. Several numerical techniques have been described and implemented in literature (Aricó et al., 2011; Hartarto et al., 2011); these include finite differences (FD), finite volumes (FV) and finite elements (FE) methods, as well as more

conceptual approaches like storage cell mehods (although these can be considered as simplified FD or FV schemes, see Sections 3.1 and 3.2). ISIS2D, JFLOW, TUFLOW, and MIKE Flood use FD schemes, whereas CCHE2D is based on a FV scheme, and TELEMAC-2D use a FE scheme. Finally, FLO2D (FLO-2D Software Inc., 2007) use a raster based approach similar to a finite volume scheme. Besides the classical numerical methods listed above, it is worth mentioning more recent methods, like FV Godunov-type schemes, FE discontinuous Galerkin (DG) schemes and TVD (total variation diminishing) schemes. In Godunov-type schemes a local Riemann problem (Toro, 1992) is solved at every cell interface, providing a high accuracy level in capturing shock waves (Soares Frazão et al., 2008; Hartarto et al., 2011). Usually, each scheme is designed for specific flow processes and topographic conditions, such as irregular or flat topography, and wetting-drying processes (Aricó et al., 2011). TRENT (Villanueva and Wright, 2006) is a river modelling software implementing a Godunov-type scheme. The TVD method is used to solve the SWE with a high order of accuracy and without unphysical oscillations in the vicinity of large gradients (Toro, 1997). A Riemann solver can also be integrated with this method to handle shock capturing (Hartarto et al., 2011). TVD schemes are used in different models like DIVAST (Liang et al., 2007), and have recently been implemented in ISIS 2D and TUFLOW models Neelz and Pender (2010). Finally, DG methods discretize the primitive form of the SWE using discontinuous approximating spaces. This approach combines Godunov and FE methods in order to provide stable solutions of highly advective flows over non-structured grids. Often, a high order Runge-Kutta (RK) is used for temporal discretization. RKDG methods are extensively used to develop accurate research models (Cockburn and Shu, 2001; Ern et al, 2008).

2.6 1D-2D models

A significant number of flood inundation models adopt a mixed 1D-2D approach, in order to exploit the avantages of both modeling schemes (Villanueva and Wright, 2006). In these models, an usual 1D scheme is used to represent flow in river reaches, coupled with a 2D scheme that activates when flow out of river banks occurs. The problem of flow at the interface can be solved either in a simplified way, (for instance using the weir flow equation), or using full SW equations to conserve momentum. The SOBEK and MIKE modeling suites (*www.deltaressystems.com/hydro* and *www.dhigroup.com*) are examples of integrated 1D and 2D hydraulic models suites, with additional modules for water quality, pipe networks and sediment transport. LISFLOOD-FP (Bates and de Roo, 2000; Hunter et al., 2005b; Bates et al., 2010) is a reduced complexity model that combines a 1D scheme for river network with a diffusive 2D scheme based on a simplified finite volume method.

2.7 3D models

3D models adopt the Navier-Stokes equations for simulating flow dynamics. Usually, the hydrostatic approximation is used when dealing with simulate flood inundation events, unless vey specific phenomena have to be simulated (e.g. tsunami waves). Although 3D models allow a detailed reproduction of flow processes in compound channels, so far a number of limiting factors usually prevented their application as flood models. The computational burden is still considerably larger than for 2D models, particularly for dynamic shallow flows with significant changes in domain extent (Hunter et al., 2007). In addition, in most flood events a detailed 3D reproduction is unnecessary for simulating flow processes, given the type and quality of data typically available for model construction and validation (Hunter et al., 2005a; Werner et al., 2005). Therefore, these models are generally used to simulate specific flow processes, like sediment transport on meander rivers, erosion processes due to bridge piers, or water quality analysis in coastal areas. Among the existing 3D models, Delft 3D (*www.deltaressystems.com/hydro*) and MIKE31 (*www.dhigroup.com*) are two widely used commercial models.

A special class of 2D models are the so called multi layer, or quasi 3D models; tridimensional flow is decomposed along horizontal planes, interconnected by mutual shear stress exchanges (Aricó et al., 2011).

2.8 Model selection for flood analysis

A wide number of research works have investigated advantages and drawbacks of each modelling approach for flood risk analysis. Although some guidelines can be drawn from literature review, a general consensus has not been reached by the scientific community, and the issue of selecting the "best" approach for a specific flood risk analysis is still being discussed and investigated (Horritt and Bates, 2002; Bates et al., 2004; Hunter et al., 2008; Neelz and Pender, 2010; Aricó et al., 2011; Castellarin et al., 2011).

2D and quasi 2D models are generally considered an appropriate choice for modelling river flood events (see previous sections of this chapter). However, as described in Section 2.5 a variety of dynamic, gravity, diffusion or kinematic wave 2D models are available in literature, each one based on different approach and including specific modeling features. Therefore a question arises: which modelling approach should be used? That is: how much complexity is required in the 2D representation to provide reliable and appropriate results (Hunter et al., 2007)? The answer implies to find a balance between the principles of model parsimony and accuracy. Given that each model is an approximation of reality, appropriate model selection for a specific flood risk analysis requires to consider different aspects: the location, extent and topographic configuration of the study area; the magnitude of the flood event; the flow processes occurring during the flood event; the quantity and quality of available information for model application and evaluation; the variables of interest and the accuracy required for the results; and, not least, the experience and expertise of the modeller (Hunter et al., 2007; Aricó et al., 2011). As described in Section 2.5, the formulation of the

shallow water equation is a key parameter, since it determines which flow processes model can be represented in the model.

Simplified 2D and quasi 2D models based on the kinematic wave or uniform flow formulae often provide an rather incomplete representation of hydraulic processes during flood events. For instance, a kinematic model is not able to compute backwater effects and provides physically inconsistent results when local minima are present in the topographic surface (Aricó et al., 2011). Therefore the kinematic wave equations are typically used within rainfall - runoff models rather than in hydraulic models.

On the other hand, the ability of diffusive wave models to simulate flooding phenomena is more debated (Hunter et al., 2007). To date, these models have been tested successfully against both analytical and numerical solutions (Xanthopoulos and Koutitas, 1976; Di Giammarco et al., 1996; Hunter et al., 2005b, 2007; Aricó et al., 2011). Less frequently, diffusive models have been tested against results from laboratory experiments (Prestininzi, 2008), and models models based on the fully dynamic SWE to simulate flood scenarios (Hunter et al., 2008; Neelz and Pender, 2010); in these works, diffusive models demonstrated several limitations, although overall good results were achieved. Actually, in different research works diffusive models provided good results in reproducing observed flood events, often performing as well as fully dynamic SWE models (Horritt and Bates, 2002; Bates et al., 2006; Yu and Lane, 2006a; Prestininzi et al., 2011).

Given these results, some authors hypothesized that uncertainties over the data set for model construction and validation could influence more model results than approximations due to a simplified mathematical description (Xanthopoulos and Koutitas, 1976; Yu and Lane, 2006a). This hypothesis has been recently verified by Aricó et al. (2011) and Guinot et al. (2009). These authors analyzed the sensitivity of fully dynamic and diffusive 2D models with respect to errors in a number of parameters, like topographic elevation, roughness coefficient and bed slope. They demonstrated that the sensitivity of computed results can be much higher for a fully dynamic model, especially when the Froude number approaches one. Since the difference between the results of the two mathematical models becomes significant only for the same range of Froude number, the better performance of a fully dynamic model can be compromised by data uncertainty (Aricó et al., 2011).

All these reasons suggest that diffusive models are the maximum degree of simplification that can be attained, in order to have a simplified, but still physically based, 2D hydraulic model. The representation of floodplain hydraulics is reduced to the minimum necessary to achieve reliable predictions at large scale when compared to typically available, non-error free validation data (Hunter et al., 2007). This hypothesis will be further discussed and analyzed in the next chapters.

Chapter 3

DEVELOPED MODELS

In this chapter, the two developed models are described in detail, including all the different versions and configurations developed during the research period. The common background of the two models includes the use of the diffusive approximation for the governing equations (Section 3.1) and a simplified finite volume (FV) integration scheme (Section 3.1.1). The description of the CA2D model is mostly taken from Dottori and Todini (2011), while part of the description of the IFD-GGA model was presented in Dottori and Todini (2010a).

3.1 The diffusive shallow water equations

The shallow water equations (SWE) can be obtained from the vertical integration of 3D Navier-Stokes equations, under the hypothesis of hydrostatic pressure distribution and adopting the Bousinnesq approximation (variations of fluid density are accounted only in pressure terms), together with an appropriate eddy viscosity closure scheme for Reynolds shear stress (Toro, 1992; Ern et al, 2008). Assuming gradual variations of flow variables (i.e. absence of shock waves), the SWE can be written in a non conservative form in Cartesian coordinates as (Casulli, 1990):

$$\frac{\partial u}{\partial t} + u\frac{\partial u}{\partial x} + v\frac{\partial u}{\partial y} + g\frac{\partial H}{\partial x} = g \cdot u \cdot n^2 \frac{\sqrt{u^2+v^2}}{h^{4/3}} \tag{3.1}$$

$$\frac{\partial v}{\partial t} + u\frac{\partial v}{\partial x} + v\frac{\partial v}{\partial y} + g\frac{\partial H}{\partial y} = g \cdot v \cdot n^2 \frac{\sqrt{u^2+v^2}}{h^{4/3}} \tag{3.2}$$

$$\frac{\partial h}{\partial t} + \frac{\partial (hu)}{\partial x} + \frac{\partial (hv)}{\partial y} = q \tag{3.3}$$

where head losses are computed using the Manning formulation. For a complete list of the variables used see Appendix A. The governing equations (3.1)-(3.3) are usually named as fully dynamic SWE, or 2D de Saint Venant equations (as in Section 2.5). The terms with time derivative of velocity components u and v represent the local acceleration; space derivatives of velocity components identify the convective acceleration (or advection) terms; space derivatives of water surface elevation H incorporate slope and pressure terms.

Although the equation set (3.1)-(3.3) can be directly integrated, it is also possible to adopt the so called diffusive approximation, by neglecting all local and convective acceleration terms (or inertial terms):

$$g\frac{\partial H}{\partial x} = g \cdot u \cdot n^2 \frac{\sqrt{u^2+v^2}}{h^{4/3}} \tag{3.4}$$

$$g\frac{\partial H}{\partial y} = g \cdot v \cdot n^2 \frac{\sqrt{u^2+v^2}}{h^{4/3}} \tag{3.5}$$

$$\frac{\partial h}{\partial t} + \frac{\partial h}{\partial x} + \frac{\partial h}{\partial y} = q \tag{3.6}$$

The resulting equations (3.4)-(3.6) are called also parabolic or zero-inertia SWE (Aricó et al., 2011). As it is immediate to see, both the momentum equations (3.4) and (3.5) can be reduced to a couple of explicit formulations $u = u(h)$ and $v = v(h)$, thus simplifying numerical integration (Prestininzi, 2008). In particular, boundary conditions can be assigned in form of an imposed arbitrary depth (Dirichlet type), an imposed arbitrary source of mass (Neumann type), or a solution-dependent condition of the type $Q = Q(h)$ or equivalently $h = h(Q)$ without a-priori awareness of super- or sub-critical flow state needed. Finally the diffusive approximation, neglecting inertial terms, leads to a shock-free evolution, allowing the use of simple numerical treatments (Prestininzi, 2008).

Several research works analysed the conditions for the applicability of 1D diffusion routing (Ponce, 1978). According to Hunter et al. (2007), the importance of advection terms in the momentum equation is a function of the lenght scale of topographic features and the model spatial discretization. Advection forces can be significant for small length scale features and high grid resolution ,whereas at larger length scales or coarse model resolution, bed friction and pressure terms will dominate and the advection terms may be neglected. Similar results were also described by Aricó et al. (2011) in a number of 2D numerical experiments. Results obtained by these authors suggested that the poor sensitivity of the diffusive SWE to small scale features can significantly smooth out local flow processes, with respect to a fully dynamic SWE description (as will be described in Section 5.4). On the other hand, this also implies a smaller sensitivity to the input data error and uncertainty, as described in Section 2.8.

It is interesting to note that in different research works, diffusive models were preferred because their simpler numerical structure resulted in higher computational efficiency with respect to fully dynamic models (Xanthopoulos and Koutitas, 1976; Di Giammarco et al., 1996). Nowadays, the methods for solving fully dynamic SWE have attained a high computational efficiency and computation times are often comparable to diffusive models (Neelz and Pender, 2010; Aricó et al., 2011).

3.1.1 Integration of equations

The diffusive equations (3.4)-(3.6) allow for the implementation of a straightforward two-dimensional cell-centred finite volume scheme. This integration method can actually be

located at the frontier between the FV approach and more conceptualized techniques, like storage cells approach (Prestininzi, 2008; Bates et al., 2010). The study area is represented by a grid of polygonal non-overlapping elements, where each single element, or cell, represents a volume of fluid connected with the adjacent cells through the contact faces. Thus, the momentum equation can be integrated along each connection k, obtaining:

$$\frac{\partial H_k}{\partial X_k} = \frac{Q_k^2 \cdot n_k^2}{b_k \cdot h_k^{10/3}} \tag{3.7}$$

The continuity equation is integrated on each elementary volume i:

$$\frac{\partial V_i}{\partial t} = \sum_k^{1,m} Q_k + q \tag{3.8}$$

It is worth noting that this computation scheme is equivalent to a pipe network, in which the nodes (that is, the cell centroids) represent the cells and the connections between nodes represent the contact faces (Di Giammarco et al., 1996). Like standard FV schemes, the proposed method can be applied to both structured and unstructured grids and any geometrical shape of the elementary volumes can be adopted (Figure 3.1). Moreover, the integral formulation of SWE automatically preserves mass balance (Toro, 1992; Soares Frazão et al., 2008).

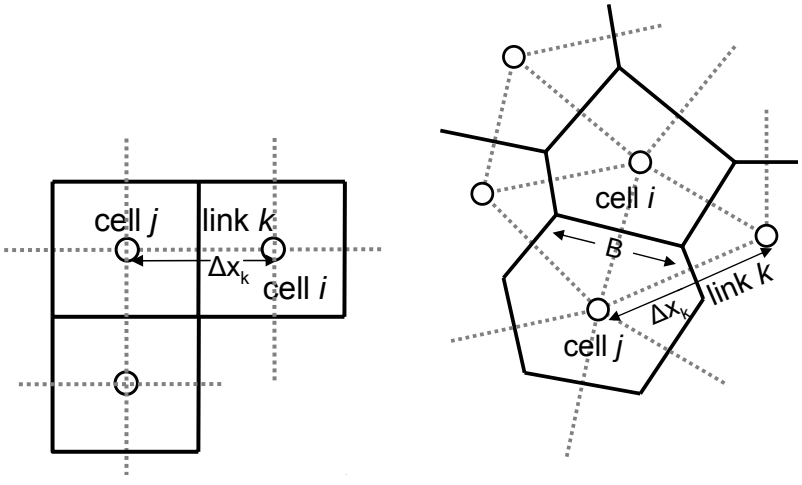

Figure 3.1: examples of computation grid in CA2D and IFD-GGA models; links are indicated as grey lines; left: square mesh; right: irregular mesh.

The choice of adopting the same schematization of the study area allows for an easy integration between the two developed models. A single case study can be simulated using the same input files, thus enabling more complete analyses as one of the models or both may be applied when required. This also facilitates the comparison between model results.

On the other hand, the two models use different schemes for the time integration of governing equations (3.7) and (3.8). The CA2D model uses an Eulero first order explicit

scheme, while the IFD-GGA model uses an implicit Crank-Nicholson scheme, with a weight coefficient θ (Di Giammarco et al., 1996).

Being explicit in time, the CA2D model is expected to be much faster than the implicit IFD-GGA model, in which an equation system must be solved at each time step. However, overall computational efficiency can be comparable since the latter is unconditionally stable and therefore can use larger time steps (Di Giammarco et al., 1996). In addition, the CA2D scheme is first order accurate in time, while in the IFD-GGA model the accuracy should depend on the weight coefficient θ.

On the other hand, implicit models may be subject to a number of drawbacks that explicit schemes don't have:

- At each time step, a linear system needs to be solved: the approximation introduced in the required iterative solution can result in a loss of precision as the simulation proceeds in time, although time step solution is still convergent.
- Although implicit models are unconditionally stable, the time step can not be arbitrarily large, and must be chosen case by case according to boundary and internal flow conditions in order to preserve accuracy; therefore a standard criteria for time step selections is difficult to establish. On the contrary, explicit models can be based on appropriate stability criteria that allow for the implementation of adaptive time stepping techniques (see Section 3.2.4).

Resuming, the feasibility of each model should be carefully tested in different conditions. Thus, these issues will be further discussed in Chapter 4.

3.2 The CA2D model

The CA2D model here described can be considered a tradeoff between physically based finite volume models and empirical cellular automata models. A cellular automaton (pl. cellular automata, abbrev. CA) is a discrete model for the description of physical dynamic systems regulated only by local laws. Typically it consists of a regular grid of cells, each in one of a finite number of states or properties, such as "on" and "off". For each cell, a set of cells called its neighborhood (usually including the cell itself) is defined. An initial state is selected by assigning a state for each cell. The system evolves in time according to some fixed rule (generally, a mathematical function) that determines the new state of each cell in terms of the current state of the cell and the states of the cells in its neighborhood. Typically, the rule for updating the state of cells is the same for each cell and does not change over time, and is applied to the whole grid simultaneously (Wikipedia, 2012)

Cellular automata are currently used to model several physical phenomena, when either the complexity of the governing equations or data scarcity prevent detailed simulations. Current fields of application include computability theory, mathematics, physics, complexity science, theoretical biology and microstructure modelling. In particular, CA have also been used to simulate specific fluid dynamics phenomena like debris flows (D'Ambrosio et al.,

2003), pyroclastic flows (Avolio et al., 2006), infiltration and water surface flow (Parsons and Fonstand, 2007). In these applications the so called macroscopic cellular automata approach was applied, which partly differs from the classical CA structure so far described. The cell lattice of a macroscopic CA forms a grid of polygonal elements of either regular or variable shape and dimension, which represents the topography of the study area. In fluid dynamics applications, each cell represents a volume of fluid to which either empirical relationships or physically based equations may be applied. It is worth noting that in some specific fluid dynamics applications (e.g. sand transport by wind) discrete CA models were used (Chopard and Masselot, 1999). Although potentially interesting, this approach is not feasible when systems composed by huge numbers of particles have to be reproduced, like in usual large scale problems of surface flow.

Given this reference background, it was decided to develop a hydraulic model based on macroscopic cellular automata approach and the diffusive equations. Previous CA models for surface flow were based either on simplified equations (e.g. Manning uniform flow equation) or approximated SWE (Parsons and Fonstand, 2007). The diffusive approximation is particularly suited to be used within a CA model: by eliminating inertial terms, flow becomes a function of water levels and the structure of 2D flow can be heavily simplified while preserving a considerable amount of "physics" in the model. For example, the diffusive approximation allows to decouple flow components.

From a practical point of view, the combination of diffusive equations and macroscopic CA leads to a simplified finite volume scheme, as mentioned in Section 3.1.1.

3.2.1 CA2D diffusive version

In the first version of the CA model scheme, the integration in time is obtained with the Euler first order explicit scheme, following the CA rule that the overall system state only depends on the previous time step. Thus, the continuity equation (3.8) is discretized at time step $t + \Delta t$ as:

$$V_i^{t+\Delta t} = V_i^t + \Delta t \sum_{j=1}^{m} Q_{i,j}^t + Q_0^t \tag{3.9}$$

where Δt is the time step in use and Q_0 is the total discharge entering or exiting the domain through cell i. Considering two adjacent cells i and j, the discharge Q through the contact face is given by the momentum equation:

$$Q_{i,j} = \frac{B h_m^{5/3}}{n} \left(\frac{H_i - H_j}{\Delta x} \right)^{1/2} \tag{3.10}$$

whereH_i, $H_j$are the water stages in the two cells; Δx is the distance between centroids of the two cells; B is the width of the contact face; n is the Manning roughness coefficient; h_m is the arithmetic mean between water depths in the two cells. The reasons for choosing this specific water depth value are reported in detail in Section 3.4.1.

As the momentum equation (3.7) is integrated along the link direction, any generic 2D

flow is decomposed in 1D flow components through the links, Δx being a vector with x and y components. Each flux component is therefore decoupled from the others, so that Eq. (3.10) may be solved separately for each link.

3.2.2 Stability problems of diffusive models

For an explicit time marching hydraulic model, the maximum allowable time step to preserve stability may be obtained from the Courant-Lewy-Friedrich (CFL) condition, written in the appropriate form. For a 2D model decoupling flow components, the CFL condition may be written in the 1D formulation:

$$\Delta t = C\Delta x / (v + c) \tag{3.11}$$

where C is a coefficient which depends on the adopted explicit algorithm and c is the wave celerity. However Eq. (3.11) only provides the upper limit value, while an explicit model may get unstable also with lower time steps, depending on the adopted computational scheme. Hunter et al. (2005b) stated that explicit models not based on the fully dynamic shallow water equations need more reduced time steps. For the LISFLOOD-FP model, based on the diffusive approximation as the CA2D model, a Von Neumann stability analysis was performed, leading to the following criterium (Hunter et al., 2005b):

$$\Delta t = \frac{\Delta x^2}{4} \min \left(\frac{2n_{i,j}}{h_{m-i,j}^{5/3}} \left(\frac{\partial H_{i,j}}{\partial x} \right)^{1/2} \right) \tag{3.12}$$

that is, for every cell i, the term between parenthesis is computed in all the j connections with adjacent cells, and the minimum time step found is chosen to proceed with the simulation. The use of Eq. (3.12) in practical applications is not straightforward, since when particular flow conditions occur it may produce too low or high time step values.

Hunter et al. (2005b) observed that time step values tend to become very small in presence of still water surface. Therefore they introduced in the LISFLOOD-FP model a linearization of the flow equation, that is applied to areas where the water surface slope is below a specified threshold. Fewtrell et al. (2007) performed a statistical analysis of the time step distribution in an experimental application of the LISFLOOD-FP model, and evaluated the effect of relaxing the time step criterion given by Eq. (3.12). The relaxation produced some degradation in the model's results as compared with the full adaptive time step solution. However, the difference was of the order of the error of elevation data. Considering these previous results, a more accurate analysis of spatial distribution of time step values computed by Eq. (3.12) was performed and it is described in Chapter 4.

3.2.3 An alternative formulation: the inertial model

A first solution to improve the performance of diffusive models like CA2D is to modify the model equations, in order to increase the maximum allowable time step up to the limit given by the CFL condition (3.11). Since its only variables are the grid size and the characteristic

velocity, the CFL condition is not affected by the problems discussed in Section 3.2.2. Heading in this direction, Bates et al. (2010) developed an equation for discharge estimation which partly accounts for inertial effects. The derivation is herein briefly summarized: the starting point is the momentum equation from the one-dimensional De Saint Venant equations:

$$\frac{\partial Q}{\partial t} + \frac{\partial}{\partial x}\left[\frac{Q^2}{A}\right] + \frac{gA\partial(h+z)}{\partial x} + \frac{gn^2Q^2}{R^{4/3}A} = 0 \tag{3.13}$$

It should be noted that Eq. (3.13) was multiplied by A, which has been considered constant in time and space to be extracted from derivation signs. Neglecting the advection term $\frac{\partial}{\partial x}\left[\frac{Q^2}{A}\right]$, dividing through a constant flow width and approximating the hydraulic radius, R, with the flow depth, h, Eq. (3.13) can be discretized with respect to time step Δt, to give:

$$\left(\frac{q_{t+\Delta t} - q_t}{\Delta t}\right) = -\frac{gh_t\partial\left(h_t + z\right)}{\partial x} - \frac{gn^2q_t^2}{h_t^{7/3}} \tag{3.14}$$

By rearranging Eq. (3.14) an explicit equation for q at time $t + \Delta t$ is obtained:

$$q_{t+\Delta t} = q_t - gh_t\Delta t\left[\frac{\partial\left(h_t + z\right)}{\partial x} + \frac{n^2q_t^2}{h_t^{10/3}}\right] \tag{3.15}$$

The same authors developed a semi-implicit version of Eq. (3.15) by replacing a q_t in the friction term by a $q_{t+\Delta t}$. After rearranging they obtained the following explicit form for discharge computation:

$$q_{t+\Delta t} = \frac{q_t - gh_{flow}\Delta t\frac{\partial(h+z)}{\partial x}}{1 + gh_{flow}\Delta tn^2\left|q_t\right|/h_{flow}^{10/3}} \tag{3.16}$$

where h_{flow} is the difference between the highest water free surface in the two cells and the highest water elevation.

Bates et al. (2010) reported that the use of Eq. (3.16) in the LISFLOOD-FP model allowed to use the following version of the Courant-Lewy-Friedrich stability condition:

$$\Delta t = C\frac{\Delta x}{\sqrt{gh_{flow}}} \tag{3.17}$$

Although Eq. (3.16) dramatically increased the model stability, with respect to the diffusive formulation, the use of the inertial formulation was not always favourable in terms of accuracy of the solution.

It must also be noted that, although (Bates et al., 2010) defined Eq. (3.16) as an inertial formulation, such definition is not completely correct, since only the local acceleration term is included, but not the advection term. However, in order to be consistent with the previous paper by Bates et al., in the present work the Eq. (3.16) is called as inertial method, following the original denomination. The structure of Eq. (3.16) is particularly suitable for the reduced complexity models; therefore it was introduced into the CA2D model, and tested in the numerical cases presented in Chapter 4.

3.2.4 The introduction of a local time step algorithm

Why a local time step algorithm? A further method to improve the performance of a hydraulic model is discussed in this section.

The great majority of explicit time marching hydraulic models include an algorithm for modifying the current time step according to flow conditions, in order to use, during the simulation, the greatest value which guarantees stability over the whole computation grid. The time step is usually adapted considering both theoretical criteria, based on the stability analysis (e.g. the CFL condition), and empirical controls (e.g. a maximum value of water depth change in a cell during a single time step).

The use of a global, adaptive time step (GTS) has a major drawback, especially in the presence of concentrated flow areas and complex topography, or when using unstructured meshes with large variations on cell size: the time step can locally assume values that are significantly smaller than values computed in the rest of computational grid, thus resulting in a considerable slowing of the simulation.

A viable approach to overcome this problem is through the use of local adaptive time step (LTS) for the time marching of simulation, whereby each grid cell is integrated according to the local flow physics and numerical stability (Kleb and Batina, 1992).

Early results on local time stepping have been published by Osher and Sanders (1983) for one-dimensional scalar conservation laws and, since then, many LTS methods have been proposed for numerical models solving the Euler and Navier-Stokes equations. In the field of hydraulic engineering, local time stepping tecniqhes has demonstrated utility both in 1D channel flow modeling (Crossley et al., 2003) and in 2D applications involving irregular topography and wetting and drying processes (Sanders, 2008). In both works, the local time step algorithm increased the computational efficiency from 25% to 70% with respect to GTS methods, with no loss in accuracy.

LTS techniques were first developed and implemented in models with unstructured meshes and local grid refinement schemes. However, according to Sanders (2008) and Crossley et al. (2003), models that use a uniform grid may also benefit from LTS schemes in applications involving a variable wave speed.

The implementation of a LTS algorithm within CA2D could be particularly favourable, since the diffusive stability condition (3.6)implies the use of locally small time steps. Hence, a local time step algorithm based on an existing method has been implemented within the CA2D model and is described here.

The proposed local time step formulation. The implementation of a local time step is obviously not straightforward: in order to maintain a time-accurate solution, a method of accurately exchanging information between cells being integrated at disparate time steps needs to be developed (Kleb and Batina, 1992).

Several methods for managing interface between regions at different time steps have been proposed in literature. Kleb and Batina (1992) presented a LTS technique based upon advancing individual cells to the level allowed by the CFL condition, then using linear interpolation at the interface to extract the information at the correct point in time. A

similar approach was used by Sanders (2008), whereas Muller and Stiriba (2007) used a predictor-corrector approach to compute fluxes at the interface.

All these techniques require to identify regions where cells are integrated with the same specific time step, and to define interfaces between regions where time integration has to change gradually. In addition, in order to avoid numerical errors the ratio between minimum and maximum time step needs to be limited (Crossley et al., 2003; Sanders, 2008). This results in an increase of computation cost and complication of code, although all the mentioned authors reported considerable increases in overall code speed.

Considering the existing techniques and the characteristics of the CA model, the developed algorithm is based on a flux-updating procedure, similar to that proposed by Zhang et al. (1994). Time steps are computed on links between nodes, assigning to each link a time step value Δt_j, which is a multiple of the smallest time step throughout the domain ΔT_m:

$$k_j \Delta T_m \leq \Delta t_j \leq (k_j + 1)\, \Delta T_m \tag{3.18}$$

The discharge on each link (Eqs. (3.10) and (3.16), depending on the model version) is updated considering the local time step value: a value computed for link j at a specific simulation time $\bar{t}$ is used until the simulation has progressed to $\bar{t} + \Delta t_j$, then new values of time step and discharge are calculated.

Temporal update of volumes in each cell (Eq. 3.9) is performed considering the smallest time step ΔT_m, using the current discharge values stored for the corresponding links; thus, Eq. (3.9) is modified and becomes:

$$V_i^{t+\Delta t} = V_i^t + \Delta t \sum_{j=1}^{m} \frac{\Delta t_j}{k_j} Q_{i,j}^t + Q_0^t \tag{3.19}$$

With such procedure, the number of temporal updates is the same of a global time step method, but the number of flux evaluations, and hence computation cost and time, is considerably reduced.

The proposed local time step algorithm presents differences with respect to the original version of the approach (Zhang et al., 1994) and successive applications (Crossley et al., 2003). In particular, there is no need to divide cells in groups with different time steps, since the maximum allowable time step is directly assigned to each link and stored after each computation step. Therefore, there is no control on the difference in time step values between adjacent nodes, as it is supposed that flow conditions always generate a gradual variation in time step. Although such hypothesis may be not always true, e.g. in areas with a transition from subcritical to supercritical flow, it is reasonable since flow dynamics in most inundation events is normally slow and the diffusive stability condition (Eq. (3.12)) imposes small time steps. The algorithm should be suitable also for the CFL condition, provided that adequate values of the coefficient C are chosen (Eq. (3.17)). The validity of such an hypothesis was tested in the numerical cases presented in Chapter 4.

Furthermore, there is no need to limit the ratio between maximum and minimum time step during a generic simulation step. Hence, the algorithm is particularly suitable for the

spatial distribution of time steps given by Eq. (3.12). For example, considering a levee breach simulation, the minimum time step may be less than 0.1s near the inflow area, due to high water depths and rapidly varying flow, while the maximum value may be 10 seconds in areas with low water depths or still water.

The only limitation introduced in the algorithm regards the minimum and maximum allowable time step (normally 0.01s and 10-20s), which are necessary considering the numerical problems given by the diffusive stability condition (see Section 3.2.2).

3.3 The IFD-GGA model

The model here described is a modification of the original Integrated Finite Differences (IFD) model developed at the Department of Earth, Environmental and Geological Sciences. In the original version of the IFD model, the solution algorithm was based on a dichotomic iterative scheme, while the resulting equation system was solved with a modified conjugate gradient method (Commission EC, 1996; Di Giammarco et al., 1996). The resulting scheme is stable and convergent in any situation, and the model was successfully used for the analysis of flood scenarios (Commission EC, 1996; Anselmo et al., 1996). However, the low convergence speed limited practical application of the model.

In order to overcome this problem, it was decided to rewrite the model code, incorporating a new solution algorithm derived from the Global Gradient Algorithm (Todini and Pilati, 1988), used for pipe network analysis. Consequently the new model has been named IFD-GGA. We consider the system of equations (3.7) and (3.8) rewritten as follows:

$$\begin{cases} \frac{n^2|Q|Q}{B_{i,j}^2(H-Z)^{10/3}} = -\frac{\partial H}{\partial x} \\ \Omega_i \frac{\partial h_i}{\partial t} = \sum_{k=1}^{ni} Q_{ij} + Q_{0i} \end{cases} \tag{3.20}$$

The system of equations (3.20) is discretized on space and time obtaining:

$$\begin{cases} \frac{3}{7}\frac{n_{i,j}^2|Q_{ij,t}|Q_{ij,t}}{B_{i,j}^2}\frac{\left(h_i^{-7/3}-h_j^{-7/3}\right)_t}{(h_j-h_i)_t} - \frac{h_{i,t}-h_{j,t}}{\Delta X_{i,j}} - S_0 = 0 \\ \Omega_i \frac{h_{i,t}-h_{i,t-\Delta t}}{\Delta t} - \theta\left(\sum_{k=1}^{ni} Q_{ij} + Q_{0i}\right)_t - (1-\theta)\left(\sum_{k=1}^{ni} Q_{ij} + Q_{0i}\right)_{t-\Delta t} = 0 \end{cases} \tag{3.21}$$

where θ is the weight coefficient of the the implicit Crank-Nicholson scheme (Di Giammarco et al., 1996). Please note that the momentum equation has been integrated in space along a generic link by using an integral average of head losses (see Section 3.4.1). The equation system (3.21) can be written in a matrix notation, extending the original GGA algorithm (Todini and Pilati, 1988) to the unsteady flow condition:

$$\begin{bmatrix} A_{11} & \vdots & A_{12} \\ \cdots & & \cdots \\ A_{21} & \vdots & A_{22} \end{bmatrix} \begin{bmatrix} Q \\ \\ H \end{bmatrix} = \begin{bmatrix} -A_{10}H_0 \\ \\ -Q^* \end{bmatrix} \tag{3.22}$$

The elements in system (3.22) are herein described:
$Q_t = [Q_{1,t}, Q_{2,t}, \cdots, Q_{np,t}]$ is the vector of discharges [1, n_p],
$H_t = [H_{1,t}, H_{2,t}, \cdots, H_{np,t}]$ is the vector of unknown water stages [1, n_n],
$H_t = [H_{nn+1,t}, H_{nn+2,t}, \cdots, H_{ntot,t}]$ is the vector of known water stages [1, n_{tot}],
$Q_t* = [Q*_{1,t}, Q*_{2,t}, \cdots, Q*_{np,t}]$ is the vector of known terms [1, $n_n - n_{tot}$],
where (n_p) is the number of links, (n_n) is the number of nodes with unknown water stage, (n_{tot}) is the total number of nodes, ($n_n - n_{tot}$) is the number of nodes with known water stage.

A_{11} is a diagonal matrix with dimension [n_p, n_p] where the elements are defined as:

$$A_{11}(k,k) = \frac{3}{7}\frac{n_{i,j}^2 |Q_{i,j}|}{B_{i,j}^2}\frac{\left(h_i^{-7/3} - h_j^{-7/3}\right)}{(h_j - h_i)} \tag{3.23}$$

The formulation (3.23) must be modified when $\varepsilon = (h_i - h_j) \to 0$; we have therefore:

$$A_{11} = \frac{n_{i,j}^2 |Q_{i,j}| \Delta x}{B_{i,j}^2} h^{-10/3} \tag{3.24}$$

A_{22} is a diagonal matrix with dimension [n_n, n_n] where the elements are defined as:

$$A_{22}(i,i) = -\frac{\Omega_i}{\theta \Delta t} \tag{3.25}$$

The generic element of the vector $Q*_t$ is defined as:

$$Q_t * (i) = Q_{i,t} + \frac{\Omega_i}{\theta \Delta t} H_{i,t-\Delta t} + \frac{(1-\theta)}{\theta}\left(\sum_{k=1}^{nn} Q_k + Q_{0i}\right)_{t-\Delta t} \tag{3.26}$$

The topology of the network (nodes and links) is described by matrix A_{12}, defined as:

$$A_{12}(i,k) = \begin{cases} -1 \text{ if flow in the link k leaves node i} \\ 0 \text{ if link k doesn't include node i} \\ +1 \text{ if flow in the link k enters node i} \end{cases}$$

In order to guarantee the existence of a unique solution, the water elevation must be known in at least one cell. This implies the partition of A_{12} in two sub-matrices:

$$A_{12} = \left[\begin{array}{c:c} A_{12} & A_{10} \end{array} \right]$$

where $A_{12} = A_{21}^T$ describes the links between the unknown water head nodes, while $A_{10} = A_{01}^T$ describes the links with the known head nodes.

3.3.1 Newton-Raphson and Jacobi methods

In order to speed up the solution algorithm of the original IFD model, different approaches have been developed. In the first one, the original dichotomic method has been substituted

with the Newton-Raphson (NR) method, coupled with the Jacobi method to solve the inner iterative cycle (Kelley, 1995; Luenberger, 2003). In order to apply the NR method, the Eqs. (3.21) must be differentiated on $Q_{ij,t}$,$h_{i,t}$,$h_{i,t-\Delta t}$, obtaining the following expressions:

$$\begin{cases} \frac{6}{7}\frac{n_{i,j}^2 \Delta X_{i,j}|Q_{ij,t}|}{B_{i,j}^2}\frac{\left(h_i^{-7/3}-h_j^{-7/3}\right)_t}{(h_j-h_i)_t}dQ_{ij,t}-1+ \\ +\frac{n_{i,j}^2|Q_{ij,t}|Q_{ij,t}\Delta x}{B_{i,j}^2}\left(\frac{3}{7}\frac{\left(h_i^{-7/3}-h_j^{-7/3}\right)}{(h_j-h_i)^2}-\frac{h_i^{-10/3}}{(h_j-h_i)}\right)_t dh_{i,t}+ \\ +1-\frac{n_{i,j}^2|Q_{ij,t}|Q_{ij,t}\Delta x}{B_{i,j}^2}\left(\frac{3}{7}\frac{\left(h_i^{-7/3}-h_j^{-7/3}\right)}{(h_j-h_i)^2}-\frac{h_j^{-10/3}}{(h_j-h_i)}\right)_t dh_{j,t}=dE_{ij,t} \\ \sum_{k=1}^{ni} Q_{ij,t}-\frac{\Omega_i}{\theta\Delta t}dh_{i,t}=dE_{i,t} \end{cases} \tag{3.27}$$

where:

$$\begin{cases} dE_{ij,t}=\frac{3}{7}\frac{n_{i,j}^2\Delta X_{i,j}|Q_{ij,t}|Q_{ij,t}}{B_{i,j}^2}\frac{\left(h_i^{-7/3}-h_j^{-7/3}\right)_t}{(h_j-h_i)_t}-(h_i-h_j)_t-\Delta X_{i,j}S_{0i,j} \\ dF_{ij,t}=\sum_{k=1}^{ni} Q_{ij,t}-\frac{\Omega_i}{\theta\Delta t}\left(h_{i,t}-h_{i,t-\Delta t}\right)+Q_{0i,t}-\frac{(1-\theta)}{\theta}\left(\sum_{k=1}^{ni} Q_{ij}+Q_{0i}\right)_{t-\Delta t} \end{cases} \tag{3.28}$$

It is possible to write the two differentials in a matrix form as:

$$\begin{cases} d\mathrm{E}^\tau=\mathrm{A}_{11}^\tau\mathrm{Q}^\tau+A_{12}\mathrm{h}^\tau+\mathrm{A}_{1\mathrm{o}}^\tau\mathrm{h}_0-\mathrm{S} \\ d\mathrm{F}^\tau=\mathrm{A}_{21}\mathrm{Q}^\tau+\mathrm{A}_{22}^\tau\mathrm{h}^\tau+\mathrm{Q}* \end{cases} \tag{3.29}$$

where τ is the iteration index and S is a vector whose elements are defined as:

$$\mathrm{S}\left(k\right)=\Delta x_{ij}S_{0,ij} \tag{3.30}$$

The non symmetric system (3.29) can be written in matrix to derive the solving algorithm:

$$\begin{bmatrix} \mathrm{D}_{11}^\tau & \mathrm{D}_{12}^\tau \\ \mathrm{A}_{21} & \mathrm{A}_{22}^\tau \end{bmatrix}\begin{bmatrix} d\mathrm{Q}^\tau \\ d\mathrm{h}^\tau \end{bmatrix}=\begin{bmatrix} d\mathrm{E}^\tau \\ d\mathrm{F}^\tau \end{bmatrix} \tag{3.31}$$

where, omitting the τ index for sake of clarity:

$$D_{11}=\frac{6}{7}\frac{n_{i,j}^2\left|Q_{i,j}\right|\Delta x}{B_{i,j}^2}\frac{\left(h_i^{-7/3}-h_j^{-7/3}\right)}{(h_j-h_i)}=2A_{11} \tag{3.32}$$

$$D_{12}\left(k,i\right)=-1+\frac{n_{i,j}^2\left|Q_{i,j}\right|Q_{i,j}\Delta x}{B_{i,j}^2}\left(\frac{3}{7}\frac{\left(h_i^{-7/3}-h_j^{-7/3}\right)}{\left(h_j-h_i\right)^2}-\frac{h_i^{-10/3}}{(h_j-h_i)}\right) \tag{3.33}$$

$$D_{12}\left(k,j\right)=1-\frac{n_{i,j}^2\left|Q_{i,j}\right|Q_{i,j}\Delta x}{B_{i,j}^2}\left(\frac{3}{7}\frac{\left(h_i^{-7/3}-h_j^{-7/3}\right)}{\left(h_j-h_i\right)^2}-\frac{h_j^{-10/3}}{(h_j-h_i)}\right) \tag{3.34}$$

Where nodes i, j indicate respectively the starting and ending node of link k. Equations (3.32), (3.33), (3.34) have to be modified when $\varepsilon=(h_i-h_j)\to 0$; in this case we have:

$$A_{11} = \frac{2n_{i,j}^2 \left|Q_{i,j}\right| \Delta x}{B_{i,j}^2} h^{-10/3} \tag{3.35}$$

$$D_{12}\left(k,i\right) = -1 - \frac{5n_{i,j}^2 \left|Q_{i,j}\right| Q_{i,j} \Delta x}{3B_{i,j}^2} \left(h_i^{-13/3}\right) \tag{3.36}$$

$$D_{12}\left(k,j\right) = 1 - \frac{5n_{i,j}^2 \left|Q_{i,j}\right| Q_{i,j} \Delta x}{3B_{i,j}^2} \left(h_j^{-13/3}\right) \tag{3.37}$$

The solution of the linear equation system can be obtained once the inverse of the system matrix is found:

$$\left[\begin{array}{cc} \mathrm{D}_{11} & \mathrm{D}_{12} \\ \mathrm{A}_{21} & \mathrm{A}_{22} \end{array}\right] \left[\begin{array}{cc} \mathrm{B}_{11} & \mathrm{B}_{12} \\ \mathrm{B}_{21} & \mathrm{B}_{22} \end{array}\right] = \left[\begin{array}{cc} \mathrm{I} & 0 \\ 0 & \mathrm{I} \end{array}\right] \tag{3.38}$$

where the iteration index τ has been omitted. From Eq. (3.38) the following relationships can be obtained:

$$\left\{\begin{array}{l} \mathrm{D}_{11}\mathrm{B}_{11} + \mathrm{D}_{12}\mathrm{B}_{21} = \mathrm{I} \\ \mathrm{D}_{11}\mathrm{B}_{12} + \mathrm{D}_{12}\mathrm{B}_{22} = 0 \\ \mathrm{A}_{21}\mathrm{B}_{11} + \mathrm{A}_{22}\mathrm{B}_{21} = \mathrm{I} \\ \mathrm{A}_{21}\mathrm{B}_{12} + \mathrm{A}_{22}\mathrm{B}_{22} = 0 \end{array}\right. \tag{3.39}$$

Therefore, the analytic solution of the equation system (3.29) is:

$$\left\{\begin{array}{l} d\mathrm{Q} = \mathrm{B}_{11} d\mathrm{E} + \mathrm{B}_{12} d\mathrm{F} \\ d\mathrm{h} = \mathrm{B}_{21} d\mathrm{E} + \mathrm{B}_{22} d\mathrm{F} \end{array}\right. \tag{3.40}$$

Replacing in Eq. (3.40) the formulation of the terms, after some simple algebraic passages the increase for the water depth is:

$$\begin{array}{l} d\mathrm{h} = \left(\mathrm{A}_{21}\mathrm{D}_{11}^{-1}\mathrm{D}_{22} - \mathrm{A}_{22}\right)^{-1} \cdot \\ \cdot \left[\mathrm{A}_{21}\left(\mathrm{D}_{11}^{-1}\mathrm{A}_{11} - \mathrm{I}\right)\mathrm{Q} + \left(\mathrm{A}_{21}\mathrm{D}_{11}^{-1}\mathrm{D}_{22} - \mathrm{A}_{22}\right)\mathrm{h} + \mathrm{A}_{21}\mathrm{D}_{11}^{-1}\mathrm{A}_{10}\mathrm{h}_0 - \mathrm{Q}*\right] \end{array} \tag{3.41}$$

As can be noticed, the matrix that have to be inverted is not symmetric but stricly diagonal dominant, thanks to the sum of matrix A_{22} on the main diagonal. This allows to solve the system (3.40) using iterative techniques like the Jacobi method. The analysis of the equations shows that it is possible to replace dh in the formulation of dQ; after an appropriate recombination of terms, dQ can be written as:

$$d\mathrm{Q} = \mathrm{D}_{11}^{-1}\left[d\mathrm{E} - \mathrm{D}_{12} d\mathrm{h}\right] \tag{3.42}$$

that can be estimated once dh has been computed. dh is computed with the Jacobi method as:

$$\left(\mathrm{A}_{21}\mathrm{D}_{11}^{-1}\mathrm{D}_{22} - \mathrm{A}_{22}\right) d\mathrm{h} = \mathrm{A}_{21}\mathrm{D}_{11}^{-1} d\mathrm{E} - d\mathrm{F} \tag{3.43}$$

Therefore, each time step the application of the iterative Newton Raphson algorithm performed by solving one by one the following relationships for each iteration τ:

$$\begin{cases} d\mathrm{h}^{\tau} = \left[\mathrm{A}_{21}\left(\mathrm{D}_{11}^{\tau-1}\right)^{-1}\mathrm{D}_{22} - \mathrm{A}_{22}\right]\left[\mathrm{A}_{21}\left(\mathrm{D}_{11}^{\tau-1}\right)^{-1} d\mathrm{E}^{\tau-1} - d\mathrm{F}^{\tau-1}\right] \\ d\mathrm{Q}^{\tau} = \left(\mathrm{D}_{11}^{\tau-1}\right)^{-1}\left[d\mathrm{E}^{\tau-1} - \mathrm{D}_{12}^{\tau-1} d\mathrm{h}^{\tau}\right] \\ \mathrm{h}^{\tau} = \mathrm{h}^{\tau-1} - d\mathrm{h}^{\tau} \\ \mathrm{Q}^{\tau} = \mathrm{Q}^{\tau-1} - d\mathrm{Q}^{\tau} \\ d\mathrm{E}^{\tau} = \mathrm{A}_{11}\mathrm{Q}^{\tau} + \mathrm{A}_{12}\mathrm{h}^{\tau} + \mathrm{A}_{10}\mathrm{h}_0^{\tau} - S \\ d\mathrm{F}^{\tau} = \left[\left(\mathrm{A}_{21}\mathrm{Q}^{\tau} + \mathrm{q}^{\tau}\right) + \frac{1-\vartheta}{\vartheta}\left(\mathrm{A}_{21}\mathrm{Q}^{\tau-1} + {\mathrm{Q}_0}^{\tau-1}\right)\right] + \mathrm{A}_{22}\left(\mathrm{h}^{\tau} + \mathrm{h}^{\tau-1}\right) \end{cases} \tag{3.44}$$

3.3.2 Linear Theory and Jacobi method

In the second solution algorithm designed for the IFD-GGA model, the equation system (3.21) is linearised by using the Linear Theory (LT) approach (Wood and Charles, 1972). In this case, the following recursive scheme is used, solving first for the water level and then the discharge:

$$\begin{cases} \mathrm{H}^{\tau} = \left[\mathrm{A}_{21}\left(\mathrm{A}_{11}^{\tau-1}\right)^{-1} A_{22} - \mathrm{A}_{22}\right]^{-1}\left[\mathrm{Q}* - \mathrm{A}_{21}\left(\mathrm{A}_{11}^{\tau-1}\right)^{-1}\mathrm{A}_{10}\mathrm{H}_0\right] \\ \mathrm{Q}^{\tau} = \frac{1}{2}\left[\mathrm{Q}^{\tau-1} - \left(\mathrm{A}_{11}^{\tau-1}\right)^{-1}\left(\mathrm{A}_{12}\mathrm{H}^{\tau} - \mathrm{A}_{10}\mathrm{H}_0\right)\right] \end{cases} \tag{3.45}$$

As can be noticed from Eqs. (3.45), the iterative solution requires the solution of a system of linear equations, which matrix $\left(\mathrm{A}_{21}\left(\mathrm{A}_{11}^{\tau}\right)^{-1}\mathrm{A}_{22} - \mathrm{A}_{22}\right)$ is a sparse symmetrical matrix with dominant diagonal. These conditions allow for the use of the recursive Jacobi approach, instead of more direct frontal Gauss-Seidel or matrix factorization approaches.

3.3.3 Discussion

Both the proposed schemes have been chosen to provide a fast and reliable solution algorithm for the IFD-GGA model. The Newton-Raphson scheme guarantees the fastest rate of convergence among the possible schemes for solving non linear systems (Kelley, 1995; Luenberger, 2003). In theory, the Linear Theory does not provide a convergence rate comparable to NR when high precision is required in the solution. However, in preliminary tests it was found that, for the accuracy requirements in typical flood inundation events (around 10^{-3} m), the LT approach required more or less the same number of iterations of the NR approach, with the advantage of a resulting symmetrical system matrix to be handled (Wood and Charles, 1972).

In addition, the use of the Jacobi scheme allows to decompose the resulting equation systems to single equations that can be solved indipendently. In this way, the algorithm can be massively parallelized, as for an explicit scheme (see Section 3.5).

However, it should be noted that the proposed approaches are not designed to be applied in hydraulic models like IFD-GGA. 2D hydraulic simulations can involve the solution of very large equation systems (more than 10^4 equations); in addition, each time step the solution

must be computed from the previous solution, with the risk of introducing increasing errors. Therefore the effective performance of the proposed solution schemes needs to be carefully evaluated.

In literature, the Newton-Raphson scheme is not recommended for problems with large number of variables (Kelley, 1995; Luenberger, 2003). Moreover, NR provides a non symmetric matrix, meaning that only specific algorithms can be applied to solve the resulting linear system. The LT approach leads to a symmetrical system matrix, but the accuracy required for the convergence, and the overall speed of the LT method with respect to the NR method should be verified.

More problems may arise from the use of the Jacobi scheme. In fact, when the method is applied to solve simulations over large time spans, a high precision of the solution (10^{-8} tolerance or less) is generally required, otherwise the error may grow as the simulation progresses in time and the results can diverge too much from the correct solution (Kelley, 1995; Luenberger, 2003). However, such a precision would slow the convergence rate as a large number of iteration is required. In addition, the convergence rate of the method for large equation systems needs to be verified.

In Section 4, all these possible drawbacks are analyzed and discussed in detail.

3.4 Further aspects of the proposed models

The two proposed models share a number of features that are described more in detail in this section. In addition, the section includes the explanation of some specific modeling details.

3.4.1 Discretization of head losses

The choice of the formulation for computing the friction slope J has a great impact on model performance. In order to find the best solution in terms of accuracy and stability, different formulations have been tested within the CA2D and IFD-GGA models. Table 3.1 reports a number of alternative formulations that were obtained considering a linear variation of the water depth along a generic link; Table 3.2 reports other formulations developed under the hypothesis of a logarithmic variation of water depth.

The formulations were tested in different numerical cases, some of which are reported in Chapter 4 (cases 2 and 3); these simulations included 1D and 2D flow conditions over different bed slopes. For the CA2D diffusive version, the best result in terms of correct flow propagation was obtained using the arithmetic mean h_m in Eq. (3.10), that is, considering a linear variation of the water depth along a generic link, and computing head losses in the middle section (Eq. (3.46) in Table 3.1). It is interesting to note that in the LISFLOOD-FP model, which is similar to CA2D, a different reference value for water depth is used. The reference value h_{flow} (Section 3.2.3) is defined as the difference between the highest water free surface in the two cells and the highest water elevation (Bates et al., 2010). Such formulation was chosen by the developers of the LISFLOOD-FP model because the use of h_m produced highly unstable results for all except horizontal planes, while the use of

Computation of head loss in the middle section of a generic link	$J = \frac{2^{10/3} n_{i,j}^2 \left\|Q_{i,j}\right\| Q_{i,j}}{B_{i,j}^2} \left(h_i + h_j\right)^{-10/3}$ (3.46)
Average of head loss between upstream and downstream sections	$J = \frac{n_{i,j}^2 \left\|Q_{i,j}\right\| Q_{i,j}}{2B_{i,j}^2} \left(h_i^{-10/3} + h_j^{-10/3}\right)$ (3.47)
Integral of the head loss along a generic link	$J = \frac{3}{7} \frac{n_{i,j}^2 \left\|Q_{i,j}\right\| Q_{i,j}}{B_{i,j}^2} \frac{\left(h_i^{-7/3} - h_j^{-7/3}\right)}{\left(h_j - h_i\right)}$ (3.48)

Table 3.1: List of formulations for the computation of the friction slope j tested within the CA2D model. The formulations were obtained under the hypothesis of a linear variation of water depth

Computation of head loss in the middle section of a generic link	$J = \frac{n_{i,j}^2 \left\|Q_{i,j}\right\| Q_{i,j}}{B_{i,j}^2} \frac{1}{h_i^{5/3} h_j^{5/3}}$ (3.49)
Average of head loss between upstream and downstream sections	$J = \frac{n_{i,j}^2 \left\|Q_{i,j}\right\| Q_{i,j}}{2B_{i,j}^2} \left(h_i^{-10/3} + h_j^{-10/3}\right)$ (3.50)
Integral of the head loss along a generic link	$J = \frac{3}{10} \frac{n_{i,j}^2 \left\|Q_{i,j}\right\| Q_{i,j}}{B_{i,j}^2} \frac{\left(h_i^{-10/3} - h_j^{-10/3}\right)}{\ln\left(h_j\right) - \ln\left(h_i\right)}$ (3.51)

Table 3.2: List of formulations for the computation of the friction slope j tested within the CA2D model. The formulations were obtained under the hypothesis of a logarithmic variation of water depth

h_{flow} did stabilize the model also in regions with complex topography (Fewtrell, personal communication). Considering these previous findings, both these formulations have been tested in the diffusive and inertial formulations of the CA2D model (see Chapter 4).

For the IFD-GGA model, Eqs. (3.21) have been integrated by using an integral average of head loss, considering a constant value of Q and a linear variation of h (Eq.(3.48) in Table 3.1). The other formulations reported in Tables 3.1 and 3.2 were unable to correctly simulate propagation in all the flow conditions and were therefore discarded.

3.4.2 Computation of velocity

In CA2D and IFD-GGA codes, velocity values are derived from the discharge values computed on the connections and divided by the link cross section A (the reference water depth value is discussed in Section 3.4.1). To obtain a consistent velocity field on the computation grid, velocities are then associated to each cell by means of a weighted vectorial average. For each cell i that has np connections to the adjacent cells, the average is performed separately on the x and y directions:

$$Ux_i = \frac{\sum_{j=1}^{np} (\cos(j)\, U_j)}{\sum_{j=1}^{np} \cos(j)} \tag{3.52}$$

$$Uy_i = \frac{\sum_{j=1}^{np} (\sin(j)\, U_j)}{\sum_{j=1}^{np} \sin(j)} \tag{3.53}$$

where Ux_j, Uy_j are the computed velocity components for cell i and $sin\,(j)$, $cos\,(j)$ indicate the direction of the connection j (x and y components are assumed to be positive in eastward and northward direction respectively). Eqs. (3.52) and (3.53) allow to easily compute the velocity field either for regular or irregular grids.

3.4.3 Simulation of wetting and drying processes

One of the most complex issues related to flood inundation modelling is the correct treatment of wetting and dying processes. Standard numerical procedure for solving SW equations may produce unphysical oscillations and negative water depths near a dry/wet front (Aricó et al., 2011). Consequently, hydrodynamic models are generally equipped with specific wetting–drying (WD) algorithms. It is important to note that hydraulic models based on implicit time marching schemes generally require more complex WD algorithms, since large equation systems have to be solved each time step; WD treatment is instead simplified in explicit models. Although some methods track the WD interfaces in time, moving the boundary nodes and deforming accordingly the computational mesh, most of the available WD methods adopt a fixed mesh (Aricó et al., 2011). In some of these methods, mesh elements (nodes or cells) are activated or deactivated according to their wet-dry condition, while other methods introduce transition elements (partially wet) to describe WD interface.

However, the application of complex algorithms for WD treatment can be not convenient, especially for reduced complexity models. Apart from fast propagating wetting fronts, like those produced by a dam break or in the proximity of a levee breach, during an inundation event wetting fronts are usually slow, wide extended and with reduced water depths, and are therefore similar to a rainfall induced overland flow. According to different authors (Horton , 1945; Guy et al., 1992; Bagarello and Ferro, 2006), such a condition is characterized by a mixture of laminar and turbolent flow in which infiltration, surface roughness and rainfall intensity play a major role (Bateman et al., 2010). Also, the gradually varied flow assumption can be not satisfied because of perturbation produced by microtopography, and the shallow water equations can lose validity (Tayfur et al., 1993). Drying processes are also strongly influenced by these factors, and their treatment is in some ways more problematic than of

the wetting front (Horritt, 2002).

Therefore, the use of simplified relationships to handle WD effects can be a reasonable alternative. In fact, it should be considered that in actual flood events the quality of experimental data is rarely sufficient to assess model results, therefore a detailed reproduction of all the mentioned processes would be scarcely useful (Horritt, 2002; Hunter et al., 2007; Neal et al., 2009a).

A current solution, adopted both by reduced complexity models and more complex models, is the use of a threshold value on water depth to distinguish dry and wet cells (e.g. the CCHE2D model, Jia and Wang (2001)). This simulates the surface storage effect due to terrain roughness. In addition, in presence of reduced water depth the ordinary flow equations can be linearized or substituted with an empiric relationship (e.g. the LISFLOOD-FP model, Hunter et al. (2005b)).

Given all these considerations, the treatment of WD processes has been undertaken with different methods in the two developed models.

WD treatment in CA2D. In the CA2D model, wetting fronts can be directly reproduced by the ordinary flow equations, thanks to the explicit solution scheme. Drying effects are handled by including a control on volumes at each discharge calculation step, to ensure mass conservation and prevent negative values of water depth. When a negative depth is detected in a cell, the outgoing discharges are reduced so that total outgoing discharge equals the available water volume. Incoming discharges are not modified, and the ratio between outgoing discharges is mantained after reduction. In addition, a surface storage value may also be used to distinguish between dry and wet cells. Each time step the control of volumes is performed iteratively until negative depths either disappear or are kept below a tolerance threshold (usually 10^{-12}). The fast convergence of this method has been extensively tested in cases with both regular and complex topography (see Chapters 4 and 5).

It must be noted that the volume control adopted within the CA2D model differs from ordinary flow limiting techniques. Generally, flow limiters are used to prevent oscillations of discharge values in deep water areas, and it was observed that such technique influences model results, that become highly sensitive to grid cell size and insensitive to surface roughness Hunter et al. (2005b). On the contrary, the volume control is applied in the model only in drying conditions, that is, where water depths are very reduced. Several tests on different flood scenarios have been performed and no significant instabilities were observed.

Thanks to the explicit solution scheme and the described drying algorithm, the CA2D model structure can deal with large variations of flow domain without stability problems. This is particularly useful when simulating rainfall-runoff process and infiltration (see Chapter 6).

WD treatment in IFD-GGA. In the IFD-GGA model, the treatment of WD processes is more complicated, since the governing equations (3.21) are defined only for positive (non-zero) water depths. This means that a minimum threshold for water depth must be established, and consequently the equation system must include all the grid cells at each time

step. In order to minimize the additional computational burden derived from large dry areas within the computation grid, a control on fluxes has been inserted, so that no flux interchange is produced between cells with a water depth equal to the threshold value. A second important problem is the threshold value can significantly influence propagation of wetting and drying front. Although a very low value can be set (e.g. 10^{-6}), the effect on flow propagation and on convergence speed of the code need to be carefully evaluated. This issue will be discussed in Chapter 4.

3.4.4 Simulation of infiltration

During lowland flood events infiltration is generally neglected. In fact, in such events infiltration is much slower than surface flow processes, and soils are usually saturated with water, resulting in very small infiltration rates. Therefore this process is currently implemented in the two proposed models using a rather simplified approach. When soil infiltration is activated in the model code, a special connection is added to each cell to represent the flow of water into the soil. Every time step, infiltration rate is equal to the hydraulic conductivity specified for each cell, until a threshold value that represents soils saturation is reached and infiltration stops.

3.4.5 Boundary and internal conditions

In the CA2D model, the ordinary flow condition of free surface 2D flow is represented by Eqs. (3.10) or (3.16) depending on model version, while for IFD-GGA the same flow condition is given by Eqs (3.21). As it is immediate to see, these equations describe the free surface 1D flow over a wide rectangular cross section with negligible lateral friction. This approximation is usually adopted by flood inundation models, and can be considered reasonable if no significant terrain slopes or no relevant vertical obstacles are present in the computation domain (however, Section 5.4 presents a case study where these conditions do not hold).

Wherever necessary, uniform or weir flow may also be imposed on specific connections. In CA2D, the uniform flow condition for a connection k which conveys flow out of the domain from cell i is written as:

$$Q_{0i} = \frac{b h_i^{5/3}}{n} \sqrt{\frac{\Delta Z}{\Delta x}} \tag{3.54}$$

For the IFD-GGA model, this flow condition is inserted in matrix A_{11} as:

$$A_{11}(k) = \frac{|Q_k| \, n_k^2}{S_0 B_k^2 (H_i - Z_i)^{7/3} \left(1 - \frac{Z_i}{H_i}\right)} \tag{3.55}$$

while the corresponding elements of matrix A_{12} are written as $A_{12}(k,i) = -1$ and $A_{12}(k,j) = 0$. The weir equation for an outgoing connection is written for the CA2D model as:

$$Q_{0i} = \alpha b \sqrt{2gh_i} \tag{3.56}$$

where α is the weir coefficient. For IFD-GGA the weir equation is written in matrix A_{11} as:

$$A_{11}(k) = \frac{|Q_k|}{2\mu_k^2 g B_k^2 (H_i - Z_i)^2 \left(1 - \frac{Z_i}{H_i}\right)} \tag{3.57}$$

In addition, in the CA2D model a simplified mixed weir-pressure flow condition can be used for outlet links. Flow is computed with Eq. (3.56) up to a threshold value of water depth, and when threshold is exceeded the following formulation is used to compute discharge (pressurized flow out of a conduct):

$$Q_{0i} = 0.99 \alpha b h_i \sqrt{h_i} \tag{3.58}$$

where α is the reduction coefficient. The treatment of incoming flow boundary conditions in the CA2D model code needs a specific description. Each time step, the inflows entering the domain are immediately converted into water level by updating water level in boundary cells, before computing flow exchanges within the computation grid. On the contrary, in the IFD-GGA model inflow boundary conditions are directly included in the overall equation system an used to iteratively compute the solution (for instance, incoming discharges are put in the continuity equation (3.21)).

In both the models, boundary or internal conditions may be assigned to cells by imposing specific water level or discharge hydrographs, as well as rainfall hyetographs.

3.4.6 Advantages of proposed modeling approaches

As already pointed out in Section 3.1, the two proposed are based on a model structure that resembles a simplified finite volumes method. At the same time, this model scheme is also assimilable to the conceptual modelling technique known as storage cell approach, that constitutes the basis of different hydraulic models (Prestininzi, 2008).

Given this framework, the proposed models combine different modelling solutions taken from other simple hydraulic models like LISFLOOD-FP (Hunter et al., 2005b; Bates et al., 2010), JFLOW (Bradbrook et al., 2004) and FLO2D (FLO-2D Software Inc., 2007). It should be noted that so far many of these modelling solutions were not available together in a single model. In addition, the models present some original solutions for specific modeling issues, in order to improve model parsimony and reproduction of flow dynamics.

- **Computation grid:** the design of the code structure takes advantage of the analogy with a pipe network: all the information and the computation cycles are partitioned between node elements and link elements, in order to optimize the code efficiency. In Chapter 4, the effectiveness of such approach to speed up the models is investigated in detail. In addition, both the two models can handle both regular and irregular meshes.

By using specific pre-processors for input data preparation (as reported in Appendix B), the two models can directly use regular grids derived from digital elevation models (DEM), as well as polygonal grids from TIN files. In this way, the two models combine the advantages of raster based models like LISFLOOD-FP FLOW and FLO2D, and those of research models based on more rigorous finite volume schemes (Prestininzi, 2008).

- **Link network:** usually, hydraulic models based on finite differences schemes, or finite volume schemes on regular grids, adopt a standard 4 direction link network (see Figure 3.1). That is, each square cell is connected with the adjacent cells along the contact faces. The same solution is adopted by different reduced complexity models like LISFLOOD-FP and JFLOW. However an alternative scheme can be obtained using a 8-direction link network, in which each cell is connected with the adjacent cells also in the diagonal directions. Such method is called Moore neighbourhood (Parsons and Fonstand, 2007) and is usually applied in CA models and GIS environments to identify flow direction over a DTM , but is less common in hydraulic modeling. The FLO2D model is one of the few models adopting an 8-direction grid (FLO-2D Software Inc., 2007). So far, no specific investigation has been undertaken to compare the two mentioned link networks, given that none of the cited models allows to select between them. However the design of the CA2D and IFD-GGA models allow to use indifferently a 4- or 8-direction link networks, when a regular square mesh is used. Therefore in Chapters 4 and 5 the two different grid configurations are compared, in order to establish advantages and drawbacks of each one. It is worth noting that the use of a 8-direction grid implies some modifications with respect to the standard 4 direction grid. While the continuity equation is not modified, the integration of momentum equation is performed by considering each cell as a regular octagon (Figure 3.2). Therefore, the effective width of each connection is given by the octagon faces, which are all equal; the lenght for diagonal links is increased with respect to horizontal and vertical links by a $\sqrt{2}$ factor. As a final remark, it should be noted that the use of a 8 direction grid almost doubles CA2D run times, since the number of connections is almost doubled in respect to 4-dir grid.

- **2D flow scheme:** the two models adopt a general 2D flow scheme instead of an integrated 1D-2D approach (Section 2.6). Although the 1D-2D approch can provide accurate results (Villanueva and Wright, 2006; Neelz and Pender, 2010) and allows for significant reduction of computation effort when 1D flow is dominant, different reasons were found to prefer a general 2D approach. First, the flexibility of computation grid costruction within the models may be used to "force" 1D flow conditions when required; for example the mesh can be adapted to the existing channel network. Besides, it must be noted that this solution avoids the problem of linking 1D and 2D grids, which is a source of additional uncertainty (Neelz and Pender, 2010). In Chapters 4 and 5, it will be shown how the general 2D approach does not produce a loss of detail even in clear 1D flow situations. Finally, the structure of the two models allows to insert

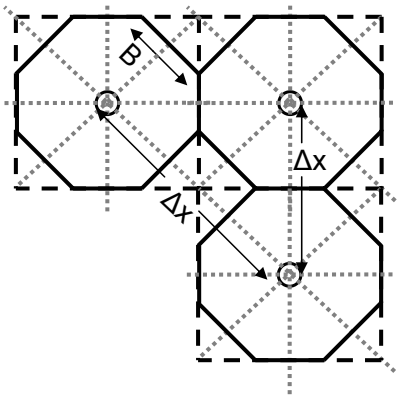

Figure 3.2: example of computation grid with 8 direction link network; links are indicated as grey lines.

specific geometry to reproduce canalized flow in more detail; for instance, a subgrid parameterization could be used to reproduce compound cross sections (Yu and Lane, 2011), although such possibility is still being implemented in model codes (see Chapter 6).

3.5 Parallelisation of hydraulic model codes

Parallelisation of computer codes is one of the recent lines of research to improve performances of 2D flood models (Neal et al., 2010). In a parallelised code, the computational burden is subdivided on different processing cores that run computations in parallel, exchanging informations according to the parallelization method in use. Different strategies can be applied to achieve this result.

Multiprocessor parallelisation methods use multiple general purpose CPU cores or clusters to solve equations concurrently and thus reduce computation time. These methods are based on message passing interface (MPI) and domain decomposition, and have been applied to different hydraulic models, including TELEMAC-2D (Hervouet, 2000),RMA (Rao, 2005), TRENT (Villanueva and Wright, 2006), LISFLOOD-FP (Neal et al., 2009b, 2010) and FloodMap-Parallel (Yu, 2010). Basically, the domain decomposition approach breaks the model domain into a number of contiguous sub-domains, with each sub-domain running on a different processing core. The speedup obtained with respect to serial model versions varied from 3.8x (Rao, 2005) to 6.2x (Hervouet, 2000) to 15x (Yu, 2010) according to the case study, the model code and the machines used for parallelisation.

An alternative method is to couple a programmable coprocessor with a general purpose CPU to handle computationally intensive tasks. The most common coprocessors are graphics processing units (GPUs), which are dedicated to performing the computation associated with graphics processing. GPUs architecture offers extensive computational capabilities when compared to conventional CPU, including massive parallelism, high memory/data

transfer between the motherboard and the GPU, and high peak single precision floating point performance (Neal et al., 2010; Kalyanapu et al., 2011). Therefore in recent years GPUs have been used in a wide range of scientific computing applications (General Purpose GPU), including flood modelling. For instance, the JFLOW model (Bradbrook et al., 2004) has recently been rewritten for GPGPUs obtaining a speedup of 112 x over the serial JFLOW code for a test case in Glasgow, UK (Lamb et al., 2009). Neal et al. (2010) implemented a simplified version of the LISFLOOD-FP model on ClearSpeed accelerator cards, that are specifically designed for computationally intensive science and engineering applications. The parallelisation method in both GPGPUs and ClearSpeed cards is based the single instruction multiple data (SIMD), where many processing elements (PEs) perform the same task on different data (Neal et al., 2010).

Neal et al. (2010) applied and compared some of the described parallelization techniques using a simplified version of the LISFLOOD-FP model. The methods included programming of multicore processors with Open-MP language and message passing interface (MPI), and use of ClearSpeed accelerator cards. The authors observed that parallelisation on multicore processors can be undertaken using dedicated programming language such as OpenMP Neal et al. (2009b), allowing a relativetly straightforward code rewriting. On the contrary, applications on GPUs require specialized hardware or dedicated complex programming languages, thus, conversion from standard CPU codes is more difficult and time consuming. However, more recent developments such as Compute Unified Data Architecture (CUDA) by the NVIDIA Corporation are likely to reduce the effort required in programming GPUs for scientific applications (Kalyanapu et al., 2011). CUDA is a software environment designed to develop parallel computations, allowing straightforward data exchange between CPU and GPU and optimizing the number of processor cores.

On the other hand, parallelisation on dedicated coprocessors allows for greater speedup of model with respect to standard multicore processors, due to the larger number of cores (usual GPU cards contain around 200 cores while nowadays a standard multicore computer has 4 or 8 cores). For instance, Kalyanapu et al. (2011) obtained a speedup of 88x and 3.5x by implementing the fully dynamic model Flood2D respectively on a 240 cores and 16 cores NVIDIA GPU. Computation times become comparable when clusters with several multicore processors are used (Neal et al., 2010), but such computational structures are rarely available with respect to standard GPUs.

Neal et al. (2010) noted that the efficiency of parallelization techniques may vary according to specific test case; for instance, models parallelised on GPUs were less efficient on partially wet domains, due to the more difficult subdivision of the effective computational burden.

3.5.1 Application to the proposed models

In order to perform parallelisation of a hydraulic model code, the code structure and must be analyzed to identify which parts can be proficiently parallelised. Generally speaking, parallelisation is effective when applied to iterations regarding the computation spatial do-

main; therefore a common practice is to decompose the study area, so that computations on each sub-domain are performed in parallel by different processors. However, care must be taken in defining how informations can be passed between parallel computation threads, for instance on boundaries between sub-domains. Moreover, some information must be shared in all the domain, therefore parts of the model code cannot be parallelised (i.e. updating of variables at each time step) (Neal et al., 2010).

According to previous research works about this topic, models based on explicit time marching schemes like CA2D are suited to be massively parallelised (Yu, 2010; Kalyanapu et al., 2011). In particular, parallelisation of diffusive models is relatively straightforward as demonstrated by the applications to LISFLOOD-FP code (Neal et al., 2009b, 2010). On the other hand, implicit schemes can only be partly parallelised, unless particular solution schemes are adopted. As described in Section 3.3, the implementation of the Jacobi scheme within the IFD-GGA model has been performed exactly for this reason.

Therefore, given the requirements from the Civil Protection, it was decided to convert the model codes from Fortran to Java language. Although Java is not a scientific language and is therefore less efficient (the model codes are written in Fortran), the advantages in terms of model performance would be consistent. First, the conversion of the codes facilitates the integration into the Civil Protection information system: this will allow to run simultaneous multiple simulations on different machines, exploiting the existing network and optimizing the availability of idle processors. Second, the Java model code could be easily adapted to run in parallel on distributed multiprocessor machines, using the domain decomposition technique (Yu, 2010; Neal et al., 2010).

As mentioned in Section 3.5 the implementation of model codes on GPU cards would be more efficient, with an expected speedup of one magnitude order with respect to multiprocessors code (Lamb et al., 2009; Neal et al., 2010; Kalyanapu et al., 2011). However, this application has not been undertaken for a number of practical reasons. The main motivation was the absence of specific requirements from the Civil Protection during the research period. It was felt not convenient to start a time consuming and costly work on the parallelization of the codes without immediate requirements. Moreover, dedicated hardware for parallel programming is rapidly evolving, as well as related programming languages (see Section 3.5); therefore some of the currently used techniques could become rapidily obsolete, and problems of compatibility could arise in the future. From this point of view, the current implementation in the information system of the Civil Protection should facilitate the updating and compatibility of the model codes (see Chapter 6).

Chapter 4

APPLICATIONS: NUMERICAL CASES

Every hydraulic model needs to undergo a detailed evaluation process in order to define its range of application,advantages and drawbacks. In the scientific community there is still no wide consensus about reliability and accuracy criteria for hydraulic models (Hunter et al., 2007), although some institutions and national agencies developed specific requirements. For instance, the U.S. Federal Emergency Management Agency (FEMA) published a list of numerical models meeting the requirements of the National Flood Insurance Program for flood hazard mapping (FEMA, 2012). On the other hand, the UK Environmental Agency (EA) developed a list of test cases to evaluate hydraulic flood models (Neelz and Pender, 2010). This latter approach has been followed to evaluate the CA2D and IFD-GGA models.

As such, in the present chapter the models are tested in several numerical cases, reproducing a wide range of flow conditions. Numerical cases allow to isolate specific flow processes, and to assess the computation scheme under simplified and well controlled conditions, reducing the number of variables to be considered and the uncertainty concerning their influence on model performance (Hunter et al., 2005b). The results are compared with analytical or semi-analytical solutions whenever possible, or alternatively with hydraulic models based on the full shallow water equations.

The majority of numerical cases presented in this sections were proposed in Dottori and Todini (2010a,b, 2011), however in the present work more information and further analyses are provided. It is important to note that, for each case, only some the possible model configurations presented in Sections 3.2 and 3.3 are tested. The main reason is that the described model versions, as well as the numerical cases, were designed and developed in different times along the research period presented in this thesis. Therefore, some of the early model versions were tested in first developed numerical cases, but were not applied to more recent cases because the observed limitations suggested to stop further applications; for the same reason the latest developments (e.g. the inertial version of the CA2D model) were tested only on more recent cases, which were more significant as benckmark tests. Nevertheless, the overall presentation and discussion of this section should provide a comprehensive overview of advantages and drawbacks of the models, including all the possible configurations.

4.1 Case 1: mild slope channel

This numerical case simulates the one-dimensional wave propagation over a regular channel with a mild bed slope; the geometry is summarized in Table 4.1. The inflow is given by the following upstream hydrogram: the simulation starts from an initial condition of uniform flow along all the channel, with a constant discharge of 10 m^3s^{-1}; at $t = 0$, the inflow discharge from upstream is linearly increased from 10 to 100 m^3s^{-1} in 5 hours; the discharge remains constant for the next 30 hours and then decrease linearly in 5 hours from 100 to 10 m^3s^{-1}. The downstream boundary condition is the uniform flow. The chosen cross section can be considered wide rectangular with respect to flow condition, thus, the standard momentum equation used in the models (Eq. (3.7)) is a good approximation.

bed slope	10^{-4}
section shape	rectangular
channel width	250 m
channel length	50 km
Manning roughness	0.05 $m^{1/3}s$
simulation time	144 hours

Table 4.1: geometry of case 1.

Given the simple geometry and relatively low energy flow condition, Case 1 is expected to be easily reproduced by the models. In order to provide a more rigorous test, simulations with the models were performed using different grid resolutions, including variable resolution grids. The results produced were compared with the well known model HEC-RAS (HEC, 2001). Besides the assessment of model accuracy, a further objective is to test the reliability of diffusive stability condition.

4.1.1 Results on regular grids

Three regular grids have been considered for the simulations: one with 400x1 cells of 125x250m size, a second with 200x1 cells of 250x250m and another with 100x1 cells of 500x250m. The three configurations are named 1a, 1b, 1c respectively. As can be seen, each grid maintains a channel width of 250m, while the longitudinal grid resolution varies. Since the channel width is only one cell, flow condition is strictly 1D. For each grid, simulations with different time steps have been performed for both the models, in order to investigate the stability of the solution (Tables 4.2 and 4.3). CA2D simulations were performed using the diffusive version and a constant time step, in order to compare simulation times with the IFD-GGA model. For IFD-GGA simulations, the two alternative versions based on the Newton-Raphson scheme (NR) and the Linear Theory approach (LT) were considered.

The first relevant observed result is that the accuracy of the models is substantially constant and is not affected by spatial and time discretization, until the solution is free of instability; instead, when the stability limits indicated in Tables 4.2 and 4.3 are exceeded, the model solutions show oscillations and are no longer comparable with the reference HEC-

Δx	1s	2s	5s	10s	15s	30s	60s	Δt_{max}
125m	Y	Y	N					1.2s
250m	Y	Y	Y	N				5s
500m	Y	Y	Y	Y	Y	Y	N	22s

Table 4.2: results of the stability analysis in cases 1a, 1b, 1c for the diffusive CA2D model; "N" indicates unstable solution,"Y" a stable solution; "Δt_{max}" indicates the maximum time step computed by the diffusive stability condition (Eq. (3.12)).

Δx	1s	2s	5s	10s	15s	30s	60s
125m	Y	Y	N				
250m	Y	Y	Y	Y	Y	N	
500m	Y	Y	Y	Y	Y	Y	Y

Table 4.3: results of the stability analysis in cases 1a, 1b, 1c for the IFD-GGA model; "N" indicates that the convergence of solution scheme was not achieved, while "Y" indicates that the simulation was successfully completed; the two versions (LT and NR) of the model provided the same convergence results.

RAS solution. In particular, Table 4.2 shows that the maximum time step computed by the diffusive stability condition (3.12) is in good agreement with the experimental maximum time step. Figure 4.1 shows the results in terms of flow profile for the 250x250m grid (case 1b) and a time step of 5s, compared with HEC-RAS results. In the figure, the profiles computed by CA2D and IFD-GGA are almost coincident and can not be distinguished. Most important, the resulting profile is also practically coincident with the HEC-RAS profile, both in general shape and position of wave front at the different time intervals. The maximum difference from the profiles given by the HEC-RAS model is below 0.5 cm., and the downstream discharges are also very similar. In conclusion, the two models accurately reproduced the wave attenuation, even if the computation scheme is not based on the fully dynamic SWE like HEC-RAS.

Table 4.4 reports some simulation times for case 1b. All the simulations were performend on a 1.86 Ghz processor and 2Gb RAM computer.

model version	time step	simulation time
CA diffusive	5 s	8 s
IFD-LT	5 s	60 s
IFD-LT	15 s	22 s
IFD-NR	5 s	36 s
IFD-NR	15 s	14 s

Table 4.4: elapsed simulation times for the model versions in case 1b, depending on time step.

As expected, CA2D is considerably much faster, given the same simulation settings ,than the IFD-GGA versions. However, the greater stability of the IFD-GGA model compensates for this drawback allowing to use large time steps, and this is true in particular for the

Newton-Raphson version. It is interesting to note that the maximum allowable time step for the two IFD-GGA versions is quite reduced, despite the implicit scheme implemented. This is necessary to achieve the convergence of the Jacobi solution method, but this is compensated by the considerable speed of the resulting solution algorithm.

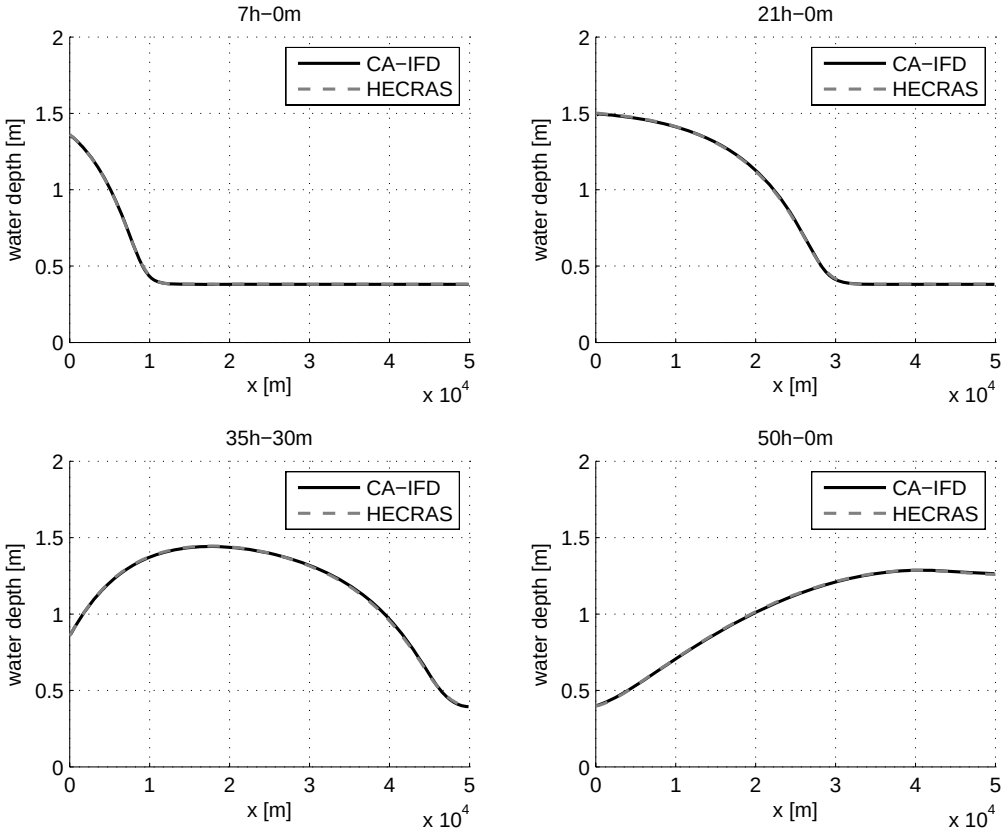

Figure 4.1: case 1b: comparison between flow profiles computed by the IFD-GGA, CA2D and HEC-RAS models.

4.1.2 Results on variable resolution grid

In addition to regular meshes, a grid with a variable longitudinal resolution was also used to test the models (case 1d). This mesh is again composed by a single row of cells of variable size: starting from upstream, there are 50 cells of 250x250m size, then 50 cells of 500x250m and 50 cells of 250x250m size. The CA2D model was tested in all its possible configurations, that is, combinining the diffusive and inertial versions with the global time step (GTS) and local time step (LTS) algorithms. The stability criteria given by Eqs. (3.12) and (3.17) were used according to the model version. For the IFD-GGA model the two alternative versions based on the Newton-Raphson scheme (NR) and Linear Theory approach (LT) were considered, based on a fixed time step.

As for the simulations with regular mesh, the profiles computed by all the different versions of the models were practically coincident (as in Figure 4.1); again, the results were also coincident with those of the the HEC-RAS model, with a maximum difference below 0.5 cm.

In Table 4.4 a comparison of overall simulation times is presented for case 1d. The simulations were performed on a 1.86 Ghz Intel Core2 processor with 0.98Gb of RAM. For the CA2D model, time steps provided by the stability conditions were found to correspond to the experimental maximum values. For the CA2D inertial version, the CFL condition with a 0.6 correction coefficient could be used. For the IFD-GGA versions, simulation times with the maximum allowable time step are reported.

CA-GTS diffusive	CA- LTS diffusive	CA-GTS inertial	CA-LTS inertial	IFD-NR (Δt 15s)	IFD-LT (Δt 15s)
14 s	9 s	3 s	1 s	24s	41s

Table 4.5: case 1d: elapsed simulation times for the different model versions.

Focusing on Table 4.5, it can be seen how the inertial formulation produces considerable improvement of CA2D model performance, in terms of reduction of computation times. The advantage given by the LTS algorithm is significant but not as important. On the contrary, computation times of the IFD-GGA versions are much larger.

4.2 Case 2: hillslope

This numerical case schematizes the overland flow produced by a rainfall over a hillslope, and it has been presented by Di Giammarco et al. (1996). The hillslope is represented by an inclined plane, which geometry is shown in Figure 4.2 and resumed in Table 4.6. The plane has a 5% slope in the x direction and null slope in the y direction; this means that the plane is equivalent to a series of one-dimensional parallel channels heading in the slope direction.

plane width	800 m
plane length	1000 m
Manning roughness	0.015 $m^{1/3}s$
slope	0.05

Table 4.6: geometry and simulation settings of case 2.

The plane is initially dry; when the simulation begins, a rainfall with a constant intensity in time and space of 10,8 mm/h is applied over all the plane; the rainfall has a 90min duration and the simulation is run for a total time of 3h, to reproduce the draining of the simulation area. A critical flow condition is imposed at the downstream boundary of the grid.

Although case 2 is in practice one-dimensional, it offers a good benchmark for a 2D model for different reasons: first of all, an analytical solution for the outflow can be derived from the kinematic wave equation, under the condition of semi-infinite plane. Secondly, the

reproduction of wetting and drying effects within the models may be tested, as well as the ability of reproducing a typical overland flow condition, with very reduced water depths and steep slopes. According to Ferro (2006), the shallow water equations are valid for terrain slopes up to 25%, so the ordinary governing equations can still be used. The simulations were performed using three computation grids with different resolutions (10x10m, 20x20m and 50x50m cell size), which have been identified as 2a, 2b, 2c.

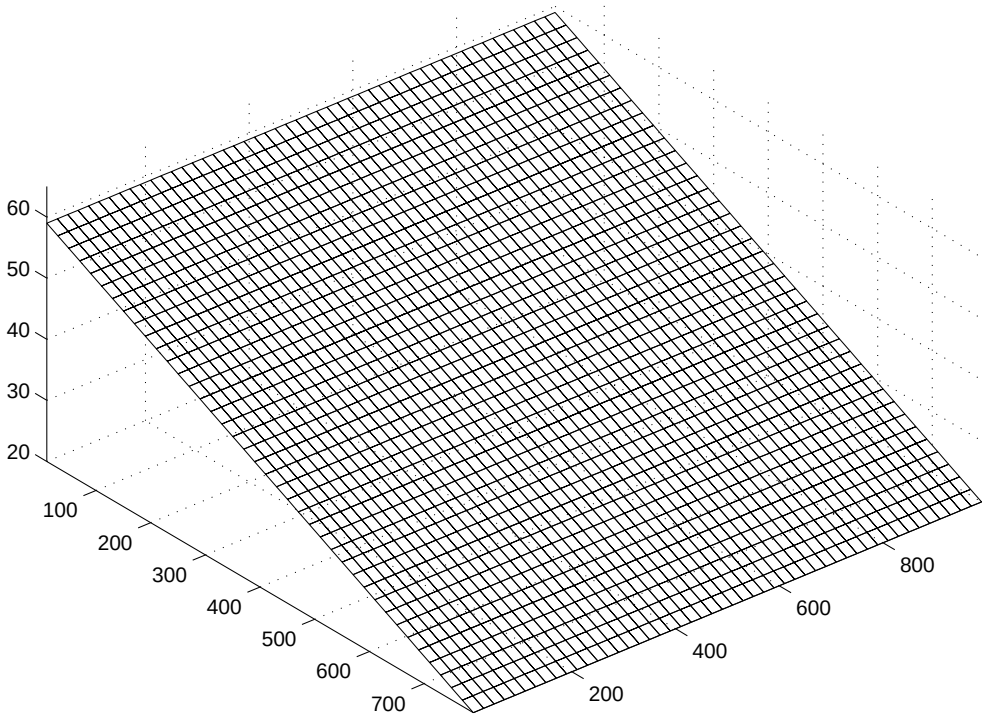

Figure 4.2: geometry of case 2a; distances are in meters.

4.2.1 Results: outflow

The results provided by the models were analysed both in terms of discharge outflow from the downstream boundary and water surface on the hillslope.

The outflow discharge hydrographs are shown in Figures 4.3, 4.4, 4.5. Figure 4.3 includes the results of the CA2D diffusive version for different grid resolutions; the graph in Figure 4.4 compares the discharges computed by the IFD-GGA and CA2D diffusive version at different grid resolutions; finally, in Figure 4.5 the hydrographs of the inertial and diffusive CA2D versions are compared. In all the graphs the discharge computed from the analytical solution is also reported.

As can be seen in Figure 4.3, after an initial transient period the outflow equals the rainfall and a steady state condition is attained; when the rainfall stops, the plane rapidly dries up. As expected, the accuracy of results improves using the 10m resolution grid (configuration

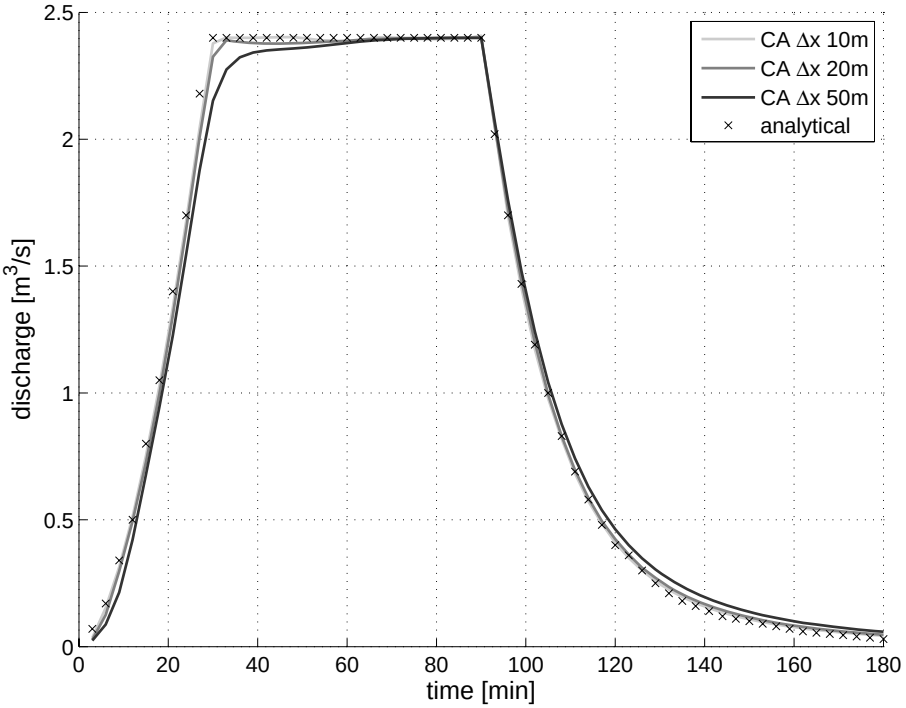

Figure 4.3: outflow computed by the analytical solution and the CA2D diffusive version at different grid resolutions

2a). Good results are obtained also with the 20m grid, while with the 50m grid a delay in the hydrograph is observed, although the differences with the analytical solution are reduced. It is worth noting that the drying phase is always well reproduced and does not instabilize the model.

Similar comments can be made also for the results of the IFD-GGA versions, although with sligth diferences with respect to CA2D diffusive model. As can be seen in Figure 4.4, the outflow computed by the two models matches well the analytic solution when the 10m and 20m grids are used (although only the IFD-LT version could finish the simulation with the 10m resolution, as reported in Table 4.8). The performance of the IFD-GGA model is better on the 50m grid. For the 20m and 50m resolution, the IFD-LT and IFD-NR configurations provided almost the same results. Finally, the inertial CA2D version produces a slight decrease in model accuracy (Figure 4.5).

4.2.2 Results: water surface profile

The analysis of water surface profiles gives provides interesting discussion points, as can be seen in Figure 4.6. Despite the good reproduction of the total discharge, the CA2D diffusive version has problems in reproducing the water surface, as along the flow direction small oscillations appear, with alternate rows of “full” and “empty” cells where the actual water depth is very low (below 0.1mm). It must be noted that such oscillations are not a

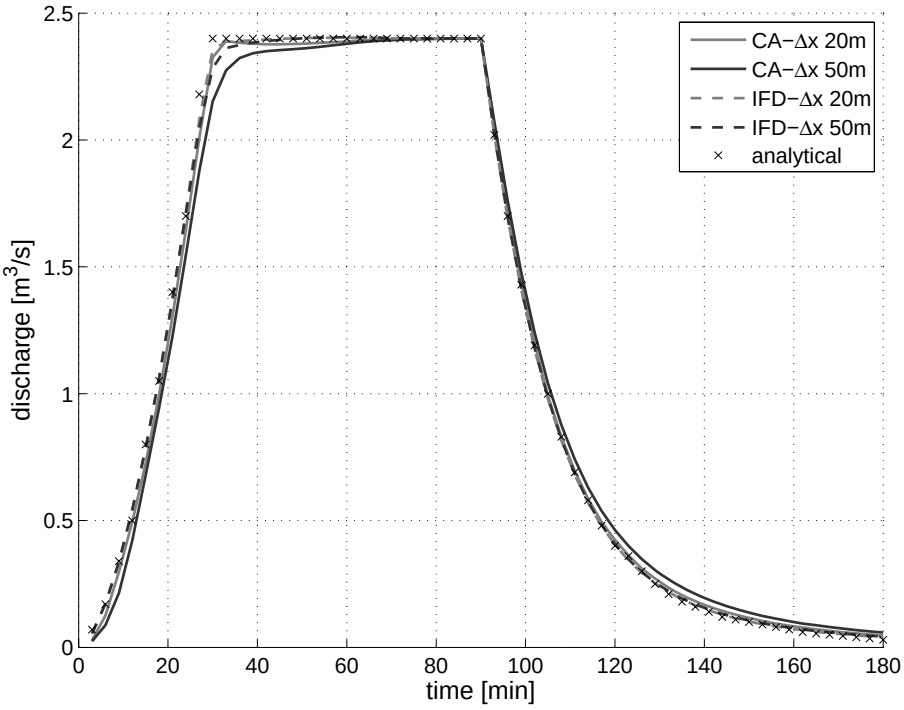

Figure 4.4: outflow computed by the analytical solution, IFD-GGA and CA2D diffusive versions at different grid resolutions.

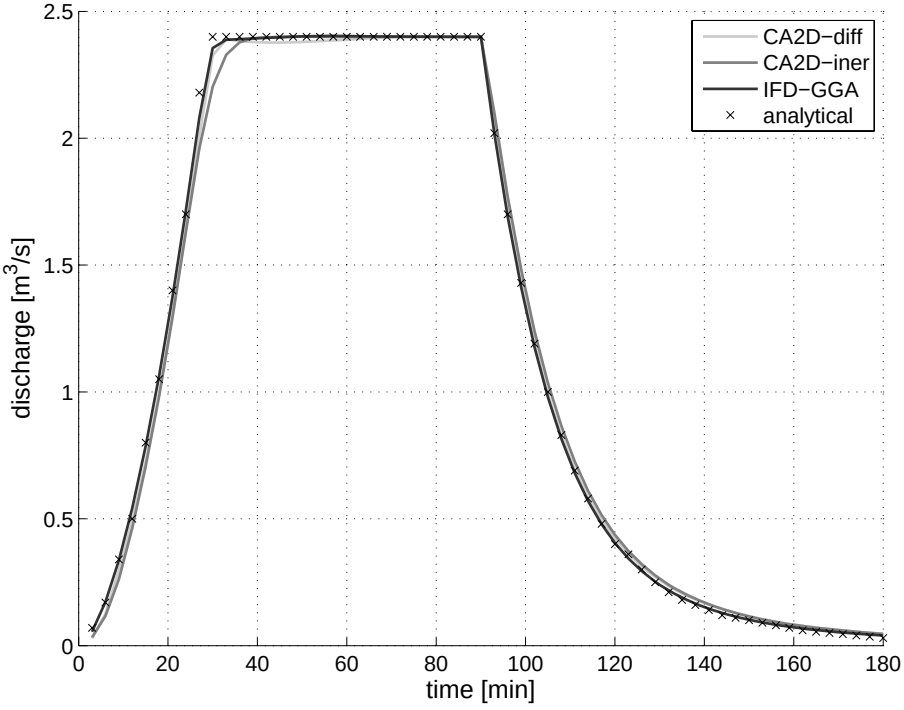

Figure 4.5: outflow computed in case 2b by the analytical solution and the CA2D diffusive and inertial versions.

consequence of too large time steps values, since they originate also for values well below those indicated by the diffusive stability condition. The amplitude of the oscillations seems to be correlated with the terrain slope rather than the water depth. It has been observed that if the rainfall intensity is increased, the amplitude also increases since there are rows which remains almost "empty" (in case of a 80mm/h intensity rainfall water depths are around 4.5 cm). However, such oscillations don't influence the downstream propagation since the discharge hydrograph still reproduces well the analytical solution. On the contrary, the problem of oscillations does not affect the CA2D inertial version: the water surface gradually increases its depth in the downstream direction until a limit value that depends on the rainfall intensity. Finally, the profile computed by the IFD-GGA model shows oscillations, although less significant than the CA2D diffusive version.

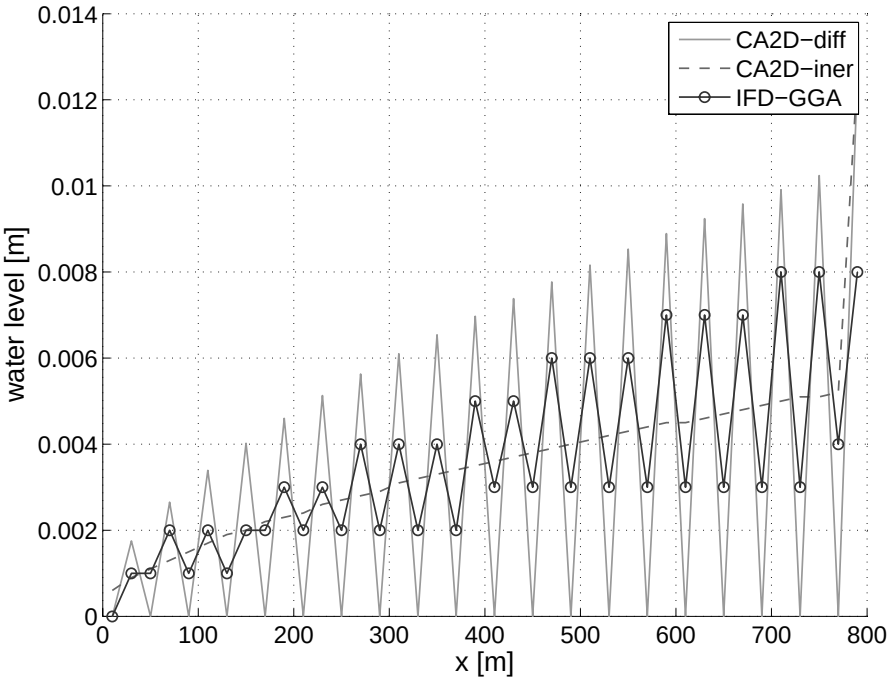

Figure 4.6: steady state water profiles along slope direction computed in case 2b.

The different performance of the CA2D versions is related with the different discretization of head losses; that is, the use of h_m produces the water surface oscillations, which are avoided by using h_{flow}. Such a difference is not readily explainable, although it has been reported also by the developers of the LISFLOOD-FP model (T. Fewtrell, personal communication). Further discussions on this topic are provided in cases 6 and 7 (Sections 4.4 and 4.5).

4.2.3 Results: stability analysis

A stability analysis for the CA2D and IFD-GGA versions was performed, in order to investigate the influence of time discretization on the accuracy of results, and to assess the

reliability of CA2D stability conditions. Results are resumed in Tables 4.7 and 4.8.

	Δx	0.2s	0.2s	0.5s	1s	2s	5s
IFD-NR	10m	N	N				
IFD-NR	20m	Y	Y	N			
IFD-NR	50m	Y	Y	Y	Y	Y	N
IFD-LT	10m	Y	Y	N			
IFD-LT	20m	Y	Y	Y	N		
IFD-LT	50m	Y	Y	Y	Y	Y	N

Table 4.7: case 2: results of the stability analysis for the IFD-GGA model versions; N indicates that the convergence of solution was not achieved, while Y indicates that the simulation was successfully completed.

	Δx	0.2s	0.5s	1s	2s	5s	Δt_{max}
CA-diff	10m	Y	Y	Y	N		2.1s
CA-diff	20m	Y	Y	Y	Y	N	4.3s
CA-diff	50m	Y	Y	Y	Y	N	12.0s
CA-iner	10m	Y	Y	Y	N		5.3s
CA-iner	20m	Y	Y	Y	Y	N	10.7s
CA-iner	50m	Y	Y	Y	Y	N	24.0s

Table 4.8: case 2: results of the stability analysis for the CA2D model versions; N indicates an unstable solution, Y indicates a stable solution; Δt_{max} indicates the maximum time step computed by the diffusive stability condition (Eq. (3.12)).

As for case 1, the accuracy of the solutions provided by the models is not dependent on time step, provided that the solution is obscillation-free. However, the stability analysis provides some unexpected indications with respect to case 1.

First of all, the IFD-GGA model shows significant convergence problems when applied to 10m and 20m resolution grids, especially the version implementing the Newton-Raphson algorithm. Surprisingly, when applied to the same grids, the CA2D was found to be more stable. Given these problems, a specific analysis was performed on the IFD-GGA code algorithm. The Jacobi iterative scheme was identified as the source of the convergence problem, due to its marked sensitivity to grid cell size.

Focusing on the CA2D model, both the diffusive and inertial stability criteria (Eqs. (3.12) and(3.17)) do not provide reliable time step values for the simulations. As shown in Table 4.8, the maximum time steps computed by both the diffusive and inertial stability criteria are well above the experimental threshold value for each grid resolution. Such difference increases with grid coarsening. It was therefore necessary to introduce a upper threshold on the time step, to avoid numerical errors and instability problems.

Possible reasons for this behavior could be the very low water depth values (lower than 1cm), and the supercritical flow condition in the lower part of the grid (see Figure 4.7). In conclusion, it seems that both the stability criteria are not adequate for overland flow con-

ditions, therefore additional empiric criteria (e.g. an upper threshold) should be considered to deal with such conditions.

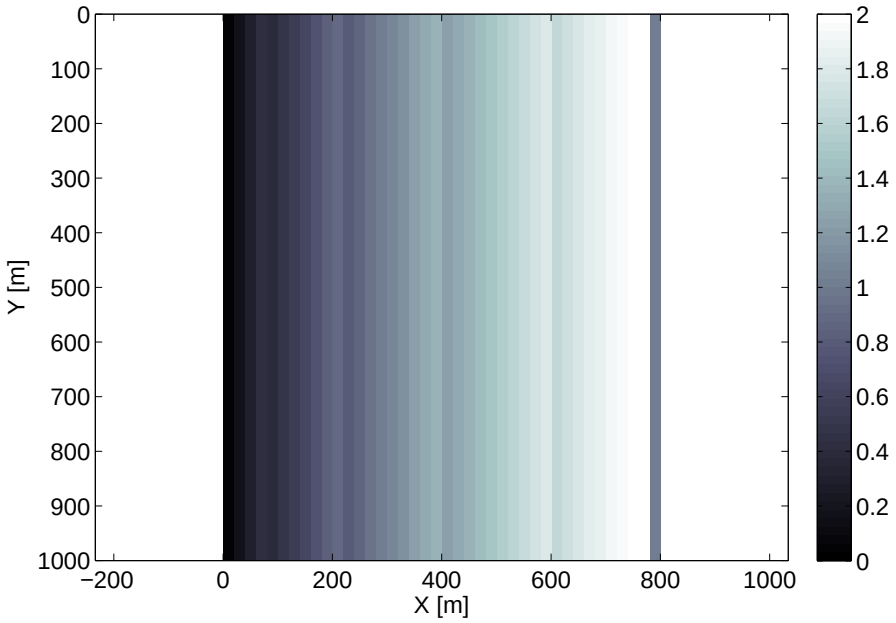

Figure 4.7: case 2b: Froude number computed by the CA inertial version after 90m from simulation start.

4.3 Two-dimensional numerical cases

In literature, 2D numerical solutions used to test hydraulic models are usually related to dam-break events, thus requiring models based on the fully dynamic shallow water equations (Soares Frazão and Zech, 2008; Neelz and Pender, 2010) .

An alternative option to establish accurate and not-trivial benchmark cases for reduced complexity models is to test them against models of greater complexity. For example, Hunter et al. (2008) compared six models of varying complexity in a single urban flood scenario, while Neelz and Pender (2010) examined the results of several models in different benchmark test cases, including both numerical cases and flood scenarios in river floodplains and urban areas.

However, more analyses are needed to investigate the behaviour of reduced complexity models when simulating two-dimensional flow dynamics. In particular, the influence of the diffusive approximation on reproducing the water surface profile and the velocity field is generally not considered (the recent works by Neelz and Pender (2010) and Aricó et al. (2011) are exceptions).

Considering this framework, the CA2D and IFD-GGA models have been tested in a number of numerical 2D cases, and compared with a 2D model based on the complete shallow water equations. The reference model is CCHE2D, which is available free of charge

on the National Center for Computational Hydroscience and Engineering (NCCHE) website (*http* : *//www.ncche.olemiss.edu*). CCHE2D is a two-dimensional hydrodynamic and sediment transport model for unsteady open channel flows over loose bed, based on depth-averaged Navier-Stokes equations (SWE). The turbulent shear stress are approximated using Boussinesq's approximation and the turbulent eddy viscosity, with the use of three different closure schemes. The set of equations is solved implicitly using a control volume approach. A detailed description can be found in Jia and Wang (2001).

The comparison between the models is carried out in three numerical cases. Case 3 is a horizontal plane made of 20x20 cells, with a 10x10m size; case 4 is a horizontal plane as well, but the flow domain is larger than case 3, being made of 50x50 cells with a 100x100m size. Lastly, case 5 has the same grid size and dimension of case 4, but the plane has a 10^{-4} slope in x direction. In all the three cases the domain is closed, except for the outlet zone, while the inflow is given by a constant discharge entering from a limited number of boundary cells (see Figures 4.8, 4.11, 4.14). The geometry and simulations settings are resumed in Table 4.9. In addition, case 4 was simulated using a slightly irregular mesh, to provide a further test for the models. The irregular mesh was obtained by modifying the position of cell centroids with a random shift, and applying the Dirichlet tessellation to obtain the cell lattice. The number of cells and the boundary were left unaltered.

	Case 3	Case 4	Case 5
grid dimension	200x200 m	5000x5000 m	5000x5000 m
cell dimension	10x10 m	100x100 m	100x100 m
slope	none	none	10^{-4}
Manning roughness	0.05 $m^{1/3}s$	0.05 $m^{1/3}s$	0.05 $m^{1/3}s$
incoming discharge	20 m^3s^{-1}	200 m^3s^{-1}	200 m^3s^{-1}
initial water depth	0.2 m	0.2 m	0.2 m
simulation time	30 minutes	10 hours	10 hours

Table 4.9: geometry and simulation settings for cases 3, 4, 5.

As can be seen from the description, the geometry and the boundary conditions were chosen to reproduce a slow propagation inundation event. Moreover the simple geometry allows for a better comprehension of flow dynamic, and for an easier comparison of models results. Since the CCHE2D model can manage only a limited number of dry cells, these simulations don't include wetting and drying phases. The LTS and GTS algorithms were used in combination with CA2D diffusive and inertial versions, while for the IFD-GGA model all the developed solution schemes were applied (NR-Jacobi, LT-Jacobi, LT-CGM, Section 3.3). Finally, all the simulations of the two models were performed using both the 4-direction and 8-direction link networks.

4.3.1 Preliminary results

Some interesting results could be observed in all the two-dimensional cases and are here summarized. First, the results of CA2D were more influenced by the reference water depth

used for discharge computation (Section 3.4.1) than by the model version. The diffusive version with h_{flow} as reference depth and the inertial version (again with h_{flow}) provide almost coincident results; results with the diffusive formulation and h_m were also similar although with local small differences (below 1cm for water depth values, and 0.1 ms^{-1} for velocity values). The same order of difference was observed between simulations with 4- and 8-direction grids. The IFD-GGA versions could be applied only in case 3, while in cases 4 and 5 the model could not be tested. In fact, the solution schemes implementing the Jacobi method could not complete the simulations due to convergence problems, while the LT-CGM version determined too large computation times with respect to CA2D and CCHE2D models.

4.3.2 Case 3: small horizontal plane

The results obtained by the models are compared in Figures 4.8,4.9 and 4.10. It must be noted that it was not possible to set exactly the same boundary condition for the outlet within the models. Therefore in all the simulations local differences are visible in this area. However, tests with different boundary conditions showed that the influence of the outlet area is limited to the nearest cells and does not affect overall flow propagation.

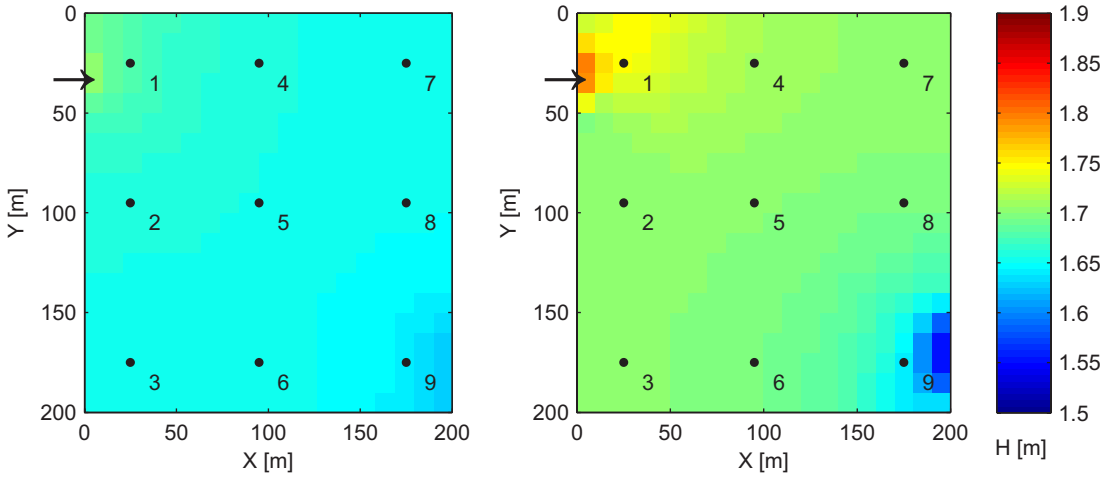

Figure 4.8: case 3: water levels computed by CA2D-IFDGGA model (left) and CCHE2D model (right) after 30 minutes from simulation start. Inflow and outflow areas are indicated by arrows.

As expected, the results produced by CA2D and IFD-GGA do not coincide with CCHE2D results (Figure 4.8). The difference between the computed water surfaces is below 10cm throughout the grid , going from 8-9% to 12-13% of the CCHE2D water depth (Figure 4.9).

Focusing on the velocity field (Figure 4.10), it can be seen in the CCHE2D results that the incoming flow produces a jet effect on the velocity distribution near the upper left boundary, because of the momentum conservation. On the other hand, the velocity distribution of CA2D and IFDGGA models does not show such effect, and the flow has a clear diffusive behaviour.

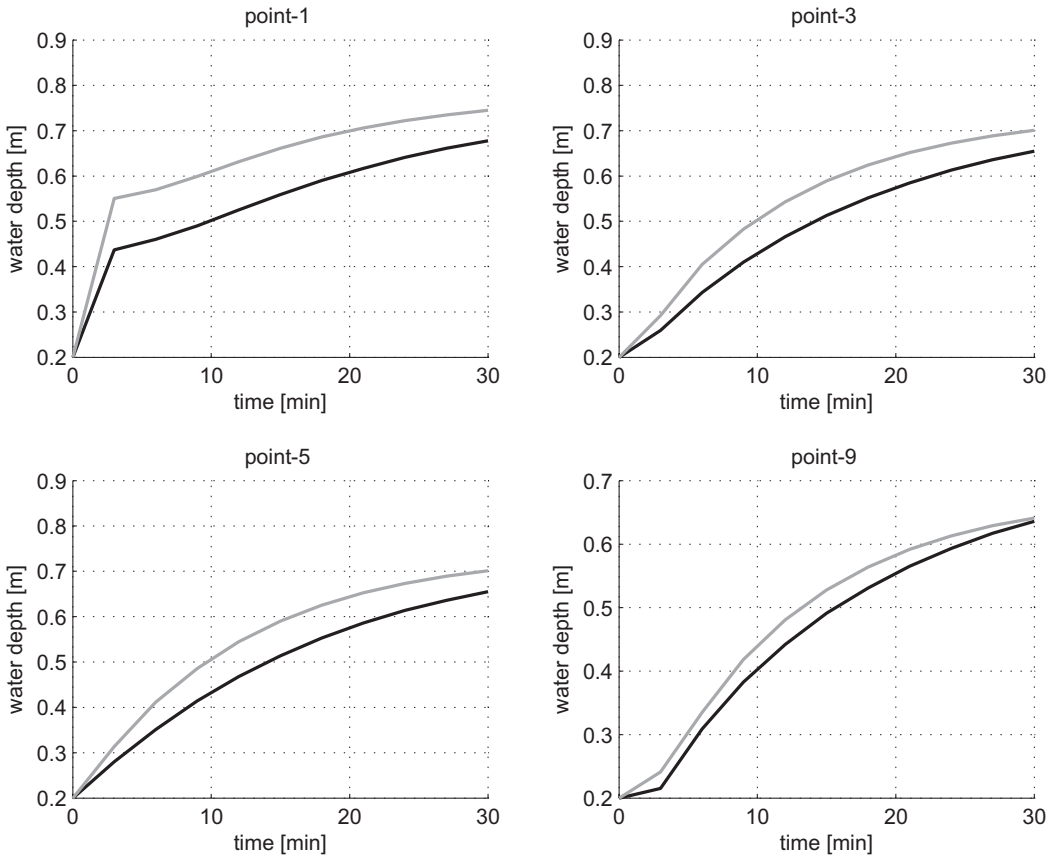

Figure 4.9: case 3: water depths computed in control points 1, 3, 5, 9 by the CCHE2D model (grey line), CA2D and IFD-GGA models (black line).

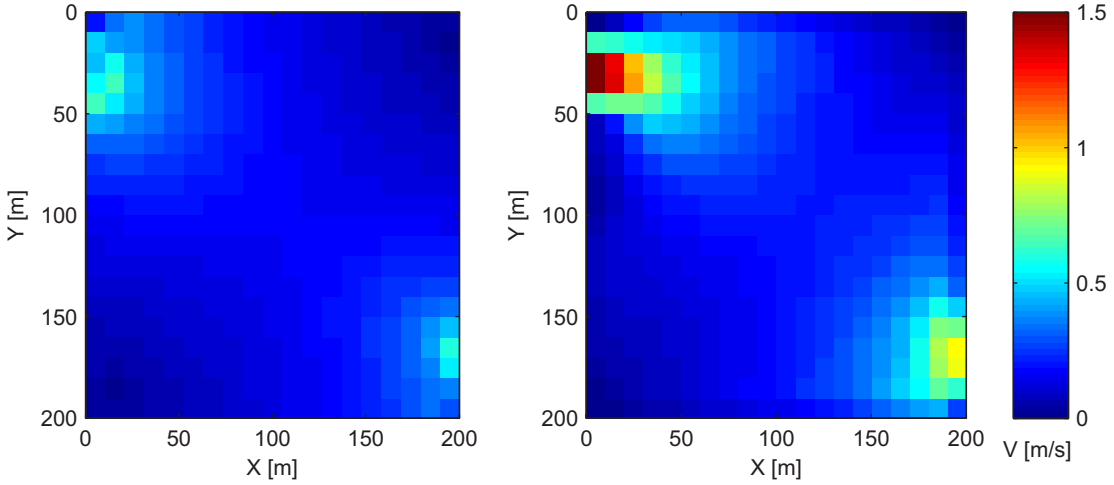

Figure 4.10: case 3: velocity fields computed by CA2D and IFD-GGA models (left) and CCCHE2D model (right) after 30 minutes.

4.3.3 Case 4: large horizontal plane

As can be seen from graphs in Figures 4.11, 4.12 and 4.13, differences between the CA2D and CCHE2D models are appreciable also in case 4. In CCHE2D simulation the flow appears to be slowed down and higher water depths are computed with respect to CA2D results. The velocity fields are similar (Figure 10), although differences are visible near the inlet and outlet area, since it was not possible to set exactly the same boundary condition for the two models. Excluding these localized effects, however, the difference between the water surface computed by the two models is everywhere below 10% of the CCHE2D water depth. Finally, results obtained with the regular and irregular meshes are practically coincident.

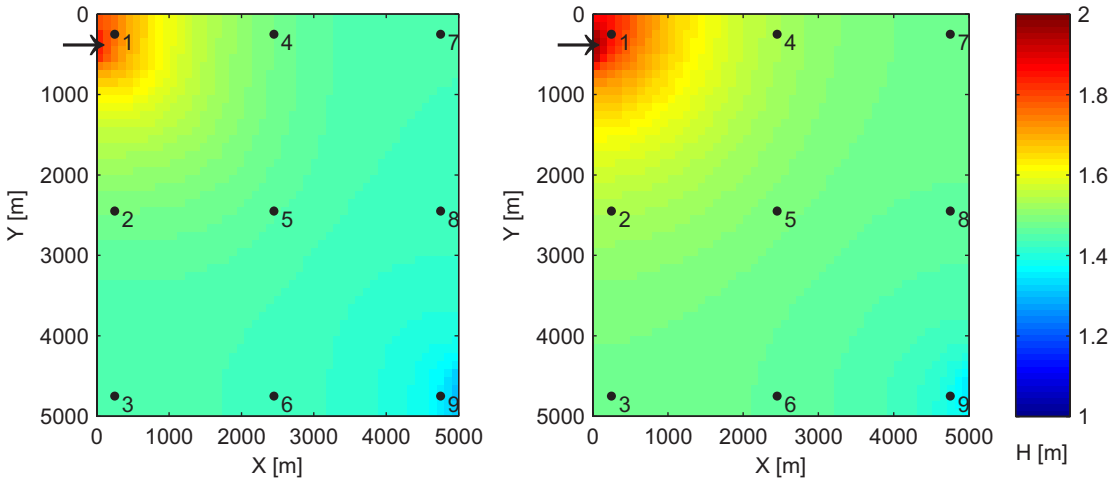

Figure 4.11: case 4: water levels computed by CA2D model (left) and CCCHE2D model (right) after 10 hours from simulation start. Inflow and outflow areas are indicated by arrows.

4.3.4 Case 5: large inclined plane

The presence of a mild terrain slope in case 5 modifies the results computed by CA2D and CCHE2D in respect to case 4. As can be seen from Figures 4.15 and 4.16, the differences between the results can be locally up to 15cm (points 3 and 7), therefore greater than in cases 3 and 4.

Focusing on the overall distribution, CCHE2D computes lower water depths where the water surface slope is steeper, while in the rest of the grid it computed higher water depths, accordingly with the results obtained in case 4 (Figure 4.14). On the contrary, the differences between velocity fields are somewhat limited, except for the inlet and outlet areas (Figure 4.17).

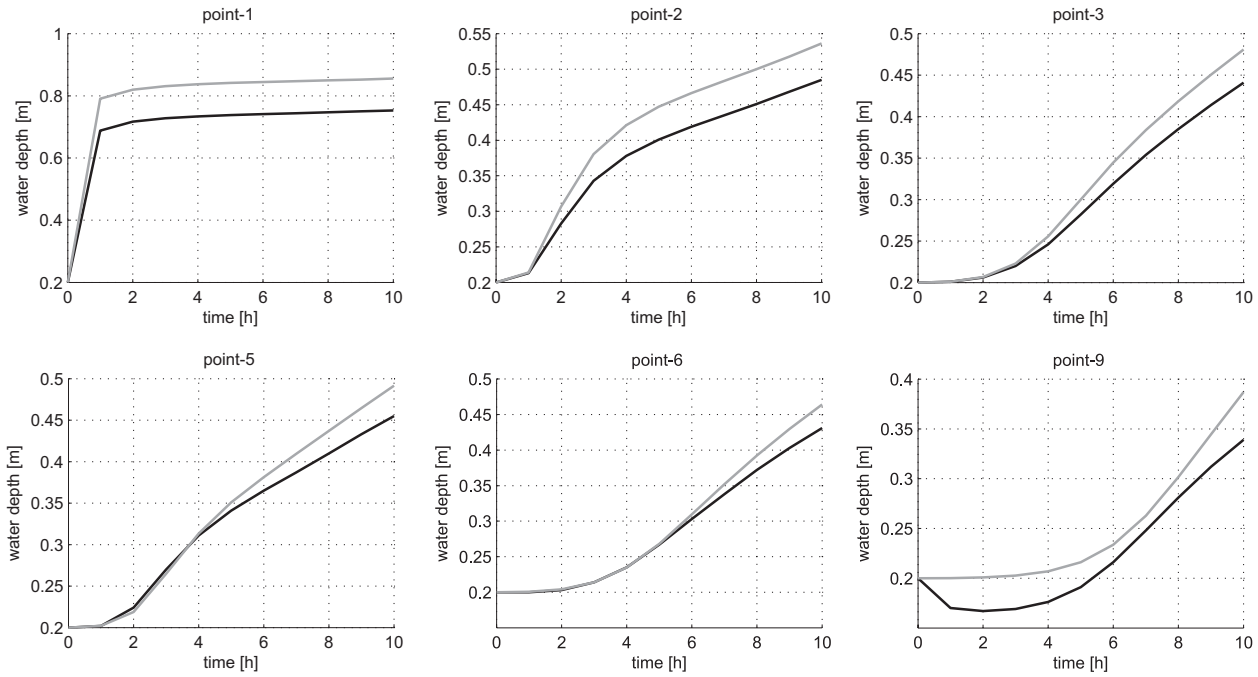

Figure 4.12: case 4: water depths computed in control points 1, 2, 3, 5, 6, 9 by the CCHE2D model (grey line) and the CA2D model (black line).

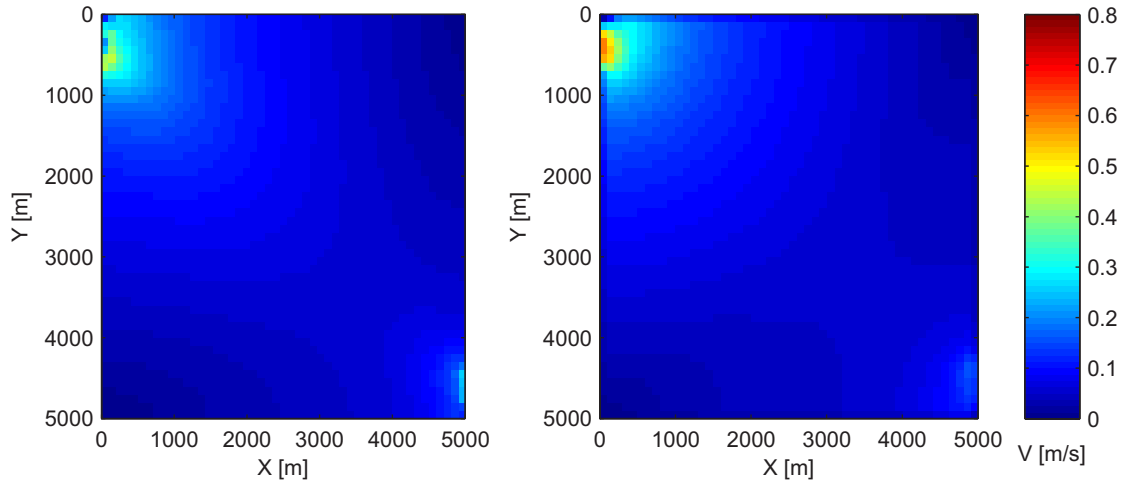

Figure 4.13: case 4: velocity fields computed by CA2D model (left) and CCCHE2D model (right) after 10 hours.

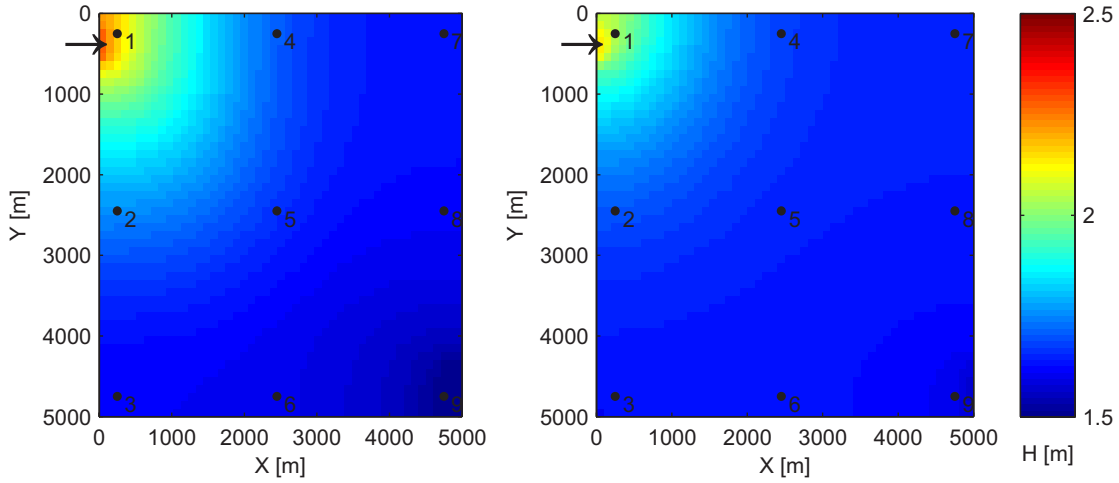

Figure 4.14: case 5: water levels computed by CA2D model (left) and CCCHE2D model (right) after 10 hours. Inflow and outflow areas are indicated by arrows.

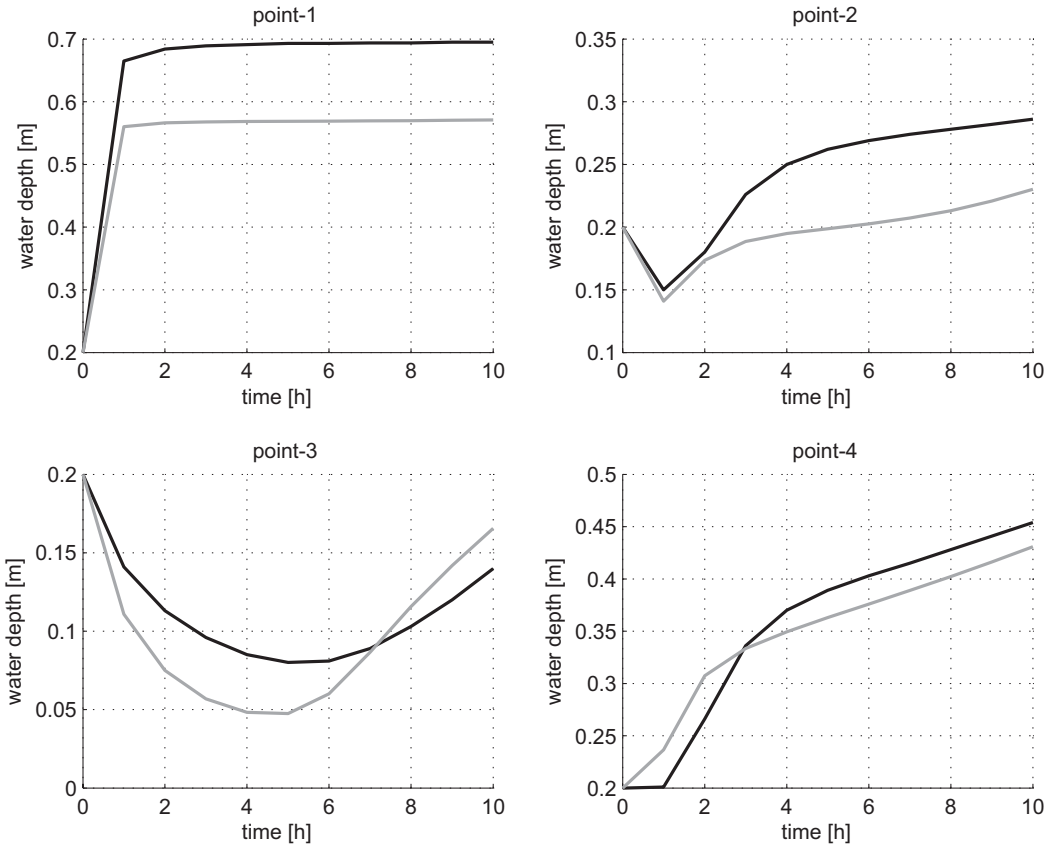

Figure 4.15: case 5: water depths computed in control points 1, 2, 3, 4 by the CCHE2D model (grey line) and the CA2D model (black line)

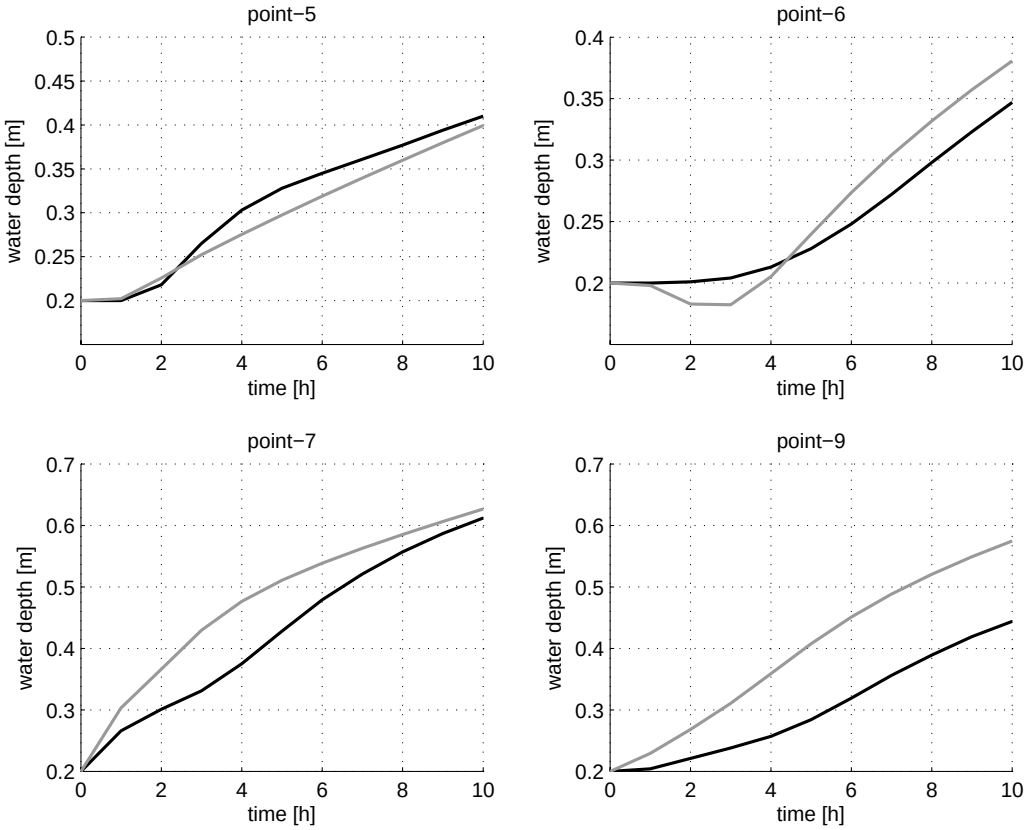

Figure 4.16: case 5: water depths computed in control points 5, 6, 7, 9 by the CCHE2D model (grey line) and the CA2D model (black line)

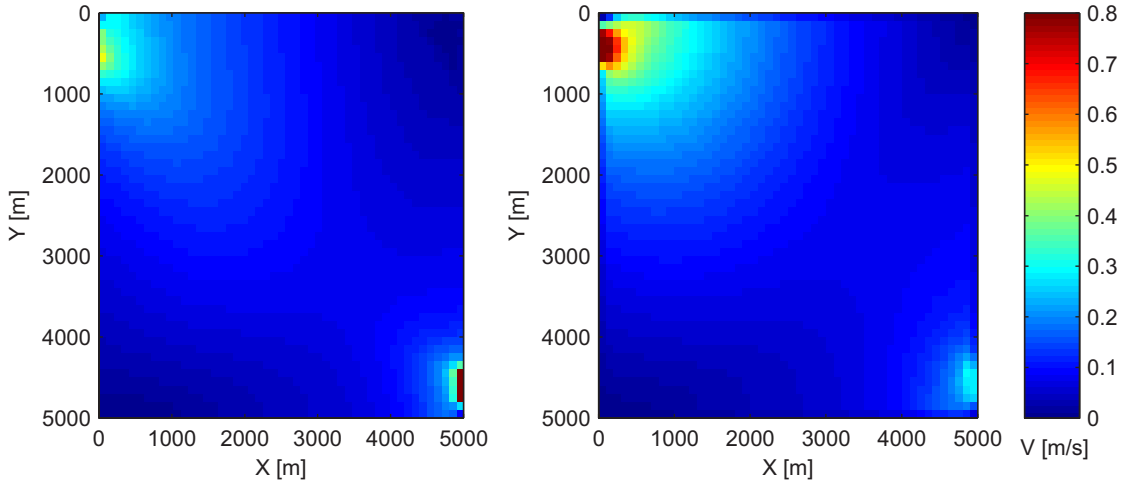

Figure 4.17: case 5: velocity fields computed by CA2D model (left) and CCCHE2D model (right) after 10 hours.

4.3.5 Discussion

Some considerations can be made about the observed results. Since the inertial and diffusive versions of the CA2D model provided similar results, the differences in respect to CCHE2D should be explained as an effect of advection terms of the momentum equation. This suggests that the importance of advection terms is not negligible in 2D flow, even though further numerical analyses are needed to investigate its magnitude in a wider range of flow conditions.

It is worth noting that the CA2D model maintained a diffusive behaviour also when using the inertial formulation, as can be inferred from the results of case 3 (Figure 4.10). This can be explained considering that in the model structure no information about the flow direction is transferred between adjacent cells: the hydraulic head is stored in cells simply as water level and flow components are decoupled. This schematization comes from the diffusive approximation but is conserved also in the inertial formulation, due to the drop of advection terms, so that momuntum conservation is still incomplete.

In conclusion, the introduction of the inertial term within the model is very effective for stabilizing the flow along the connections, but it seems to add little further description of flow dynamics, at least in the presented cases. Similar results were observed also by Bates et al. (2010) in applying the inertial and diffusive versions of the LISFLOOD-FP model to a urban flood scenario.

These observations can be used to draw some preliminary conclusions about the performance of the diffusive approximation in the simulation of flood events. Further analyses will be presented in Chapter 5.

Results obtained in case 3 indicate that the CA2D model can reproduce locally concentrated flows only with some approximation. Nevertheless, the overall results in cases 3,4,5 suggest that localized flow conditions may have a minor influence on overall 2D flood propagation, as concluded by previous research studies (Hunter et al., 2008; Neelz and Pender, 2010).

In particular, the observed differences between CA2D and CCHE2D are comparable with the uncertainty normally associated to available "real world" data for flood events. For example, according to Fewtrell et al. (2007) and Hunter et al. (2008), LiDAR data have a typical vertical error of ± 15 cm, comparable with the maximum difference in water depths observed in case 5. High level of uncertainty are also associated with calibration and evaluation data, like inundation extent maps from SAR imagery, or measurements of water level from water marks (Horritt et al., 2007; Neal et al., 2009a).

4.3.6 Simulation times

Table 4.10 reports run times for the simulations performed with CCHE2D, IFD-GGA and the CA2D models. All the simulations were run on a 1.25 Ghz Intel processor with 2.00 Gb of RAM. The CCHE2D model uses an implicit time marching scheme with a constant time step, so the maximum allowable values reported in Table 4.10 were chosen with a trial-and-error procedure. As reported in Section 4.3.1, the IFD-GGA model could be run only in case 3, while in cases 4 and 5 the model was too slow (run times exceeded two hours).

For the diffusive versions of the CA model, simulation time steps were first computed considering Eq. (3.12) alone. However, during the simulation analysis it was observed that the stability criterium locally computed very low time step values, thus slowing down the simulation. These low values were found to be not necessary for stability: in case 3 for example, according to Eq. (3.12) minimum time step values around $5{\cdot}10^{-3}$s are needed; however, it was experimentally observed that a minimum value of 0.02s was sufficient to preserve stability, while producing the same results both in terms of water surface and velocity. Therefore the CA simulations were run again introducing a minimum time step value, which obviously reduced computation times (Table 4.10). It must be pointed out that this finding does not allow for a generalized use of larger time steps, since the stability condition (3.12) was still valid in most of the computation grids.

In particular, it was observed that the velocity field is more subjected to instability than the water surface; for example, in case 3 the water surface computed with a time step limit of 0.05s does not show oscillations, whereas relevant oscillations are visible in velocities, both in module and direction. Further research should be necessary to establish a general rule for the application of the lower limit to time step, as a function of flow condition and cell size.

Such limitations can be completely avoided if the inertial formulation is used, since the maximum allowable time step can be obtained directly from the CFL stability condition (Eq. (3.17)), using an appropriate value for the coefficient C. For cases 3, 4, 5 the adopted values were between 0.4 and 0.5. As for the one-dimensional cases, the inertial formulation produces a dramatic speed up of the model especially in case 3 (33x) but the improvement is remarkable also for cases 4 (4.3x) and 5 (3.1x).

	Case 3	Case 4	Case 5
CA- diffusive v. GTS	170 s	221 s	450 s
CA- diffusive v. GTS (lim.)	42 s	57 s	55 s
CA- inertial v. GTS	1 s	12 s	12 s
CA- diffusive v. LTS	57 s	68 s	105 s
CA- diffusive v. LTS (lim.)	33 s	39 s	28 s
CA- inertial v. LTS	1 s	9 s	9 s
IFD-GGA (CGM)	1800 s	–	–
CCHE2D	30 s	112 s	113 s

Table 4.10: total simulation time, in seconds, for two-dimensional cases (3,4,5); the results obtained by setting a minimum time step value for the CA2D model are identified by "(lim.)"

Focusing on the comparison between the LTS and GTS algorithms, it can be seen that the diffusive LTS version is significantly faster than the GTS version, with a speed up from 2.5x to 4x. When the inertial formulation is used the run time reduction is less important although it should be noted that the numerical cases include only grids with a limited number of cells.

A further consideration can be made about the comparison between CCHE2D and diffusive CA2D run times. In case 3, the CCHE2D model is significantly faster than the diffusive CA2D model, mainly because the computation grid includes few cells and the CA2D model

needs to use very low time step values to preserve stability. On the contrary the diffusive CA2D model with a lower limit to time step value is faster in cases 4 and 5, in which the grid extension is larger. However, it must be remembered that CCHE2D is an implicit time-marching model, therefore the procedure for finding the optimum value of time step in a practical case could require running different simulations, thus being time-consuming. This is avoided with an explicit model like CA2D, in which the maximum available time step is directly computed by the model.

4.4 Case 6: 1D flow over horizontal plane

This numerical case, proposed by Hunter et al. (2005b) and applied also by Bates et al. (2010), reproduces the one-dimensional propagation of a non-breaking wave over an horizontal plane. The computation grid has a length of 6km in the flow direction, and a width of 0.8km; grid dimensions are therefore comparable to an ordinary 2D simulation, although the flow propagation is one-dimensional due to the constant discharge along the width.

This case was used to test the possible configurations of the CA2D model over different grid resolutions, from 10m to 100m. For each grid the LTS and GTS algorithms were used in combination with the diffusive and the inertial versions; in addition, the diffusive formulation was tested using the two reference values of water depth h_m and h_{flow} , respectively adopted by CA2D and LISFLOOD-FP (see Section 3.4.1 and the variables of Equations (3.12) and (3.16)). An attempt to use the arithmetic mean h_m within the inertial formulation was also made, but this caused strong instability and accuracy problems, so the obtained results are not represented. The 4- and 8-direction link networks were also tested.

The IFD-GGA was applied using the available solution schemes, but as for cases 4 and 5 the model could not complete the simulations, either because of convercenge problems or too slow algorithm speed. In addition the model could not simulate the dry bed initial condition, requiring minimum positive depths around 0.1mm to avoid instability; this affected propagation and relevant errors in wetting front were observed.

Hunter et al. (2005b) developed a one-dimensional analytical solution for the propagation of a non-breaking wave over an horizontal plane where the full De Saint-Venant equations can be simplified to yield an ordinary non-linear differential equation. The equation for the water depth h, at any point in space x and in time t is therefore:

$$h_{x,t} = \left[\frac{7}{3}\left(C_0 - n^2 u^3 \left(x - ut\right)\right)\right]^{3/7} \tag{4.1}$$

Where u is the component of depth-averaged velocity in the x direction and C_0 is a constant of integration, which can be fixed by referring to the initial conditions of the problem. Here the solution was implemented using parameter values of u=1ms^{-1} and n=0.03m$^{1/3}s$, for a simulation of duration 3600s.

4.4.1 Results

The results of CA2D (4 direction network) are shown graphically in Figures 4.18, 4.19, 4.20, together with with the analytical solution and the results of the LISFLOOD-FP model obtained by Bates et al. (2010). Table 4.11 summarizes the root mean square error (RMSE) and the minimum time steps (ΔT) computed for the diffusive CA model with h_m, applied both with the LTS and GTS algorithms. Finally, Tables 4.12 and summarize the RMSE and ΔT values for the different versions of the CA and LISFLOOD-FP models; results for the CA model are referred to the LTS version since, as can be seen from Table 4.11, the LTS and GTS algorithms have the same level of accuracy and stability.

	global time step				local time step			
Δx	10m	25m	50m	100m	10m	25m	50m	100m
ΔT	0.0059	0.0369	0.1490	0.6016	0.0059	0.0369	0.1490	0.6016
RMSE (20min)	0.0111	0.0116	0.0143	0.0517	0.0114	0.0130	0.0192	0.0514
RMSE (40min)	0.0058	0.0062	0.0125	0.0398	0.0063	0.0073	0.0151	0.0369
RMSE (60min)	0.0044	0.0047	0.0113	0.0339	0.005	0.0056	0.0128	0.0308

Table 4.11: case 6: minimum time step during the simulation (ΔT) and RMSE values for simulation steps 20,40,60 minutes for the GTS and LTS versions of the diffusive CA2D model.

	CA diffusive (h_m)			
Δx	10m	25m	50m	100m
ΔT	0.006	0.037	0.149	0.602
RMSE (60min)	0.004	0.005	0.011	0.034
	CA diffusive (h_{flow})			
Δx	10m	25m	50m	100m
ΔT	0.006	0.037	0.149	0.602
RMSE (60min)	0.07	0.130	0.150	0.172
	CA inertial			
Δx	10m	25m	50m	100m
ΔT	0.4	2.5	5	10
RMSE (60min)	0.308	0.117	0.054	0.100

Table 4.12: case 6: minimum time step during the simulation (ΔT), and RMSE values at 60 minutes for the diffusive and inertial versions of CA2D.

As can be seen from Figures 4.18, 4.19, 4.20 and the RMSE values in Tables 4.11 and 4.12, the three CA2D model versions produced quite different results. The original diffusive version, based on the arithmetic mean of water depth h_m, seems to be substantially insensitive to grid resolution and reproduces well the analytical solution. Differences are visible on the wave front when using the 50m and 100m resolutions, where the grid is too coarse to describe the flow profile (Figure 4.18).

On the contrary, the water profile computed with versions using h_{flow} is significantly influenced by the grid resolution, and the results are less accurate, especially near the wave

	LISFLOOD-FP diffusive version				LISFLOOD-FP inertial version			
Δx	10m	25m	50m	100m	10m	25m	50m	100m
ΔT	0.006	0.04	0.15	0.6	1.450	3.62	7.25	14.51
RMSE(60min)	0.013	0.03	0.06	0.09	0.065	0.05	0.03	0.05

Table 4.13: case 6: minimum time step during the simulation (ΔT), and RMSE values at 60 minutes for the diffusive and inertial versions of the LISFLOOD-FP model, from Bates et al. (2010).

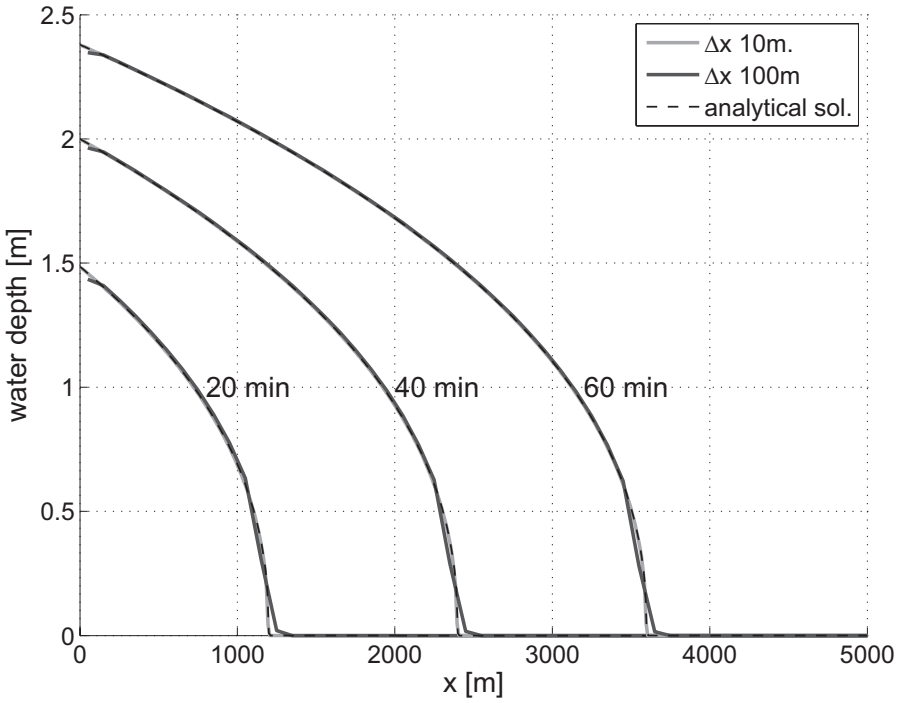

Figure 4.18: case 6: comparison between the analytical solution and the flow profiles computed by the diffusive version of the CA2D model with h_m for different grid resolutions.

front (Figures 4.19 and 4.20). The use of h_{flow} within the diffusive formulation seems to worsen the accuracy of the model, especially with coarser grids. The inertial version produced better results than the diffusive version in coarser grids, while the opposite is true for the 10m grid. It is worth noting that a similar result was observed by Bates et al. (2010) with the analogous versions of LISFLOOD-FP, as can be seen from Table 4.13.

Hence, in this particular case, the assumption of a linear variation of water surface along the link produces more accurate results, probably because of the marked differences in water depth between adjacent cells; on the contrary, the use of h_{flow} seems to introduce some errors in the computation of head losses.

A further explanation for the errors produced by the inertial formulation can be made from the hypotheses assumed for the derivation of Eq. (3.16): the flow area A is considered as a constant in time and space between two cells, and this means that the equation becomes

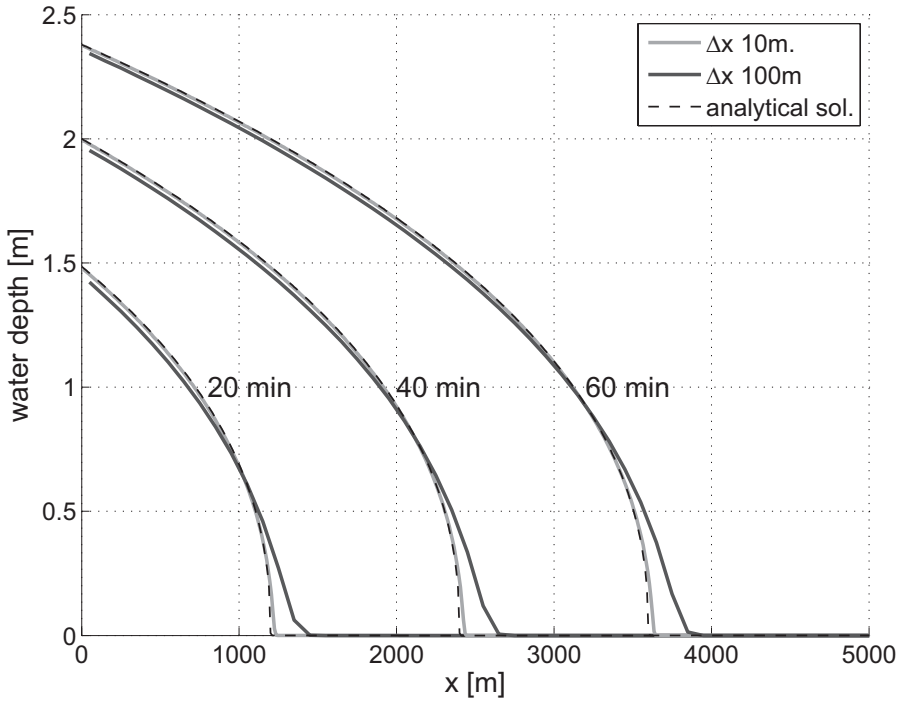

Figure 4.19: case 6: comparison between the analytical solution and flow profiles computed by the diffusive version of the CA2D model with h_{flow} for different grid resolutions.

non-conservative, thus introducing a further error in addition to the use of h_{flow}. It must be noted that in the numerical cases performed by Bates et al. (2010), the use of Eq. (3.16) was not always favourable in terms of accuracy with respect to the diffusive version, although in cases with complex topography the differences were limited.

As can be seen in Tables 4.12 and 4.13, the maximum allowable time steps values are coincident for the diffusive versions of the CA2D and LISFLOOD-FP models, and were directly derived from the diffusive stability condition (Eq. (3.13)). Minor differences between the two inertial versions were observed, but this depends on the values of the coefficient C used within the CLF stability condition (3.17). For the CA2D model, values of C between 0.3 (for 10m mesh resolution) and 0.5 (100m mesh resolution) were found appropriate, while the in the LISFLOOD-FP model a value of 0.7 was adopted. Hence, the introduction of the inertial term within the CA2D model produces a remarkable improvement in model stability.

	RMSE		
	20min	40min	60min
4-dir. grid	0.0111	0.0058	0.0044
8-dir. grid	0.0922	0.2145	0.3254

Table 4.14: case 6: RMSE values for simulation steps 20,40,60 minutes for the diffusive CA2D model using 4 and 8 direction grids.

Table 4.14 and Figure 4.21 illustrate the results obtained using the 4- and 8-direction

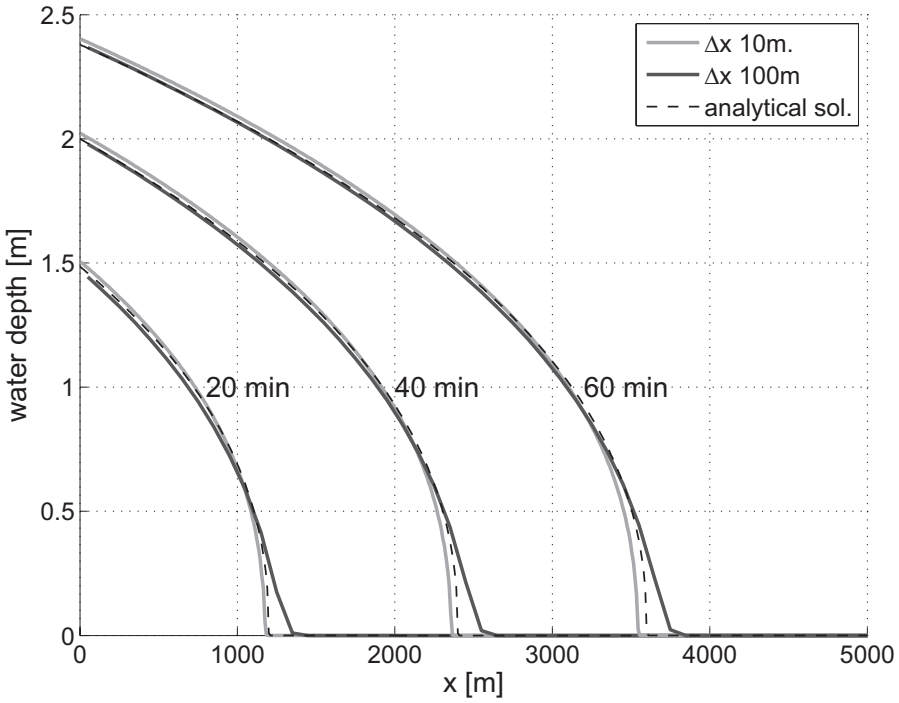

Figure 4.20: case 6: comparison between the analytical solution and flow profiles computed by the inertial version of the CA2D model for different grid resolutions.

link networks, in combination with the CA2D diffusive version with h_m. As can be seen, the accuracy of the model is decreased by the 8 direction grid; in particular, wave routing is faster and the difference with the analytical solution increases as the simulation progresses in time. The error in term of depth is more reduced if wave front is not considered, although it increases with the increasing of water depth. It should be noted that in this test case the 4-direction grid takes advantage from the 1D straight flow condition; the performance of the 8-direction grid could improve in situations with a variable flow direction (see Section 5.3).

4.4.2 Simulation times

Table 4.15 reports run times for the different versions of the two models. Simulation times for LISFLOOD-FP model are taken from Bates et al. (2010). The simulations with the CA2D model were performed on a 1.86 Ghz Intel Core2 processor with 0.98Gb of RAM, while simulations with the LISFLOOD-FP model were run on a single 2.66 Ghz node of a dual-core Intel Core2 Duo processor with 3Gb of RAM. Run times for the diffusive versions of the CA2D model were approximately the same. The CA2D run times are referred to simulations with a 4 direction grid (run times are almost doubled using the 8 direction grid).

When using a grid resolution of 25m or coarser, the CA2D model versions result faster than the corresponding LISFLOOD-FP versions. On the contrary, the LISFLOOD-FP versions are considerably faster on the 10m grid. The difference between the run times for this resolution is partly due to the data preparation time. For application of the inertial version

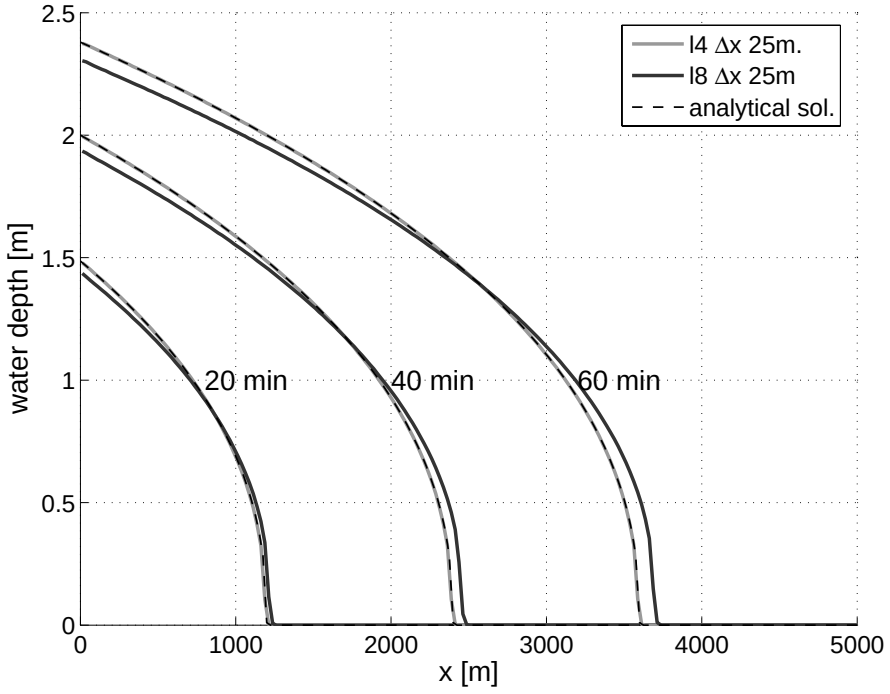

Figure 4.21: case 6: comparison between the analytical solution and flow profiles computed by the CA2D model with 4- and 8-direction grids (diffusive version with h_m).

to the 10m grid, the effective run time is less than 40 seconds, comparable to LISFLOOD-FP overall run time. It must be also considered that LISFLOOD-FP simulations were run on a more powerful processor, so the comparison of run times is just qualitative.

As for the LISFLOOD-FP model, the implementation of the inertial formulation within CA2D produces a dramatic decrease of run times, with an overall speedup of 39x for the 10m grid.

Finally, in this case the LTS technique produced a limited advantage compared to GTS version. This can be explained considering the small number of cells and the one-dimensional dynamics.

	CA diffusive		CA inertial		LISFLOOD	
	GTS	LTS	GTS	LTS	diffusive	inertial
10 m	6711 s	5275 s	177 s	135 s	1921.2 s	21 s
25 m	135 s	110 s	6 s	6 s	156 s	7.2 s
50 m	8 s	7 s	1 s	1 s	19.8 s	1.2 s
100 m	1 s	1 s	1 s	1 s	3 s	1.2 s

Table 4.15: case 6: total simulation time, in seconds, for CA and LISFLOOD-FP models versions with different grid resolutions (LISFLOOD-FP values are taken from Bates et al. (2010)

4.5 Case 7: channel with variable slope

This test case was proposed by Hartarto et al. (2011) and is designed to test the model ability to represent flow transitions (subcritical to supercritical and vice versa). In the simulation, a 1D steady flow condition is generated using a 5 km long channel with a variable bed slope (0.03, 0.01 and 0.001), as shown in Figure 4.22.

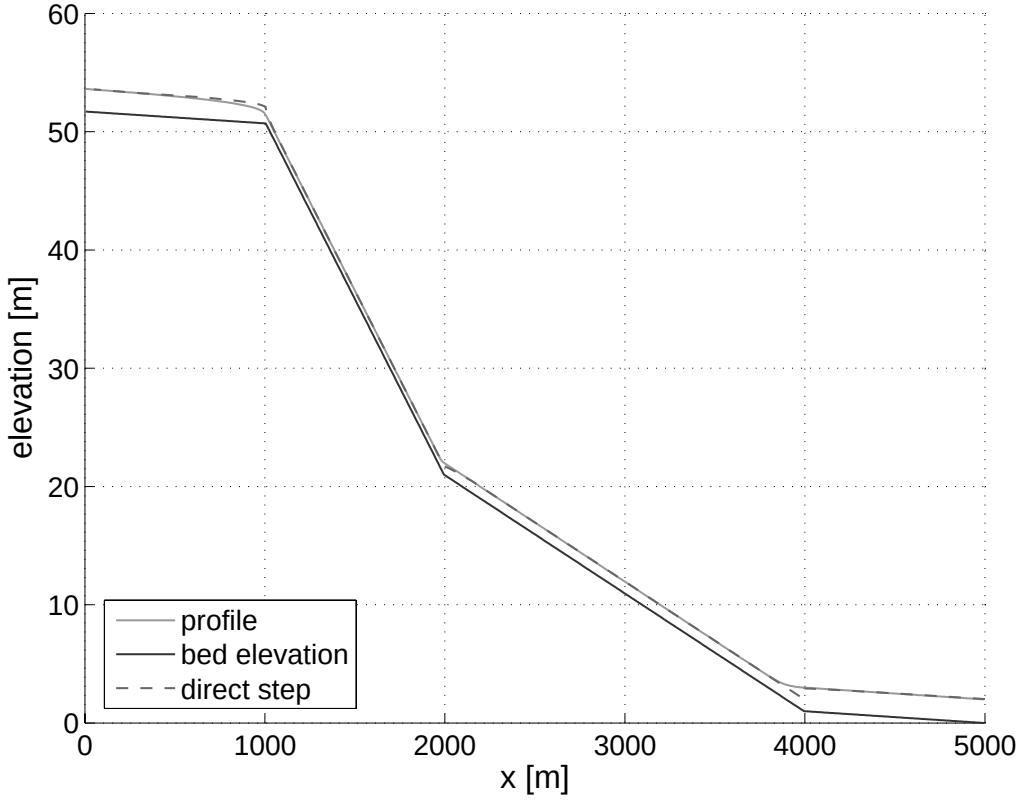

Figure 4.22: case 7: channel bed profile and computed flow profile in steady state.

The initial condition is dry bed, then ustream discharge is linearly increased from 0 to $500 \mathrm{m}^3 \mathrm{s}^{-1}$ in 1 hour, then a constant discharge is set until a steady state is reached in all the channel; a uniform flow downstream boundary condition is set, which corresponds to a 2.15 m water level at steady state. The geometry and the other simulation settings are resumed in Table 4.16. When steady state is reached, the discharge value and the various slopes produce an alternance of subcritical (upstream part with slope 0.001), supecritical (intermediate part with slopes 0.03 and 0.01) and again subcritical flow (downstream with slope 0.001). According to the notation of Chow (1959), a S2 flow curve occurs after the transition from the first slope change (0.001 to 0.03), then a S3 profile at the second slope transition (from 0.03 to 0.01), and finally a S1 profile in the last slope change (0.01 to 0.001). Given the steady state, a semi-analytical reference solution can be obtained using the direct step method. The channel has been discretized using a regular 10m resolution mesh, and a 4 direction link network.

bed slope	variable
section shape	rectangular
channel width	100 m
channel length	5 km
Manning roughness	0.02 $m^{1/3}s$
simulation time	1 hour

Table 4.16: geometry and simulation settings of case 7

4.5.1 Results and discussion

Both the inertial and diffusive versions of the CA2D model were tested, but surprisingly the inertial formulation was not able to compute a stable solution: strong oscillations are produced as the flow reaches the 0.03 slope during the initialization phase (increasing upstream discharge), and it was not possible to stabilize the model solution even when very reduced time step were used.

Further analyses were carried out using different values of discharges in order to vary the water depths, and varying grid resolution. Results suggest that the triggering factor of instability could be the supercritical flow condition due to steep slope. In such conditions, the inertial formulation could conserve stability only with very reduced water depths (less than 4-5 cm), while grid resolution did not seem to affect stability.

A possible explanation could be the use of h_{flow} to discretize water depth in the inertial formulation (Eq. (3.16)). In fact, the diffusive formula shows the same instability problems if h_{flow} instead of h_m is used in Eq. (3.10). It is likely that such discretization of head losses is not accurate enough where significant variations of water depth between adjacent cells occur. Bates et al. (2010) reported that the inertial formulation was subject to instability when using low roughness values (around 0.01 $m^{1/3}s$), therefore high velocity could be another triggering factor. However, more accurate analyses should be necessary to investigate the problem. On the contrary, the diffusive formulation could provide stable solution, coherently with the stability criteria given by Eq. (3.12). Anyway, since in this case only the steady flow condition is considered, the local acceration term included in the inertial formulation would not influence model results.

The computed flow profile is shown in Figure 4.22, while Figures 4.23, 4.24, 4.25 show the details of the computed and semi-analytical flow profiles where flow transitions occur. As was expected, the CA2D model was not able to correctly reproduce flow transitions, because the absence of advective terms eliminates the influence of local changes in geometry (Aricó et al., 2011). At x=1000m, the infuence of the supercritical flow transition is visible on the upstream computed profile for a much longer distance, with respect to semi-analytical solution, thus determining lower water depths (Figure 4.23).

In the other two transition points the differences between semi-analytical and computed solution are more limited. At x=2000m, the error propagates downstream for a short distance and after 100m the two profiles are almost coincident (Figure 4.24). At x=4000m, the hydraulic jump is not reproduced by the CA2D model and the transition from supercritital

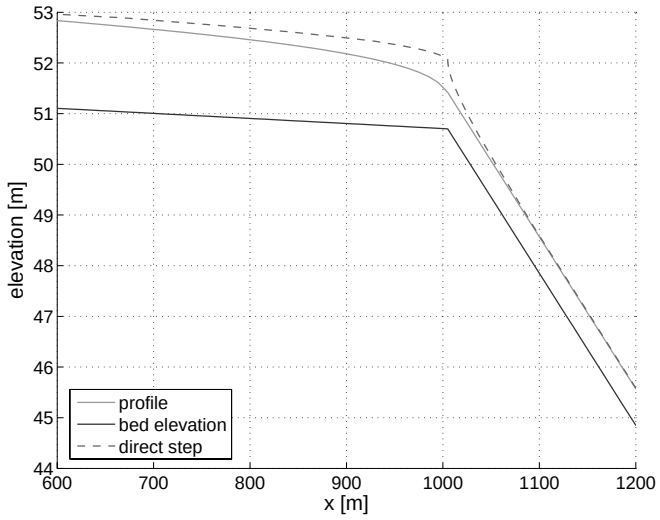

Figure 4.23: case 7: detail of computed and nunerical flow profiles (transition from subcritical to supercritical flow).

and subcritical flow has a continuous profile. Again, such behaviour was expected, as the non-conservative form of the model govening equations does not allowto reproduce shock waves and therefore hydraulic jumps.

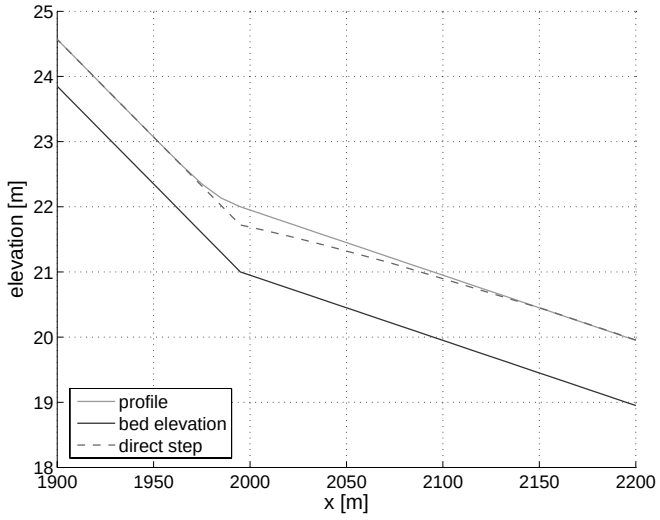

Figure 4.24: case 7:detail of computed and nunerical flow profiles (transition between supercritical flows).

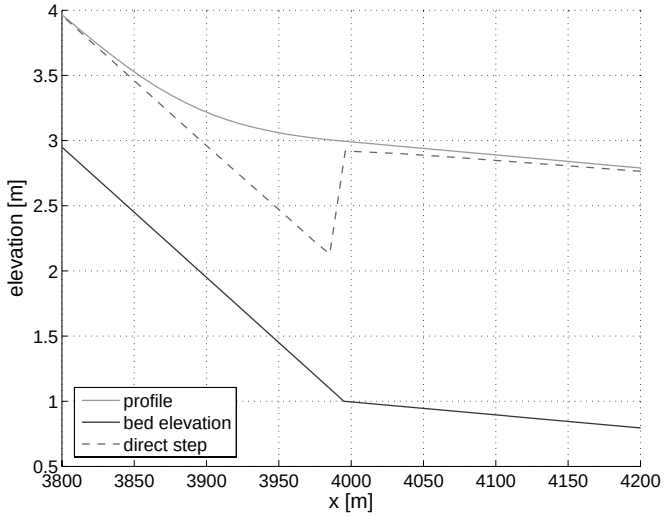

Figure 4.25: case 7:detail of computed and nunerical flow profiles (hydraulic jump).

4.6 Overall considerations about the models

The analysis of the numerical cases allowed to investigate the reliability of the CA2D and IFD-GGA models, and their performance in different flow conditions. Overall results highlighted relevant differences between the performance of the two models, that are below summarized.

4.6.1 performance of the CA2D model

The overall performance of the CA2D model was very satisfactory. First of all, the model proved to be robust and could be applied in all the considered test cases. Run times were small and comparable to other established hydraulic models. As expected, the accuracy of CA2D varied according to flow conditons. The model provided accurate results in one-dimensional flow conditions over with mild slopes, as well as in reproducing overland flow conditions, with reduced water depths and steep slopes. The model performance was less satisfactory when flow transitions over steep slopes were simulated, and relevant local errors were observed, due to the non-conservative governing equations. When applied to two-dimensional numerical cases, the model showed some limitations with respect to the fully dyinamic CCHE2D model. Such results were partly expected since the original formulation of the model does not account for acceleration and advection effects. However, in 2D cases the magnitude of observed errors was limited and below the typical uncertainty level of data and observations in actual flood events, e.g. topography and inundation extent maps.

In order to increase model performance and to reduce run times, two existing techniques were implemented and tested, both with overall good results. The incorporation of a local adaptive time step algorithm reduced the computation time in all the simulations, with no loss of accuracy in the results. On the other hand, the implementation of the inertial

formulation proposed by Bates et al. (2010) was even more effective, reducing computation times up to 97%. However, compared to the original diffusive formulation, the inertial formulation did not improve the accuracy of results, and the formulation showed serious instability problems when applied over steep slopes. The analysis of two dimensional cases suggested that the inclusion of the advection terms within the model equations will be necessary for a more accurate simulation of flow dynamics. Given these good results, the CA2D model has been further applied to reproduce flood events and scenarios (Chapter 5).

4.6.2 performance of the IFD-GGA model

The overall results of the IFD-GGA model in the considered numerical cases were not satisfactory. The model performed well in simple 1D cases with a limited number of cells, both in terms of accuracy and reliability of solution methods. On the contrary, in the 2D cases the versions of the model using Jacobi solution scheme had serious convergence problems that prevented its application. Better results were obtained by applying the CGM, however the resulting computation times were too slow with respect both to the CA2D model and the fully dynamic CCHE2D model. Hence, it was decided to interrupt the work on the IFD-GGA model, and reconsider its development (see Chapter 6).

Chapter 5

APPLICATIONS: FLOOD EVENTS AND SCENARIOS

Different issues are currently being addressed in research applications of hydraulic models in flood events and flood scenarios. Among them, the assessment of model performances is a key issue to improve the reliability of flood inundation studies. In fact, the current large amount of topographic information (Section 2.8) is not supported by a comparable availability of field information regarding the development and the dynamics of flood events. Experimental data of flood extent, water levels and velocities are generally limited in terms of spatial and temporal coverage, and affected by a significant uncertainty (Hunter et al., 2007). In some cases, different types of observed data were available to perform model validation and calibration (Hunter et al., 2005a; Werner et al., 2005; Bates et al., 2006; Neal et al., 2009a). However, even in these data-rich events the sparsity and uncertainty of observed data did not allow for rigorous assessment of model results. As a result, possible limitations of a simplifed model can be disguised by the calibration procedure, while a more complex model can not exploit its better potential because of data scarcity (Bates et al., 2004; Horritt et al., 2007; Di Baldassarre et al., 2009b). This was confimed in different research works where the performances of 1D or diffusive 2D models were comparable to fully dynamic 2D models, as mentioned in Section 2.8.

In this framework, the evaluation procedure of a 2D model should include applications to different flood events and scenarios, with the purpose of testing model performance using typical data set for model construction and validation. This is carried out in the present chapter by analyzing four test cases which differs in terms of location, topography configuration, extent and ongoing flow processes. Only applications of the CA2D model are here described, given the relevant problems of the IFD-GGA model highlighted in Chapter 4. Although during the research period CA2D has been applied in several flood risk and flood hazard analyses, for reasons of conciseness only a limited number of applications are here reported. These applications have been selected because they provide a good overview of model capabilities; moreover, observed data are available for model evaluation.

Section 5.1 describes CA2D application in a lowland rural flood event originated by a levee breach, where overland 2D flow is dominant. In section 5.2 the model is used to

reproduce a flood event affecting the floodplain of a wide river over a long reach; this event was characterized by a dominant 1D flow with local 2D flow processes. Section 5.3 describes the simulation of a high discharge event in a mountain river, characterized by steep slopes and the alternance of natural and artificial bed. Finally, Section 5.4 reports the application of CA2D to a series of physical experiments, representing urban flood scenarios.

5.1 1990 inundation event on the River Reno

The present section describes the application of the CA2D model to the inundation event that affected a small area near the Reno river, in Northern Italy, in 1990. This first test case can be considered as a typical application for a 2D flood model, regarding a flood event over lowland rural area. The event was mainly characterized by slow overland flow processes, although 1D flow over drainage network did play a role. The available data set is also representative of data sets typically available in similar events.

This event was analyzed and simulated within the European project AFORISM (Commission EC, 1996) using an early version of the IFD model (Section 3.3). However, the results obtained in that study were limited by the absence of an adequate data set for model validation. Recently, the existing topographic data set could be integrated with different field observations. Both qualitative information describing the development of the event, and measured field observations including maximum flood extent and high water marks, were collected, providing an adequate data set for testing the performance of a hydraulic model. Hence, a more comprehensive analysis of the flood event was planned. In addition, the new collected data showed that the flood event was significantly influenced by the minor structures of the drainage network. Flow processes related to minor structures are generally not considered in current literature, mainly because data scarcity does not allow to perform adequate analyses (Bates et al., 2006). Therefore it was decided to integrate the existing topograhic data with surveys of the drainage network, to investigate this issue.

5.1.1 Description of the test site

The site involved in the 1990 event is located in the lowland plain of the River Reno. The area is included in the municipalities of Galliera and Malalbergo, near the city of Bologna (Figure 5.1). The site is enclosed by a number of road embankments and levees: on the NE side the Reno levee; on the east side the embankment of the National road SS64, near Malalbergo; on the SW side the levee of the Riolo drainage channel; and, on the west direction, a railway embankment. During the flood event these embankments played a major role, retaining the flooded volumes within a limited area and influencing flow direction and timing.

The area is crossed in a south-west/north-east direction by the A13 motorway embankment, with a height above the surrounding ground from 4 to 6 meters. Other minor embankments are the Ca' Bianca secondary road and the Ponte Bosco road; the area also includes many minor roads and footpaths which join the smaller hamlets and border the various farm holdings.

The test site is characterized by a number of field drains, mostly oriented in the NE/SW direction. They convey water to the San Prospero drain, which runs parallel to the Riolo drainage channel (Figure 5.2). In spite of its small size and limited hydraulic capacity, this drain acquired great importance during the 1990 flood event, as described in Section 5.1.2.

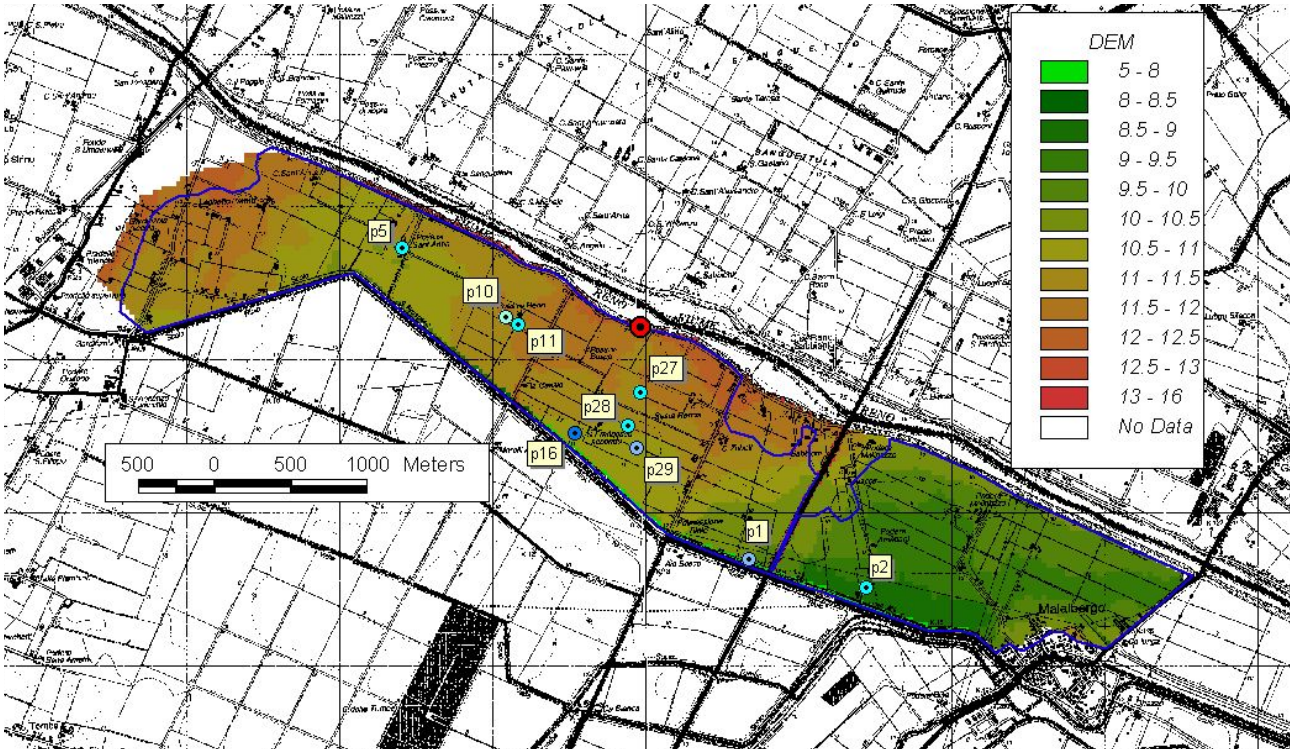

Figure 5.1: DTM of the area involved in the 1990 flood event; the map includes the maximum flood extent (blue line), the location of the levee breach (red point), and the measured high water marks.

5.1.2 Dynamics of the flood event

The dynamics of the flood event was reconstructed thanks to the field observations reported by the Civil Protection and the Technical Service of the Reno basin. A detailed description is available on the final report of the Aforism project (Commission EC, 1996), which is here resumed.

The flood event started on the 26th of November. The triggering cause was a siphoning process that originated on the foot of the River Reno right levee around 16.30 h. The resulting seepage could not be stopped despite the attemps made by the Civil Protection, and eventually caused the collapse of a large section of the levee (Figure 5.3). During the overflow, the breach was progressively widened up to a 28 m width. The overflow of water continued for almost 20 hours until the 27th, when the decrease in the water level inside the River Reno bed allowed to close the breach.

Figure 5.2: the San Prospero drain near Malabergo; the roughly triangular cross section is 10m wide and 3.3m deep; on the left side the levee of the Riolo drainage channel is visible.

During the flood event, the water was first held back in the western part of the site by the embankment of the A13 motorway. In a second time, the water could underpass the embankment through the San Prospero drain, inundating the eastern part between the motorway and Malalbergo. Since the urban area is elevated with respect to the surrounding fields, the water passed by the village, flowing in the NW direction and reaching the embankment of SS64 National road; the only damages in the urban area were due to local sewer surcharge, that caused the flooding of some basements. However, a number of isolated houses located out of Malalbergo were severely affected.

In order to facilitate the drainage of water from the flooded areas, as soon as the flow from the breach had ceased on the 27th, the Riolo levee was cut into upstream of the motorway embankment and, on the 28th, at another point downstream. Such measures were needed because the outflow structures within the area (namely, a culvert connecting the San Prospero drain with the Riolo drainage channel, and an culvert under the SS64 embankment, both of them near Malalbergo) were largely insufficient to drain the huge amount of water stored in the flooded area.

5.1.3 Available data

Some of the data used in the present work, namely the breach hydrograph and a triangulated irregular network (TIN) topography, could be taken from the AFORISM simulations

Figure 5.3: the breach before the beginning of repair works (27th of November). The overflowing water eroded the levee creating a 28m wide, 6m deep breach (Cremonini, 1994).

(Commission EC, 1996). The breach hydrograph was reconstructed using visual observations made by the personnel monitoring the breach, integrated with hydraulic analysis in the River Reno. The TIN was obtained from the surveyed points of the regional topograhic map 1:25000. In order to obtain the topographic information needed by the CA2D model, the TIN was eleborated in ArcGis to produce a 30 resolution DTM. In a second time levees and embankments were manually introduced in the DTM, using elevation data from the regional topograhic map.

Given their importance in the hydraulic simulations, the geometry of the San Prospero drain, the related hydraulic structures and other minor structures of the drainage system were surveyed during dedicated field inspections, reported in Section 5.1.4.

As already mentioned, the topographic data set was integrated with observations and measurements concerning the dynamics of the flood event. Most of this information was taken from the field work of Cremonini (1994) few days after the flood event. In a number of sites, high water marks were clearly visible on trees and buildings, and other useful information of flow conditions could be inferred from ground sedimentation (Figure 5.4, left). These field observations were integrated in 2010 during the field inspections for the present work; the interviews with people affected by the flood and with personnel of the Malalbergo municipality improved the knowledge of the event dynamics and the set of observed data for model calibration. In addition, the maximum flood extent was captured by an aerial photo taken during the event, before the Riolo levee was cut to drain the water.

5.1.4 Reproduction of the drainage system

As already mentioned, the San Prospero drain played a major role during the flood event, therefore special care was used in modeling its geometry and the associated structures into the computation grid. The drain is parallel to the levee of the Riolo drainage channel; the outlet point is located near Malalbergo and consists of a box culvert under the Riolo levee (Figure 5.5). From the outlet to the culvert under Ponte Bosco road, the cross section is roughly triangular, with a width of 10m and a depth of 3.3m; in the rest of the drain, the cross section is almost rectangular, with a width between 5 and 6 meters and a depth from 1 to 2 meters. The slope in the drain is around 0.1% and is roughly constant.

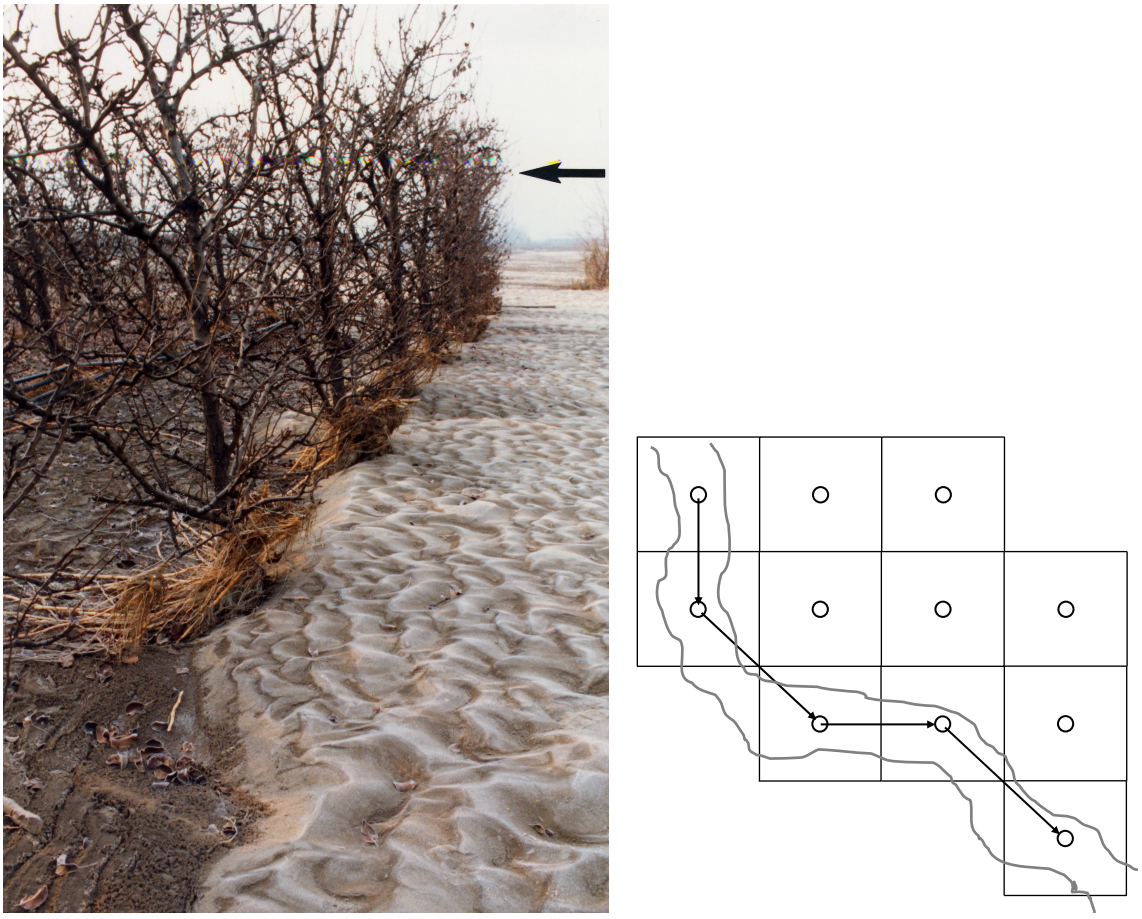

Figure 5.4: left: a picture taken in 1990 few days after the flood event; the increased resistance given by fruit trees slowed down the flow and produced sedimentation of sand; the black arrow indicates the probable flow direction (Cremonini, 1994); right: reproduction of the San Prospero drain in the grid.

Considering the real geometry, the drain has been reproduced in the model by adding a row of cells along the south-west border of the computation grid (Figure 5.4, right); these cells have a reduced size with respect of ordinary cells, and the connections between drain cells reproduce the drain cross section adopting a simplified rectangular section, even for the part with a trapezoidal section. In order to test this approximation, a number of simulations with the 1D HECRAS model were performed; a 5m wide rectangular cross section was found

Figure 5.5: box culvert connecting San Prospero drain and Riolo drainage channel; the culvert passes under the levee of the latter.

to be roughly equivalent to the real one when bankfull discharge flows in the drain; that is, water depths were almost the same. Moreover, 2D simulations demonstrated that the drain geometry has a limited influence in flood dynamics, since water rapidly fills up the drain and starts overflowing. The drain slope measured during the field inspections was introduced into the model grid.

Along the drain, a number of culverts and small bridges at the intersection with the motorway, secondary public roads, and private roads can be found. Bridges and minor culverts were not represented in the model, due to the limited obstruction on the drain section. On the contrary, some of the culverts and the two outlet points have been explicitly modelled within the grid, due to their importance in the overall flow processes (Figure 5.6):

- culvert under Ca Bianca road: the structure has a conspan arch cross section with a 2m width and 2.5m heigth; the dynamics of flooding suggest that this culvert was partially or totally obstructed during the event, therefore it has been represented as a part of the Ca' Bianca road embankment (see discussion in Section 5.1.6);

- culvert under Ponte Bosco road: the structure has a conspan arch cross section with a 2m width and 2.5m heigth; it has been reproduced as a connection with a mixed weir-pressure flow;

- culvert under the motorway: this is a box culvert with a rectangular 4.5m high cross section; due to its considerable size and the observed upstream maximum water levels (see Figure 5.1), it has been represented as an ordinary free surface connection, although with a reduced cross section;

- outlet points (box culvert under the levee of Riolo drainage channel (Figure 5.5), and conspan arch culvert under SS64); these two culverts have been reproduced as outlest connections with mixed weir-pressure flow; for both of them, the original geometry (width and height) has been considered.

Buildings were not reproduced in the grid, given the relatively coarse grid resolution and the fact that most of the buildings are isolated and could not influence overall flow.

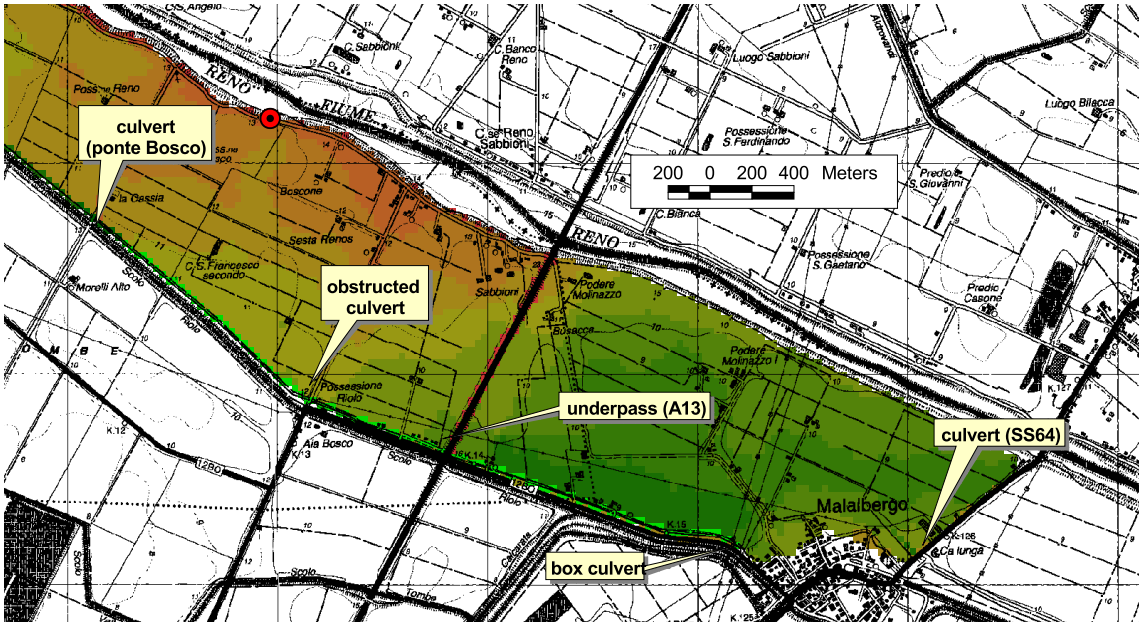

Figure 5.6: location of the hydraulic structures included in the computation grid.

5.1.5 Methods

The applicaton of the CA2D model to this case study is based on a sensitivity analysis to calibration parameters. This is an established modeling approach in current literature (Romanowicz and Beven, 2003; Hunter et al., 2005a; Di Baldassarre et al., 2009b) and can be used in place of a standard calibration procedure when calibration and validation data are scarce and affected by uncertainty. A number of studies pointed out that model overcalibration for a specific case study can compromise the capability of simulating events of different magnitude, unless recalibration is performed (Aronica et al., 1998; Di Baldassarre et al., 2009b). In this case different types of observed data are available for calibration, however the dataset has some limitations: only few observed high water marks are available and their distribution is not regular over the site (see Figure 5.1); in addition, only the maximum flood extent has been observed therefore no data about the dynamics are available; finally, observations are not completely consistent. Within this framework, a sensitivity analysis allows to take better into account the uncertainty in both modeling approach and available data (Götzinger and Bárdossy, 2008).

In addition to incompleteness of calibration data, there is a significant uncertainty regarding land use configuration when the flood event occurred. From the pictures, it can be observed the alternance of crop fields and orchads in the flooded area, which do not entirely correspond to current land use. Observations of deposition after the flood event suggested a relevant influence of lande use on water flow (Figure 5.4). In addition, flow dynamics was probably influenced by minor drains within the fields, that could not be reproduced in the model grid due to their reduced dimension.

Focusing on model uncertainty, the experiments on numerical cases reported in Section 4 suggest that the model approximations should not produce substantial errors in the reproduction of overall flow dynamics. However, errors are expected to be locally relevant neat the breach and where section narrowings cause an acceleration of flow.

For the sensitivity analysis several simulations with different combinations of roughness values were carried out; in order to simplify the analysis, only two roughness values were used, one for the San Prospero drain and an uniform value for the rest of the area. The problem of the influence of land use was therefore not considered. In the simulations, the drain Manning parameter varied from 0.03 a 0.05 $m^{1/3}s$, with a 0.005 span, while for the floodplain the values went from 0.1 to 0.2 $m^{1/3}s$, with a span of 0.02. Results were evaluated using several indexes based on observed data. The comparison between observed and simulated maximum water depths is based on the absolute and relative root square mean error (RMSE), and the standard deviation. The performance in reproducing flood extent is based on the difference between the observed and simulated flooded areas, and the computation of two established performance indexes (Hunter et al., 2005a). The two indexes $P1$ and $P2$ are defined as:

$$\begin{cases} P1 = W1/\left(W1 + W0 + D0\right) \\ P2 = \left(W1 - W0\right)/\left(W1 + W0 + D0\right) \end{cases} \tag{5.1}$$

where: $W1$ is the area that is correctly predicted as flooded in the model, $W0$ indicates the area wrongly predicted as flooded in the model, $D0$ is the flooded area that was not flooded in the model simulation. For a number of reference simulations, the differences between inertial and diffusive versions were also analyzed.

5.1.6 Results

A first evaluation of model results can be done comparing the observed and simulated flooded area (Figure 5.7). It can be seen that the simulation matches well the observation, as confirmed by the high values of $P1$ and $P2$ indexes (Figure 5.8). However, most of the area is actually delimited by dikes and embankments, therefore flood extent is not a good benchmark variable as the model results are constrained by the topography; this is demonstrated by the low sensitivity of model performance to roughness calibration (values of $P1$ and $P2$ show little variation, as can be seen in Figure 5.8). Anyway, it can be noticed how the flooded area is underestimated near the west boundary, and overestimated in the eastern sector near the motorway.

More information on model performance can be inferred from the comparison between

observed and simulated water depths, where high water marks are available. As can be seen in Figure 5.9, even with an optimal calibration the mean absolute error is around 30cm, and the relative error is around 33%. These values are relevant, however, the analysis of single points shows that the level of error is not uniform (Figure 5.10). Whereas differences are limited to 15–25 cm in most of the points, errors up to 50 cm are recorded for point 16, near the drain in the central area, and in point 2, in the west sector (Figure 5.1).

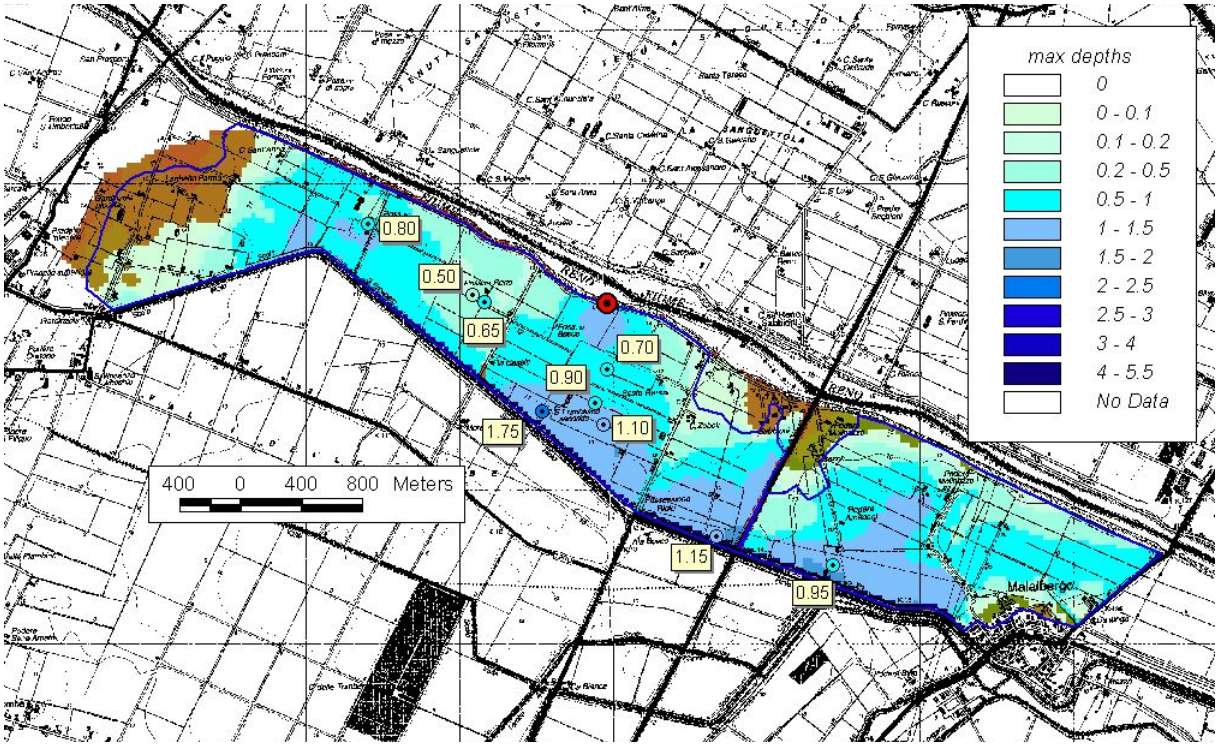

Figure 5.7: comparison between simulated maximum flood extent and observed data. Simulation results are referred to a roughness values of 0.04 $m^{1/3}s$ for the drain and 0.15 $m^{1/3}s$ for the floodplain.

Despite the uncertainty in observed data, the analysis of performance indexes confirm the consistency of model results (Figures 5.8 and 5.9); all the indexes indicate an optimal calibration area, centered around roughness values of 0.03 $m^{1/3}s$ for the drain and 0.18 $m^{1/3}s$ for the floodplain. The high value for the flooplain can be explained considering the mixed land use of the test site, where fruit orchads posed a relevant obstacle to flow. Moreover, the low DTM resolution does not take into account the microtopography (i.e. field drains) and must be compensated by higher friction losses (Yu and Lane, 2006a). A more comprehensive discussion about the calibration of roughness is reported in Section 5.4).

Generally speaking, the model underestimated flood extent in the west sector, with subsequent lower water depths. Thus, in the simulation more water flowed eastward beyond the motorway underpass, producing higher water depths around Malalbergo.

The comparison between the diffusive and inertial versions did not show significant differences, with localized maximum differences in water depth around 10cm, and average differences below 5 cm.

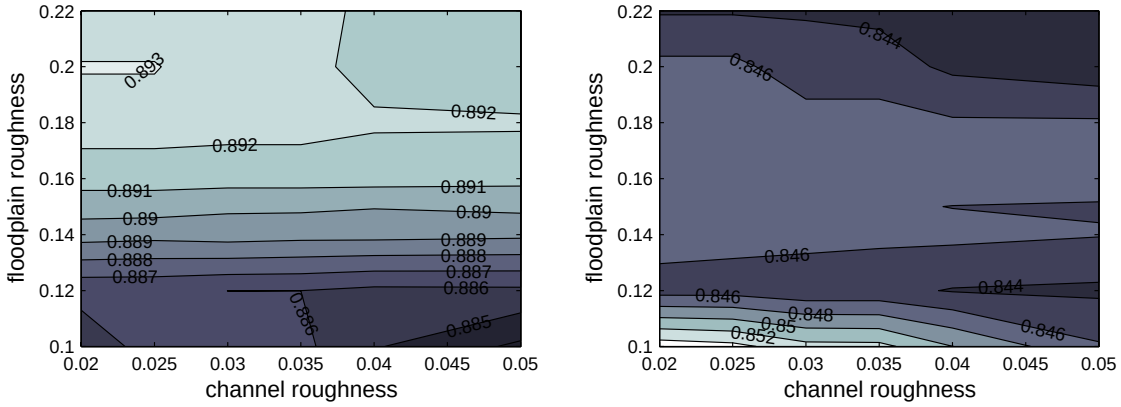

Figure 5.8: variation of the performance indexes $P1$ (left) and $P2$ (right) as a function of floodplain and channel roughness (expressed in $m^{1/3}s$).

Finally, although observed data do not allow a proper assessment of the time evolution of the event, some indications can be taken considering the qualitative descriptions. The blockage effect of the obstructed culvert underpassing Ca' Bianca road produces a relevant ponding in the central area, and a similar ponding effect can be seen around Malabergo, due to the insufficient drainage from the two outlet structures (Figure 5.11). As the simulation progresses the central area remains partially flooded, although most of the water is drained from the central to the east sector of the study area. This is consistent with the observed flood pattern, as it was necessary to cut the levee of the Riolo channel in the central area.

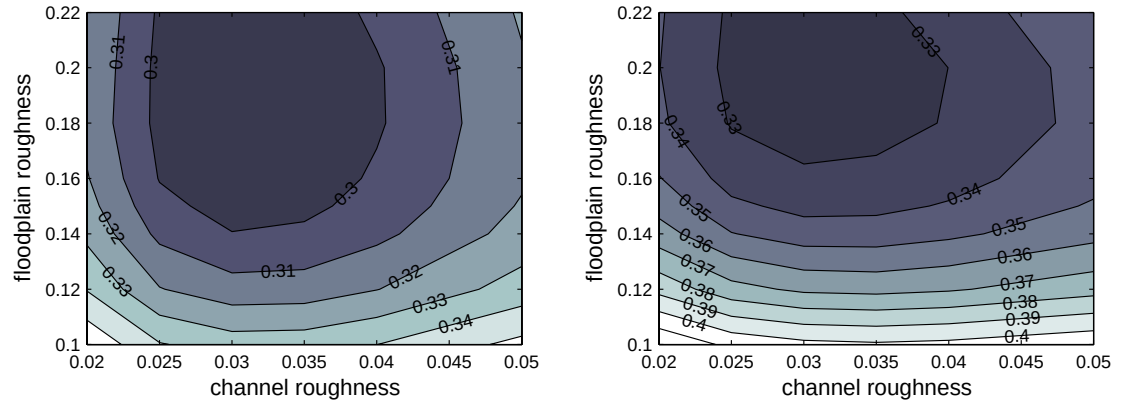

Figure 5.9: variation of RMSE (left) and normalized RMSE (right) considering simulated and observed maximum water depths as a function of floodplain and channel roughness (expressed in $m^{1/3}s$).

As a further evaluation, a number of simulations in which the Ca' Bianca culvert was not obstructed were run; the western and central sectors resulted almost completely drained at the end of each simulation, unlike the observed dynamics. Hence, this suggests that during

the event the culverts along the S Prospero drain were partially or totally obstructed.

5.1.7 Discussion

Several reason can be proposed to explain the difference with the dynamics inferred from observed data. Götzinger and Bárdossy (2008) identified three main sources of uncertainty (and therefore errors): (i) observation uncertainty, which is the approximation in the observed hydrological variables used as input or calibration data; (ii) parameter uncertainty, which is induced by imperfect model parameterisation; and (iii) model structural uncertainty.

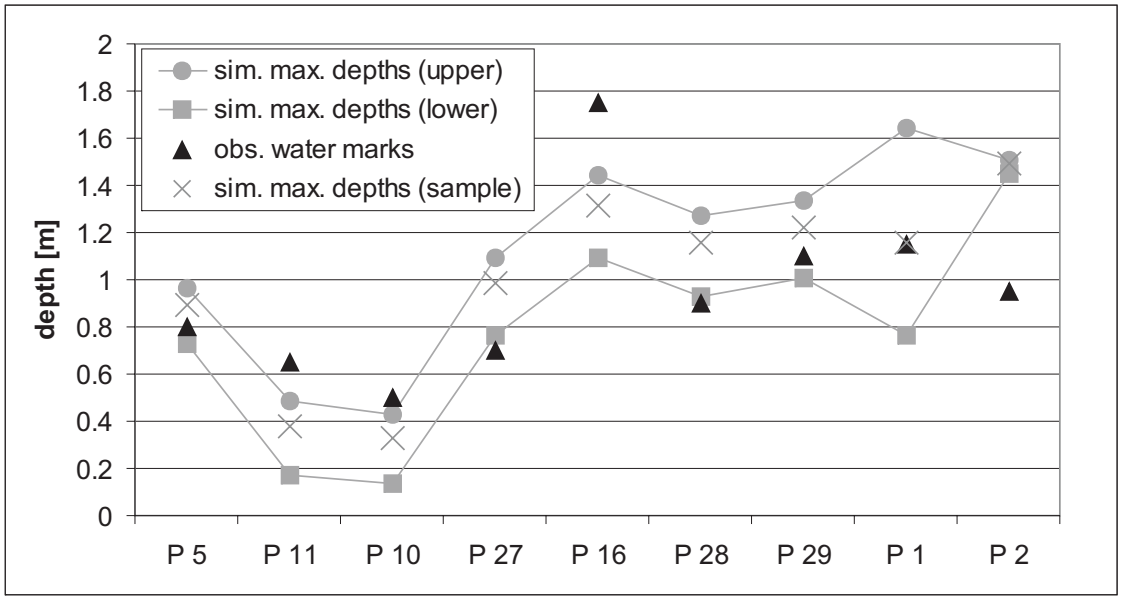

Figure 5.10: comparison of high water marks with computed max depths, with the indication of upper and lower bounds depending on roughness coefficients; the "sample" simulation refers to 0.03 $m^{1/3}s$ floodplain roughness and 0.18 $m^{1/3}s$ channel roughness.

Focusing on the latter, the CA2D diffusive approach (even for the semi-inertial formulation) could influence the correct reproduction of the flood processes; for instance, during the event the water flowed out of the breach mainly in the N-S direction, and could have produced more relevant water depths near the Riolo channel levee, with respect to model results (as indicated by point 16). Actual higher water depths could explain the larger propagation eastward.

Besides model theorecal assumptions, also the representation of the study area within the model grid was necessarily approximated. The drain cross section is simplified, and the minor drainage network is not represented. As mentioned, it is likely that the hydraulic structures along the drain were partially or completely obstructed during the event, thus modifying flow patterns and blocking the drainage. Actually, The Ca' Bianca road culvert was represented as an obstruction, but such a decision can not be properly verified. The use of a uniform roughness parameter for the floodplain is a further significant approximation,

since areas covered with fruit trees slowed down flow producing a consistent increase of water dephts.

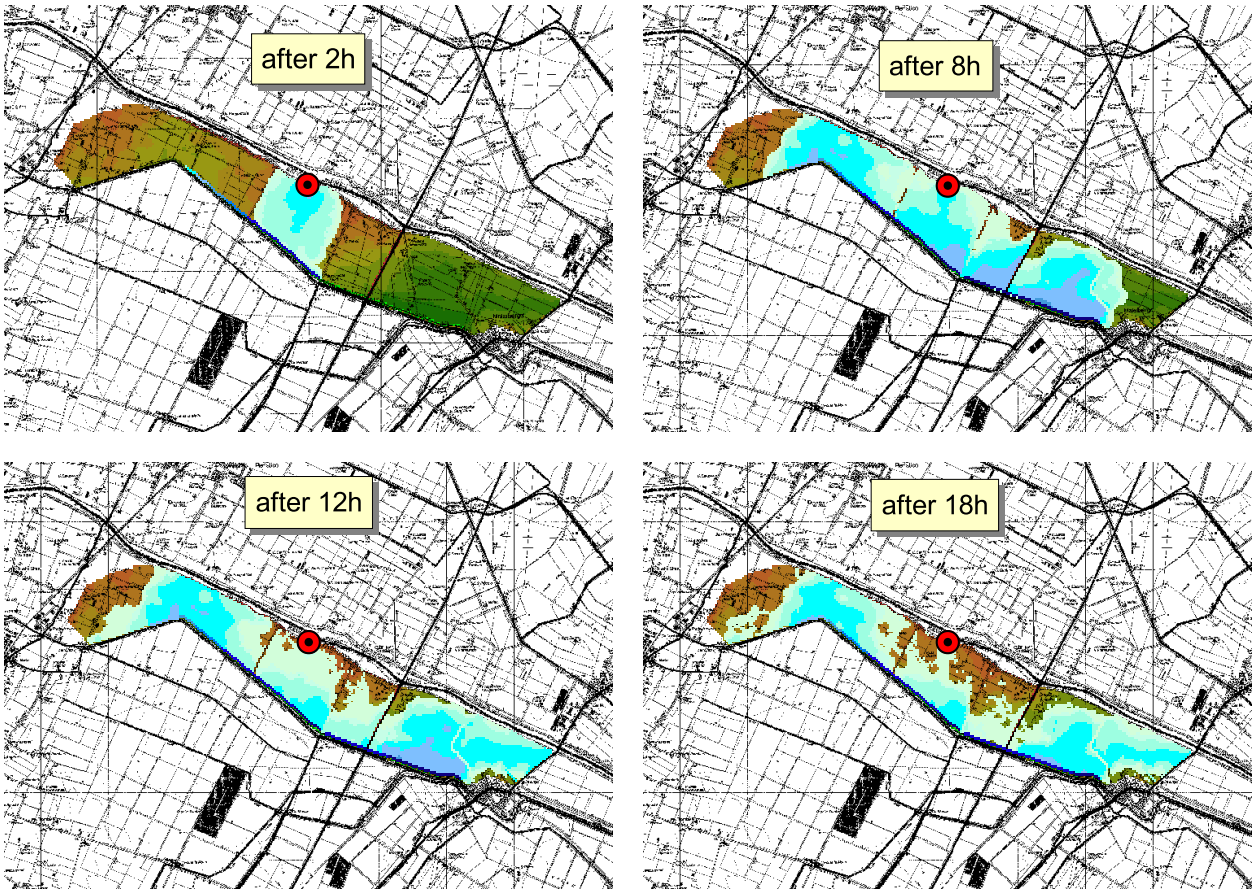

Figure 5.11: time evolution of flood extent (floodplain roughness 0.03 $m^{1/3}s$, channel roughness 0.18 $m^{1/3}s$).

However, the differences between observations and simulations are probably also influenced by the uncertainty of data for model construction and validation. The DTM was obtained from the interpolation of the surveyed points of the regional cartography, while the embankments were manually introduced. Therefore some uncertainty could result with respect to real topography, influencing the timing and entity of volumes overtopping. To have a reference value, Neal et al. (2009a) reported a RMSE of 0.18m for a DEM based on LIDAR surveys.

In addition, some incoherences between high water marks and observed flood extent can be seen:

- cells on west border of the flooded area have higher bed elevation than maximum water levels in point 5, but were observed inundated;
- in the east sector, border cells of the flooded area have higher bed elevation than maximum water levels in point 2;

- the water level in point 16 is considerably higher with respect to neighbour points 27, 28, 29 (differences between 50 and 70cm);

The effective uncertainty of each measurement is difficult to evaluate. It is possible that point measurements derived from sedimentation under estimate water level, given that wrack marks can deposit on the hydrograph receding limb, and not necessarily at peak. In a previous study Neal et al. (2009a) reported a mean underestimation of 0.5m for wrack marks. The observed flood extent derived for aerial photographs could also not correspond to effective maximum extent.

In conclusion, the CA2D model performance can be considered accurate enough for a large scale flood analysis, given the available dataset.

5.2 2008 flood event on the River Po

This test case considers an ordinary flood event occurred in the River Po, in Northern Italy. The area considered in this case study is a 96-km reach of the river between the gauging stations of Cremona and Borgoforte (Figure 5.12). This portion of the river consists of a main channel (around 200-300m wide) and a floodplain (overall width ranging from 400 m to 5 km) confined by two continuous artificial embankments. The middle-lower reach of the River Po is characterized by a system of minor dykes that protect part of the floodplain against frequent flooding. Previous studies demonstrated that this dyke system has a relevant influence on the hydraulic behaviour of the river during major flood events (Di Baldassarre et al., 2009a; Castellarin et al., 2011).

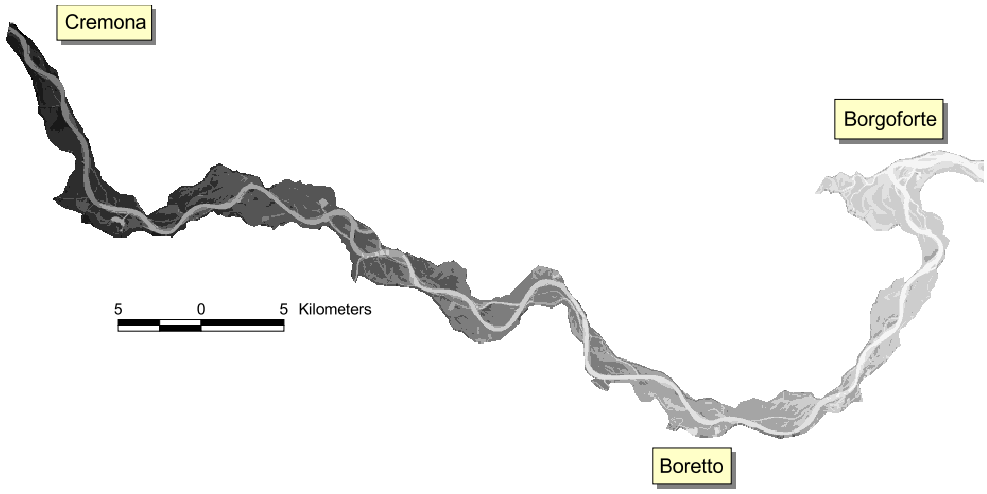

Figure 5.12: DEM of the considered reach of the River Po.

For the present research work, the flood event occurred in May–June 2008 was simulated with the CA2D model. The return periods was estimated to be around 2–3 years. The peak flow at the upstream boundary of Piacenza was 5736 m3/s, while maximum channel

discharge for this reach is about 3500 m3/s (Prestininzi et al., 2011). As a result part of the floodplain was inundated during the event, with relevant 2D flow processes occurring (Di Baldassarre et al., 2009b; Prestininzi et al., 2011). This flood event has been already analyzed in a number of studies with either 1D models (Di Baldassarre et al., 2009b) and 1D2D models (Prestininzi et al., 2011), while 2D models have not been used so far to reproduce the whole event. Although in a similar test case a 2D model is probably not as efficient as a 1D2D model in terms of computation times, the application can provide interesting information about model performance.

5.2.1 Available data

Stage and discharge hydrographs of the event are available from the two gauging stations of Cremona and Borgoforte, at the upstream and downstream ends of the river reach (Figure 5.13). In addition, discharge data are available at the Boretto gauging station, located approximately 30km upstream of the Borgoforte station. The discharge data were converted in stage data using the rating curve available for the Boretto cross section. Although the available records at Boretto include only one measurement each 24h, the long duration and slow propagation of the flood event allows to have enough data between the duration of the event, allowing to reconstruct the intermediate hydrograph.

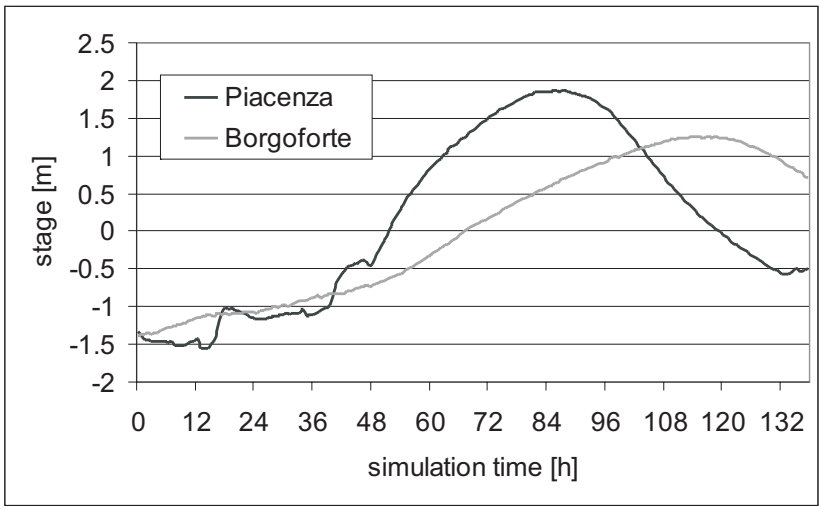

Figure 5.13: upstream (Piacenza) and downstream (Borgoforte) stage hydrographs for the 2008 event.

For the 2008 event a flood extent map is also available. The map derives from a coarse resolution (75 m) ASAR imagery acquired the 1st of June at 9.30 am, one hour before the peak flow at Cremona (Di Baldassarre et al., 2009b). The geolocation error of the ASAR image was estimated to be within 100 m, while it accuracy was not assessed as no other flood extent data were available. Di Baldassarre et al. (2009b) and (Prestininzi et al., 2011) used the satellite image for validating their models, but did not consider the available stage

recording. A 64m resolution DEM was used to describe both the river channel and floodplain areas. The DEM was obtained by resampling the 2 m DEM produced by the River Po Basin Authority (Di Baldassarre et al., 2009b).

5.2.2 Simulation settings

For all the simulations, upstream and downstream boudary conditions are given respectively by the stage hydrographs recorded at Cremona and Borgoforte (Figure 5.13). Since at initial time only the upstream and downstream stages are known, warm-up simulations were run in order to provide the initial stage condition in all the river reach.

As for the River Reno flood event (Section 5.1), a sensitivity analysis was carried out to investigate the influence of roughness coefficients. Given the uniform morphologic configuration and land use along the reach, separate roughness values were used for the channel and floodplain, with the assumption of no spatial variation within these zones. The same assumption was made in previous studies on the same reach (Di Baldassarre et al., 2009b; Prestininzi et al., 2011).

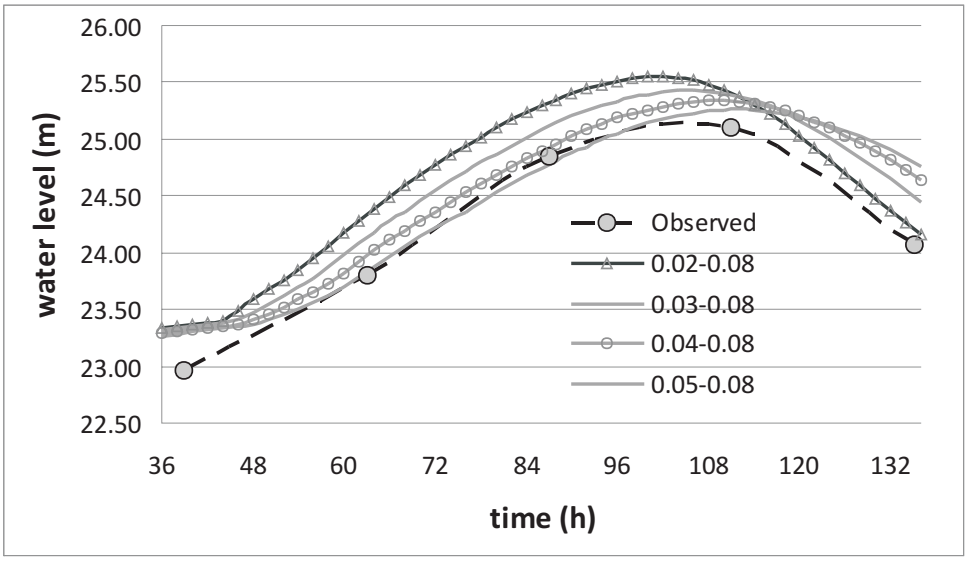

Figure 5.14: comparison between simulated and observed water levels at Boretto gauging station; results refer to simulation with a fixed channel roughness and a variable floodplain roughness (expressed in $m^{1/3}s$).

5.2.3 Results and discussion

The graphs in Figures 5.14 and 5.15 show simulated and observed water levels at the gauging station, and describe the different influence of floodplain and channel roughness. The large error in the model profiles before $t = 48h$ depends on the difficult setting of the warm-up

simulation: due to the considerable lenght of the reach, the upstream condition needs more thant 30h to propagate up to the Boretto station.

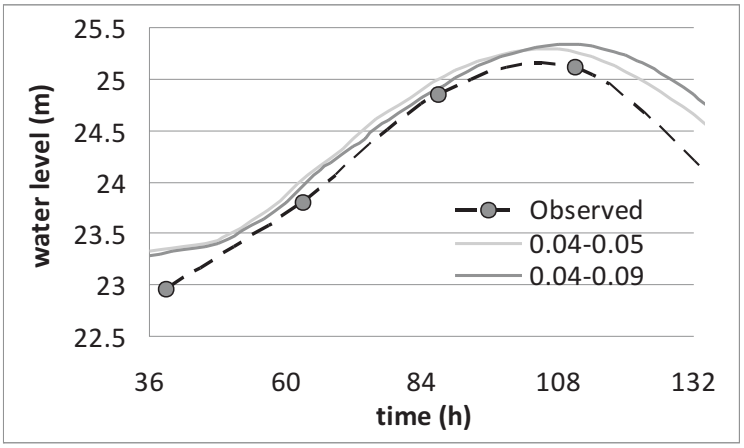

Figure 5.15: comparison between simulated and observed water levels at Boretto gauging station; results refer to simulation with a fixed floodplain roughness and a variable channel roughness (in $m^{1/3}s$).

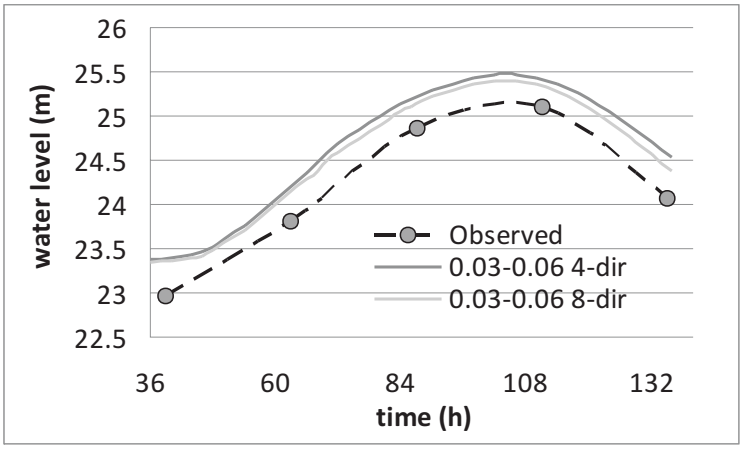

Figure 5.16: comparison between simulated and observed water levels at Boretto gauging station; profiles are referred to 4 and 8 direction grids with the same roughness coefficients (in $m^{1/3}s$).

As expected, model results are more sensitive to channel roughness, due to the predominance of channel flow: as the Manning coefficient increases the peak is delayed and the water level at the peak is lowered down. Floodplain roughness has a smaller influence on falling limb stage while and peak timing. The overall performance of the model is good: excluding the first phase of the raising limb the error on water stage using roughness values of 0.03 and 0.04 $m^{1/3}s$ is generally well below 50cm, and well below 10% of the observed water depths. These values are comparable with those obtained by Di Baldassarre et al. (2009b) in previous applications with HEC-RAS on the same reach of the River Po.

Some simulations were performed using both 4- and 8-direction link networks. The differences in terms of stage and wawe celerity are not relevant, (Figure 5.16), while run times are halved when the 4 direction grid is used.

The good results obtained by comparing observed and simulated stages are in sharp contrast with the poor model performance resulting from flood extent validation. The model computes a significantly larger flooded area (Figure 5.17), and the performance indexes P1 and P2 (5.1) have very low values, indicating a large discrepancy between observation and simulation. It should be noted that similar poor results were obtained also by Di Baldassarre et al. (2009b) and Prestininzi et al. (2011).

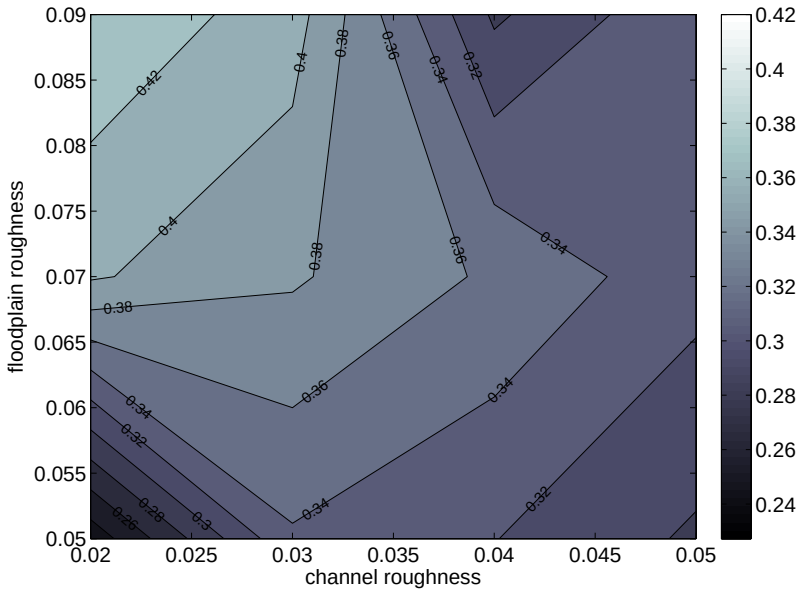

Figure 5.17: normalized error of simulated flood extent with respect to observed extent.

However, these results can be explained considering the high uncertainty on the reference observed map. As can be seen in Figure 5.18 the map is affected by significant scattering, with a large number of flooded pixels being isolated. On the contrary in the CA2D results the flooded area is continous, as would be expected since the maps are both referred to the raising limb of the flood wave.

An estimation of the error due to scattering in the observed map can be done at the Boretto cross section using the stage records. Assuming a constant stage on the cross section extrapolated from the DTM, it can be seen that the wetted area indicated by the satellite image is inconsistent with the geometry, while the result of the CA2D model is much more consistent (Figure 5.19). This can be seen also in the comparison on a cross section located 1km upstream (Figure 5.20, see Figure 5.18 for the exact location with respect to Boretto section). This errors have to be added with the mentioned georeference error.

In conclusion, the analysis of observed data suggests that in this case the satellite image is probably not a reliable benchmark for model validation, while a more traditional data

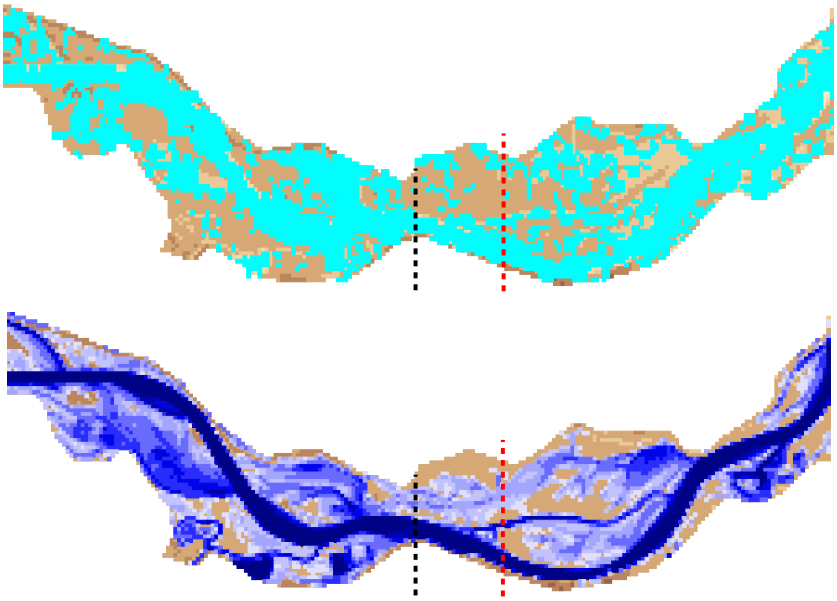

Figure 5.18: comparison between simulated and SAR flooded areas; the gauging cross section (Figure 5.19) and the upstream section (Figure 5.20) are indicated respectively by the red and black dashed lines; the model results are referred to simulation with Manning coefficients of 0.08 $m^{1/3}s$ for floodplain and 0.04 $m^{1/3}s$ for the channel.

source like observed water levels seems more consistent. This confirms the need for multiple data sources when evaluating model performances.

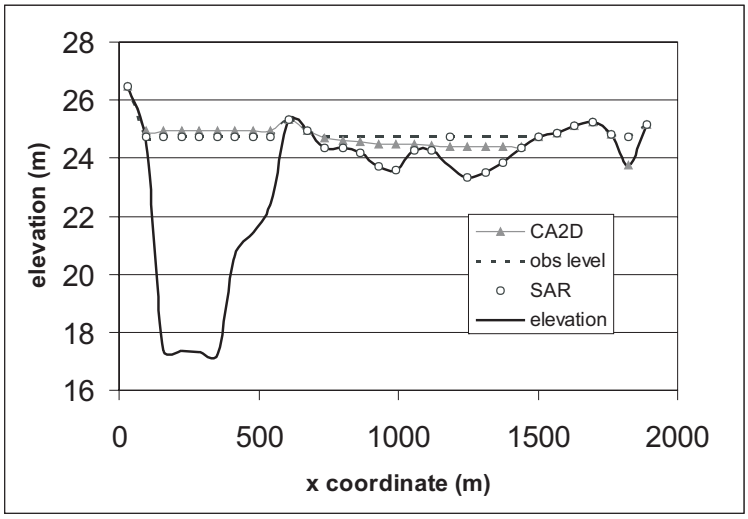

Figure 5.19: comparison between satellite data, simulated and observed water levels at Boretto gauging station; the observed stage is set as the water level of satellite data; CA2D results are referred to simulation with 0.04 $m^{1/3}s$ (channel) and 0.08 $m^{1/3}s$ (floodplain) roughness values.

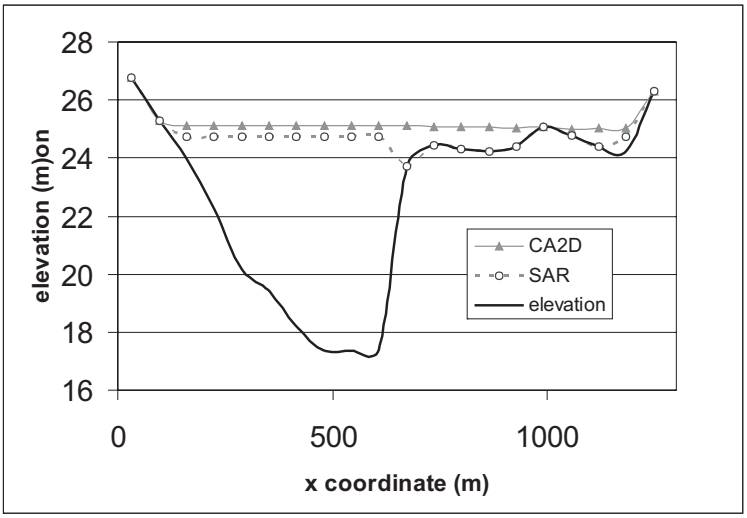

Figure 5.20: comparison between satellite data and simulated water levels 1km ustream of Boretto gauging station (Figure 5.18); CA2D results are referred to simulation with 0.04 $m^{1/3}s$ (channel) and 0.08 $m^{1/3}s$ (floodplain) roughness values.

5.3 Flood risk mapping on the River Ubaye

The case study described in this section is part of the research work carried out for the European project KULTURisk (*www.kulturisk.eu*). The area is located in the upper part of the valley of the River Ubaye, in the French Alps. The study area includes the river bed and the sorrounding floodplain, which is partly occupied by the urban area of Barcelonnette (Figure 5.21).

The river is mainly characterized by a large unconfined gravel bed, typical of mountain rivers. However, near the urban area the river is canalized and constrained by embankments in a narrow trapezoidal artificial section. Therefore the test area includes both the artificial bed reach and portions of bed in natural conditions upstream and downstream.

Barcelonnette was affected by a major flood event in 1957, that caused the flooding of a significant portion of the village. After that event, the existing system of dykes were reinforced and heightened. In 2008, another significant flood event occurred in the River Ubaye. The water remained within the river bed, but the recorded water levels were the highest since the 1957 flood. This is the event that has been simulated with the CA2D model.

Although 1D flow routing is not an usual application for a 2D model, this case provides a good benchmark for testing the ability of CA2D to reproduce 1D flow over a steep slope, with alternance of subcritical and supercritical flow and considerable changes of river cross section. Given the presence of dykes, in this case the use of a 2D–based model could be advisable to simulate both in–bed and floodplain flow and the consequent complex interaction.

It is worth noting that most applications of 2D models in literature are carried out on flat floodplain areas, especially when mixed 1D-2D flows are simulated. Applications to

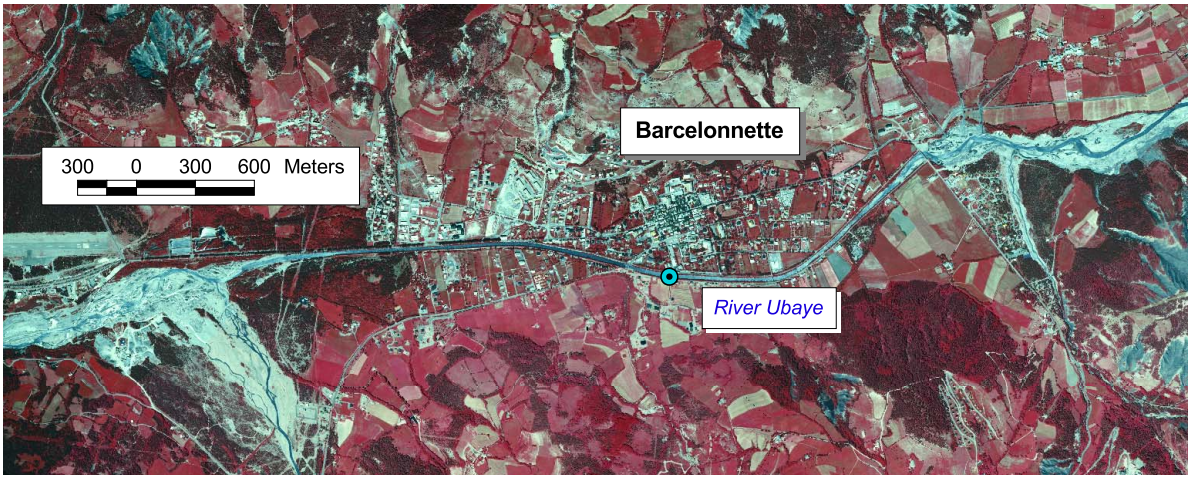

Figure 5.21: aerial photograph showing the study area; the natural and artificial reaches of the River Ubaye and the urban area of Barcellonette are visible; the gauge point is marked.

mountain valleys are rare, especially for reduced complexity models, therefore the present test case would provide valuable information.

As for cases described in Sections 5.1 and 5.2, available observed data allow for model calibration and validation.

In the research work carried out for the KULTURisk project, the CA2D model was used also to produce probabilistic flood maps for the Barcelonnette area (Dottori et al., 2011). An ensemble of hydrographs based on the estimation of the 1957 hydrograph was simulated, and a large number of different flood maps were obtained. Then the maps were integrated to obtain a single probabilistic map, using an established procedure described by Di Baldassarre et al. (2010b). The resulting map was evaluated using the value of information approach (Dottori et al., 2011). This part of the research is not described here in detail, since it was not possible to evaluate the results due to the absence of observed data for the 1957 event. However, some results are used to evaluate the performances of different model configurations.

5.3.1 Available data

The topographic information for the test site consists of a 10m DTM developed by the Observatoire Multidisciplinaire des Instabilités de Versants (OMIV, $http://omiv.osug.fr$), and a detailed survey of the canalized reach, realized within the KULTURisk project. These topographic datasets were merged together to have an accurate reproduction of the dykes and the river bed and the dykes.

Besides the topgraphy, a land use map dated 2000 was available, together with the observed stage hydrograph at the gauging station of L'Abattoir, located on a bridge inside the urban area of Barcelonnette (Figure 5.21). In addition, discharge–water level measurements used for calibrating the rating curve at the gauging station are available. The calibration of

the rating curve was performed the year before the considered 2008 event.

5.3.2 Simulation settings

In order to obtain the upstream boundary condition for the simulation, the available stage hydrograph was converted into a discharge hydrograph using the rating curve, and used as the upstream condition. Although such operation is not theoretically correct, it can be considered acceptable for the present case. The bed slope is steep in all the considered reach (more than 0.5%), and this means that the flow condition can be considered almost kinematic, and the flood wave should travel along the reach without significant attenuation. Therefore, the hydrograph at the Abattoir cross section was simply anticipated by estimating the time of delay between the upstream and the gauging station cross sections. It also worth noting that due to the kinematic condition the rating curve should not be affected by a significant hysteresis.

The Manning coefficient for the canalized reach was estimated by applying the uniform flow formula to the available coupled measurements of stage and discharge. For water depths over 2m, a value of 0.037 $m^{1/3}s$ was estimated. For the natural portions of the reach a value of 0.05 $m^{1/3}s$ was set. Although effective roughness can be different when evaluated in different flow conditions (Horritt, 2002; Hunter et al., 2007), given the regularized section it is reasonable to assume a constant roughness value for high discharge rates. Given these friction coefficients, some simulations with simple wave hydrographs were used to estimate the wave travel time between the upstream boundary and the gauging station, resulting in 1 hour delay. The calibration showed also that the assumption of large rectangular section within the model is consistent in this case, with a depth/width ratio below 0.1.

Since this case study deals with a 1D flow over a narrow channel with considerable changes of direction, the simulations have been performed using both 4 direction and 8 direction link netwoks, in order to test the reliability of each grid configuration under such flow conditions.

A critical flow was set as downstream boundary condition. Since the area of interest is limited to the canalized reach, and given the steep slopes, such a choice do not influence model results.

5.3.3 Results

Figure 5.22 shows the comparison between simulated and observed water dephts at the gauging station using both 4- and 8-direction grids. As can be seen, the model computed slightly lower water depths, which can be due to the wave attenuation. Attenuation is higher in 4 direction than in 8 direction grid, whereas the hydrograph profile is well reproduced by both link networks.

Figures 5.23, 5.24 and 5.25 illustrate the model results in the upstream part of the study reach, in terms of maximum water depth, velocity and Froude number. It can be seen that where the river bed narrows a transition from subcritical to supercritical condition occurs. As discussed in Section 4.5, the CA2D model is not able to reproduce the exact profile of

flow transitions, therefore an error in computed depths is expected, although its magnitude can not be evaluated.

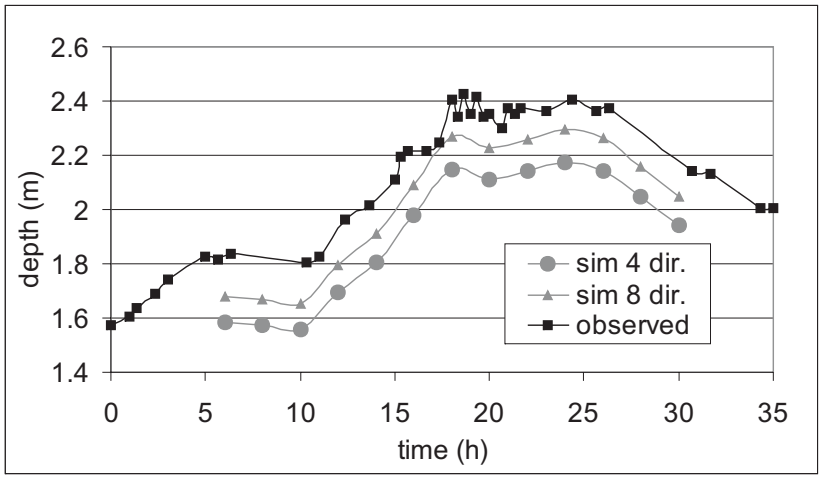

Figure 5.22: comparison between observed water dephts at Abattoir gauging station and CA2D results using 4 and 8 direction grids.

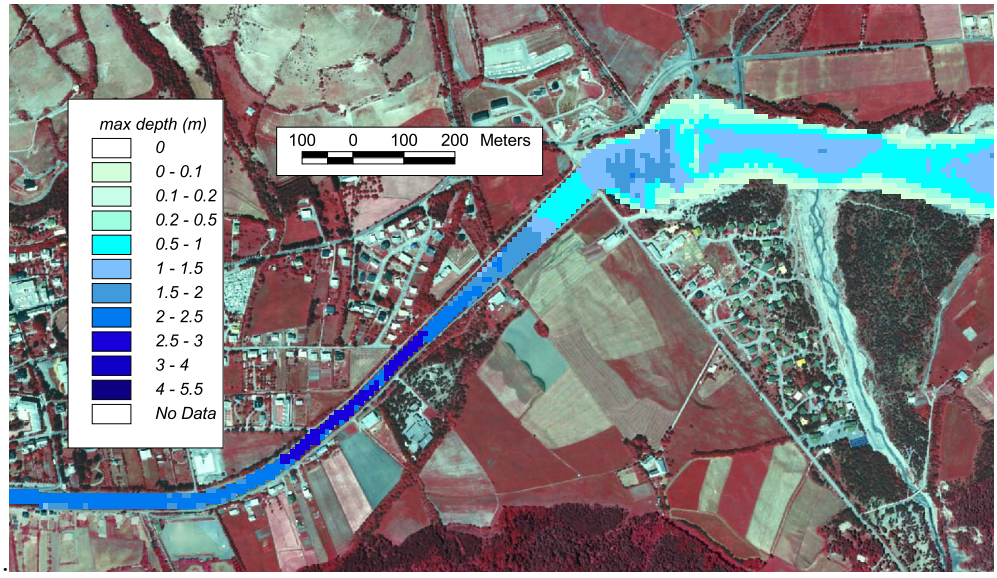

Figure 5.23: maximum water depths computed by CA2D in the upstream part of the test site (4 direction grid).

The high velocity values computed are consistent the available couples of stage and discharge observations at the gauging cross section. The largest measured value of discharge is 274 m^3/s, corresponding to a 2.7m depth; given an average section width of 26.5m ,the resulting velocity is 3.8 m/s, while the computed maximum velocities at the gauge section

(for a 230 m^3/s discharge) are 3.7 m/s and 3.6 m/s, respectively for the 4- and 8-direction grids. Again, a detailed evaluation of the velocity field would require specific data.

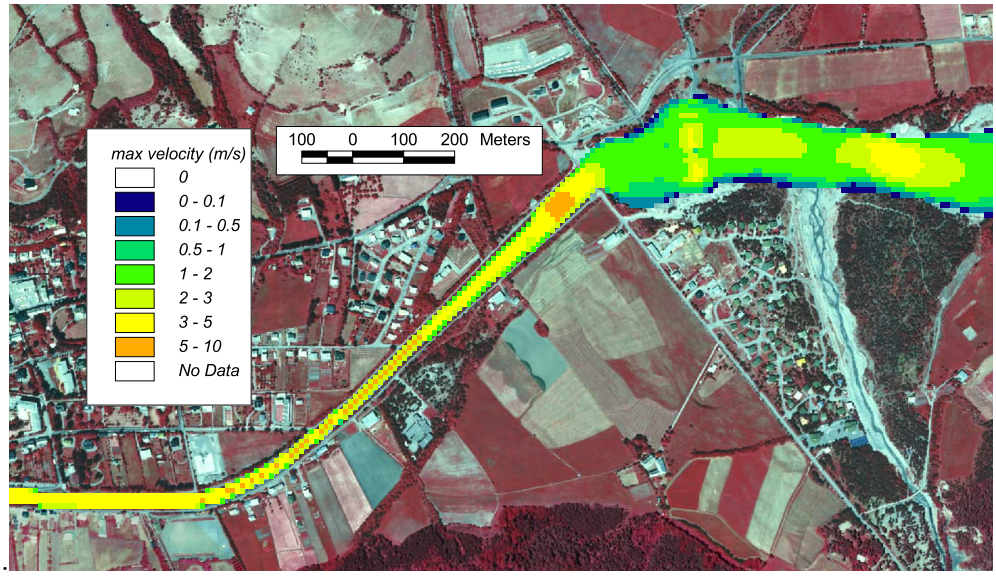

Figure 5.24: maximum velocities computed by CA2D in the upstream part of the test site (4 direction grid).

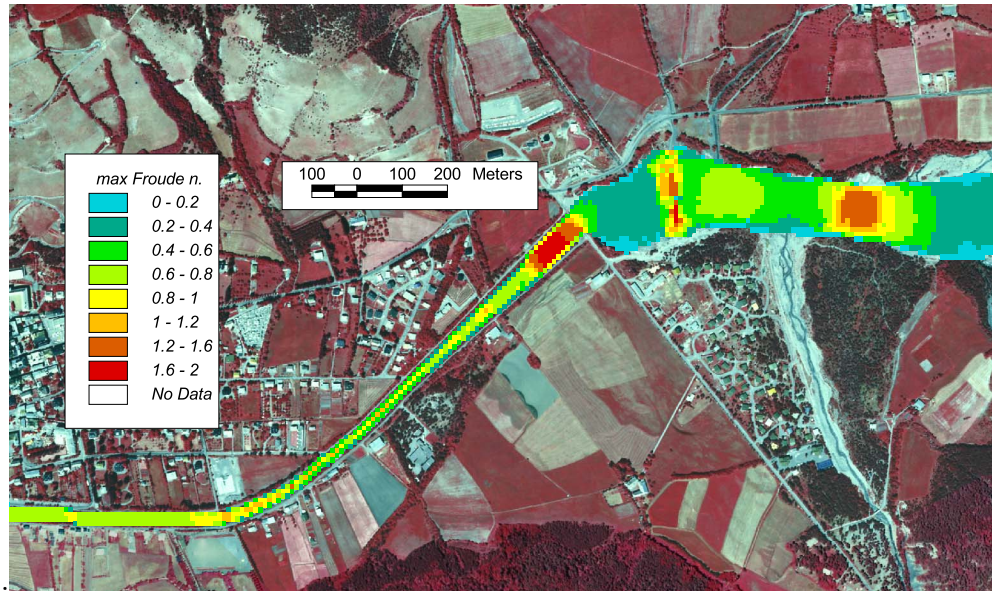

Figure 5.25: maximum Froude number computed by CA2D in the upstream part of the test site (4 direction grid).

In conclusion, the CA2D model provided reliable results despite the complex 1D flow conditions. The available data were not sufficient to undertake an in–depth model evaluation,

however, results suggest that the model should be suited to simulate effective flood events involving mointain river floodplains.

5.3.4 Discussion

The better performance of the 8 direction grid in this case is in partial contraddiction with the results of numerical case 7 (Section 4.5). Such a difference could depend on the diagonal orientation of a significant part of the river reach, that probably complicates flow representation within a 4 direction grid.

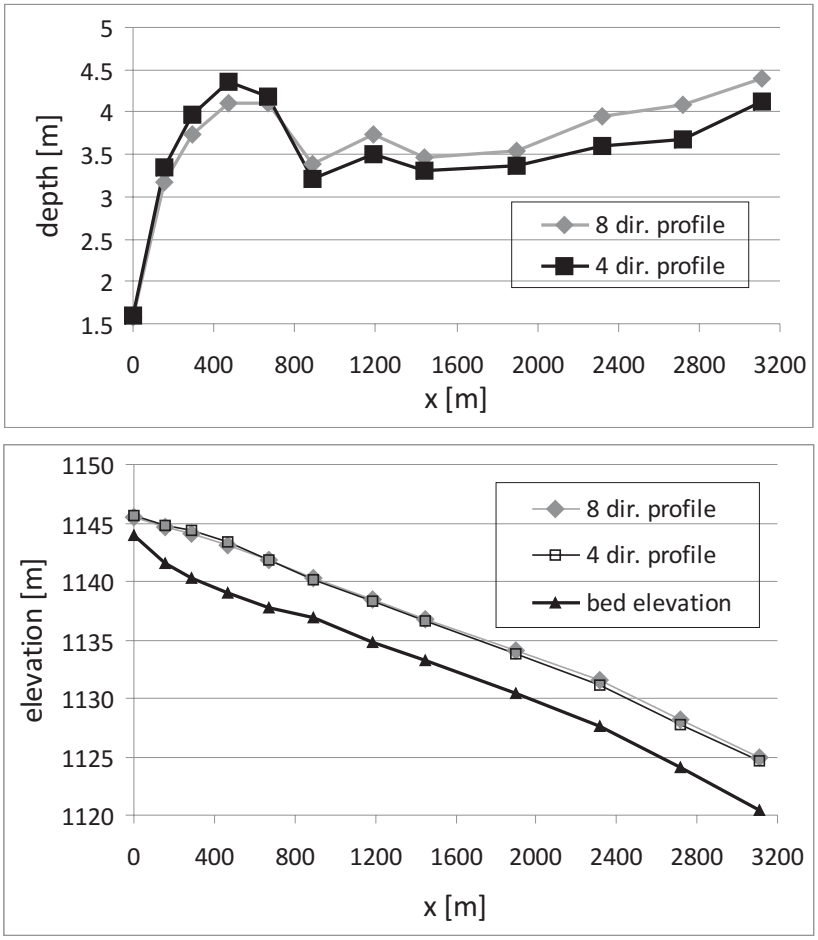

Figure 5.26: water depth and water level profiles computed by the CA2D model for a syntetic flood event, using 4–dir and 8–dir link networks.

Although in this case the difference with the 4 direction grid is reduced (Figure 5.22), during events with higher discharges such differences could be more relevant. In order to investigate this issue, a number of simulations using syntetic triangular hydrographs with high peak values were analyzed, comparing stage profiles computed from the 4 and 8 direction grids. These simulations are taken from the work for the KULTURisk project. Figure 5.26 illustrates an example of computed stage profiles. A peak discharge of 444 m^3s^{-1} with a

base discharge of 90 m^3s^{-1} and time to peak of 20 hours were used. Figure 5.26 represents results after 21 hours, therefore with nearly maximum water levels. It is worth noting that a similar peak discharge was estimated for the 1957 event.

As can be seen, in this case the difference between the two grids is more relevant and, most important, such a difference can influence flooding pattern and timing. In this specific simulation, the water overtops the dykes at different locations depending on grid configuration 5.27. In other simulations, thedifferent grid configuration could also determine a different timing for the inundation of the areas out of the river bed.

According to these results, the 8 direction link network seems to be more appropriate to simulate 1D flow in reaches characterized by narrow cross sections and changes in flow orientation. In order to improve model performance in similar test cases, an integration of a 8- and 4 direction grids respectively for the river and the floodplain could be a good solution.

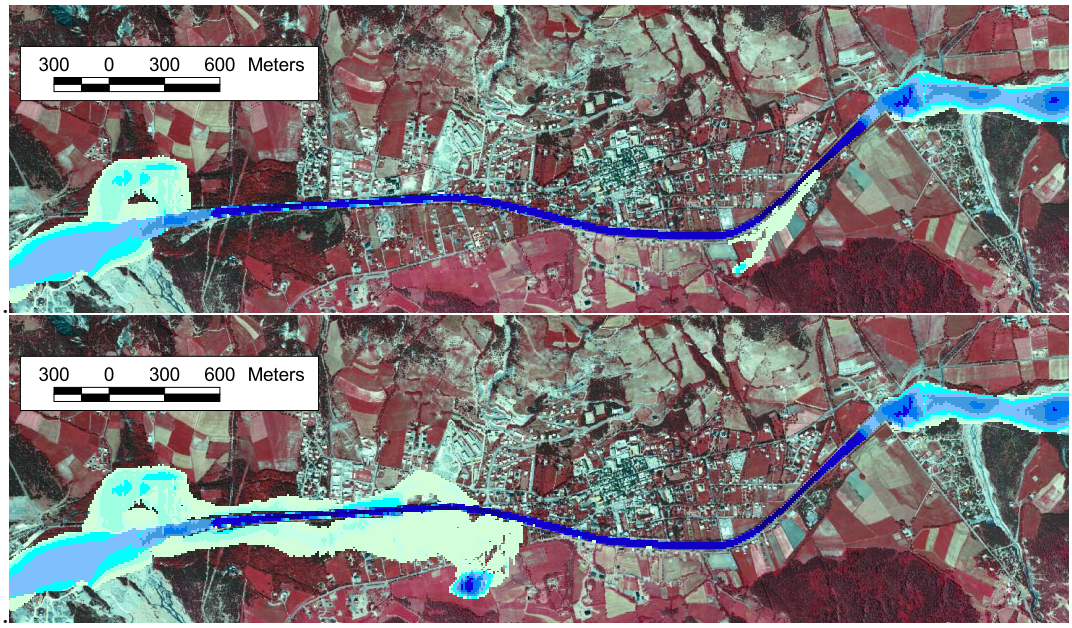

Figure 5.27: maximum flood extent computed by the CA2D model for the same syntetic flood event, using the 4–dir (top) and 8–dir (bottom) link networks.

5.4 Physical experiment of urban flood inundation

The hydraulic modelling of flood events involving urban areas has become an important topic of research in the recent years. Despite the considerable number of dedicated works (Fewtrell et al., 2008; Hunter et al., 2008; Mignot et al., 2006; Schubert et al., 2008; Gallegos et al., 2009; Neelz and Pender, 2010), the degree of complexity needed by a model to provide reliable simulations of urban flood events is still under debate. It is generally recognized that these events are a difficult benchmark for any hydraulic model, due to the complexity of topography and flow dynamics which characterise urban environments. The use of complete

2D models based on full SWE should be recommendable (Cunge, 2003; El Kadi et al., 2009), but in most of the cases the scarcity of observed data prevents an adequate evaluation (Hunter et al., 2007; Neal et al., 2009a). As a consequence, many research works used reduced complexity models for simulating urban flood events, exploiting their simplicity of development and application and their low data requirement (Yu and Lane, 2006a; Hunter et al., 2008; Fewtrell et al., 2011).

However, caution should be used. Reduced complexity models are designed to simulate only part of the flow processes, therefore risks of inappropriate application are likely to arise. Indeed, detailed analyses of the effective ability and limitation of simplified models in reproducing floods processes are still rare, especially for urban environments.

Hunter et al. (2008) compared a number of 2d models of varying complexity in a single urban flood scenario, and observed that the overall performance of reduced complexity models were comparable to more complex models. Prestininzi (2008) used a simplified 2D model, based on parabolic equations, to reproduce an experiment carried out in a physical model, observing a generally good performance. Neelz and Pender (2010) performed a detailed analyses of different 2d models in a number of numerical cases, including dam break physical experiments.

Considering this framework, the use of laboratory experiment data can be seen as a good solution for evaluating reduced complexity models. Experimental data allow the possibility to test model performances in detail, since flow conditions may be accurately controlled and reliable data for model calibration and evaluation are available Sanders (2008); El Kadi et al. (2009). Therefore, in this test case, the CA2D model is used to simulate different experiments of urban flood, carried out using a physical model.

5.4.1 Case study description

The description of present case is taken from Dottori and Todini (2012). For reasons of conciseness, not all the simulations performed in that paper are here described.

The model has been tested by reproducing the results of a number of experiments, included in the IMPACT European project (Investigation of extreMe flood Processes And unCerTainty, Alcrudo (2004)). These experiments are part of a broader study of flood propagation in urban areas, and have been described in detail by Testa et al. (2007). In the experiments, a series of concrete blocks was placed in an instrumented physical model of a short reach of the Alpine Toce River at a 1:100 scale, to simulate the ooding of an urban district. Two building configurations were tested: either aligned in a regular pattern, or placed in checker board (staggered) layout. Figure 5.28 shows the aligned and staggered layouts.

Flooding of the model is achieved by rapidly raising the water level in a feed tank located at the upstream end of the model. Different hydrographs were used in the experiments; this paper only includes the results for low and medium hydrographs described by Testa et al. (2007). In Figure 5.29 the hydrographs are reported. The average terrain slope is between 2% and 3%, with local values in the channel up to 20%. Time series of water depth at

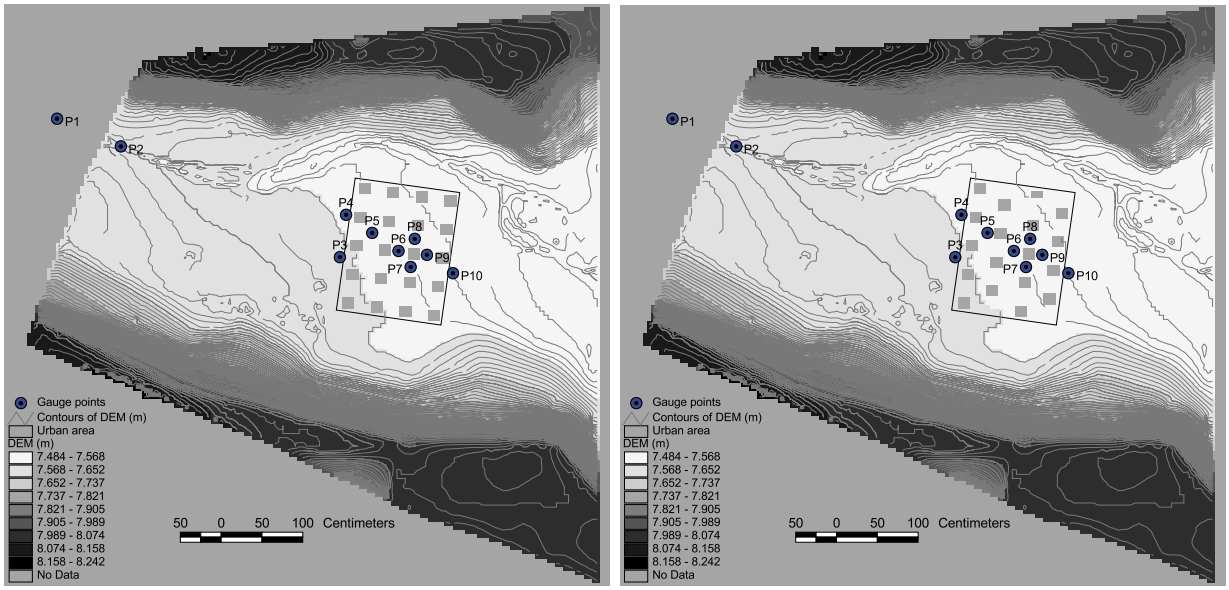

Figure 5.28: digital elevation models of the physical model with the position of gauge points. The aligned (left) and staggered (right) building layouts are represented.

different locations were recorded for all the configurations of the model city, surrounding terrain and flooding conditions. These data provide exhaustive information on spatial and temporal flow dynamics and therefore allow a detailed evaluation of the model performance.

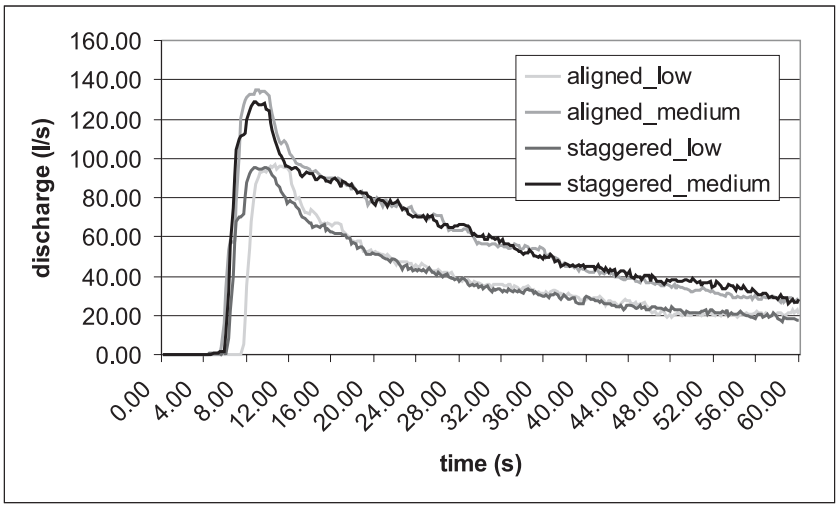

Figure 5.29: discharge hydrographs used in the simulations.

Testa et al. (2007) provided a general description of flow processes. In all the configurations, the presence of the urban district produced a strong hydraulic jump immediately upstream of the buildings, and a complex ow pattern inside the urban district. Differences in water depth readings at various locations among the buildings arose from the complexity

of the flow pattern induced by the obstacles. However, as water progressed further downstream into the city, friction and reections damped out the wave pattern and the ow became more uniform, resembling that in a porous medium. In addition, the authors observed that the differences between observed water depths inside the urban district depended on the magnitude of incoming flow, so that flow was more uniform for low flow simulations.

The simulations of the described experiments have already been undertaken in previous works by Guinot and Soares-Frazão (2006); Soares Frazão et al. (2008); Sanders et al. (2008). All these authors adopted various finite volume schemes to solve the fully dynamic shallow water equations (SWE); in addition, they developed modified versions of the SWE with a porosity parameter, to represent the effects of obstructions not explicitly resolved in the grid. The numerical scheme by Soares Frazão et al. (2008) included also a shock-capturing, Godunov-type algorithm. El Kadi et al. (2009) applied a fully dynamic model to other experiments based on the same physical model with a different configuration, described as well by Testa et al. (2007). In those cases the geometry was modified by inserting two lateral walls along the river valley, in order to further constrain the flow through the urban district. As can be noticed from the mentioned research works, so far the IMPACT experiments have not been analysed using diffusive models. The main reason is that these experiments reproduce severe urban flood events; in fact, given the1:100 scale of the physical model, the rescaled water levels would be several meters high with considerable velocities even in the low flow simulations, as the generalized supercritical flow conditions suggest. Therefore, diffusive models are expected to provide an incomplete representation of flow processes, given the absence of inertial terms and shock-capturing methods in the governing equations. Nevertheless, the application in these cases could be extremely useful to investigate diffusive model limitations, and quantifying the errors that could be expected. As mentioned before, a similar study was carried out by Prestininzi (2008), who applied a diffusive 2D model on the same physical model here considered. However, in the present paper different experiments of the IMPACT project are used; in particular, flow conditions are different and the idealized urban district that constitutes the main focus of the present analysis was absent in the cases considered by Prestininzi.

5.4.2 Setup of numerical experiments

The physical model has been represented with a regular raster grid with a 5 cm resolution (Figure 5.29). In simulations with the aligned or staggered layout, buildings are represented by eliminating the correspondent cells of the computation grid, (each building has a size of 3x3 cells) so that they are completely impervious. The original position of the buildings is slightly rotated in respect to the axes of the chosen regular grid, therefore they could not be exactly reproduced. However, the difference is small in respect to the relative position of gauge points.

Table 5.1 illustrates the relative position of the gauge points with respect to staggered and aligned building configurations. Gauge 1 is located out of the test area, and measures the water level in the tank used to create the upstream hydrograph. Gauge 2 is located on

the upstream border of the test area: since the available data did not include a complete description of the upstream boundary condition, the water level in gauge 2 was used with the hydrographs of Figure 3 as additional boundary condition for the CA2D model. Therefore, only the records for gauges from 3 to 10 are here used to evaluate model performance. The downstream boundary conditions is given by a uniform flow condition.

Gauge point	Position (aligned grid)	Position (staggered grid)
1	water tank	water tank
2	boundary of study area	boundary of study area
3	upstream (road)	upstream (road)
4	upstream (building)	upstream (building)
5	road	in front of building
6	behind building	in front of building
7	road	road
8	road	road
9	behind building	behind building
10	dowmstream (road)	downstream (behind building)

Table 5.1: relative position of gauge points in the two grid configurations.

Both the inertial and the diffusive version of the model were applied, but only the diffusive version of the model was able to provide results. In all the simulations, the inertial version was subject to strong increasing oscillations that destroyed the solution stability, like in numerical case 7 (Section 4.5).

5.4.3 Results: simulations with aligned buildings

The first simulation with this configuration was run with a uniform Manning roughness coefficient of 0.0162 $m^{1/3}s$, as suggested by Testa et al. (2007). Figures 5.30, 5.31, 5.32 show respectively the water depth, velocity and Froude number values at different time steps. In order to explore the model sensitivity to roughness parameter, more simulations were carried out for each discharge hydrograph (low and medium), using roughness values ranging from 0.02 to 0.04 $m^{1/3}s$.

The analysis of time graphs in Figures 5.33 and 5.34 and errors reported in Tables 5.2 and 5.3 reveals the limitations of the CA model in reproducing the experimental results. Generally speaking, it can be observed that the water depths computed by the model inside the urban district are much more uniform than observed values. This indicates that the model is not able to capture the complex interaction of obstacles with the flow, such as the blockage and wake effects. In particular, the hydraulic jump profile upstream of the urban district is not represented by the model, as the water depths are much lower than observed values in gauge points 3 and 4. The calibration of the roughness coefficient improves the results, but can only partially compensate for model limitations.

The water levels computed in gauge points show a faster flow propagation with respect to observed levels (Figures 5.33 and 5.34). However, an earlier wave arrival time was reported

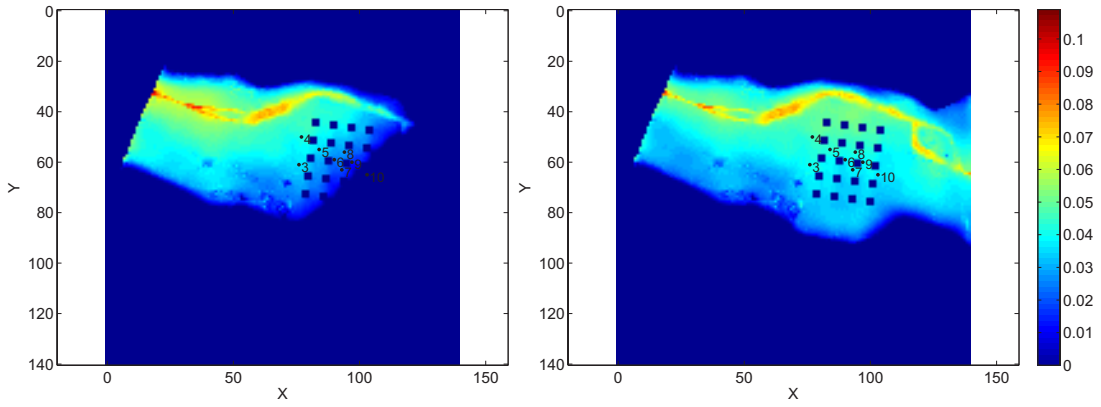

Figure 5.30: water depths (in m) after 9 s (left) and 15 s (right); simulation with roughness value of 0.0162 $m^{1/3}s$, aligned buildings configuration and medium hydrograph.

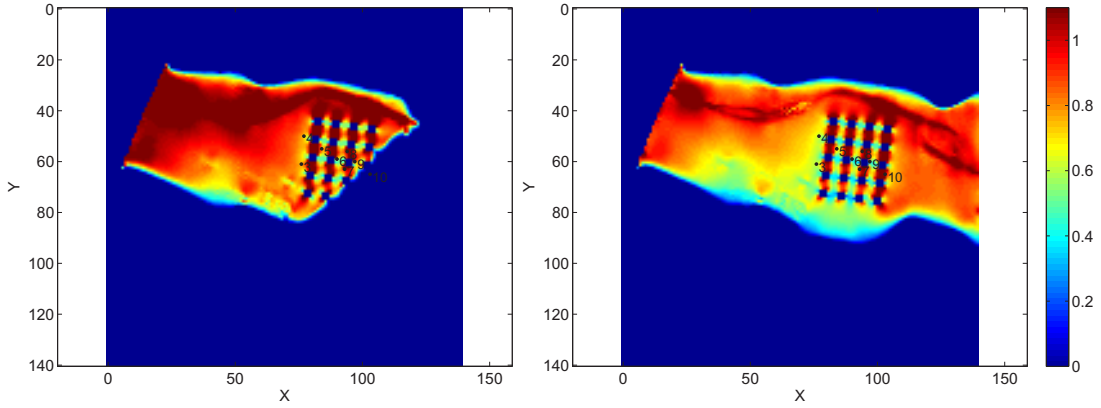

Figure 5.31: velocities (in m/5) after 9 s (left) and 15 s (right); simulation with roughness value of 0.0162 $m^{1/3}s$, aligned buildings configuration and medium hydrograph.

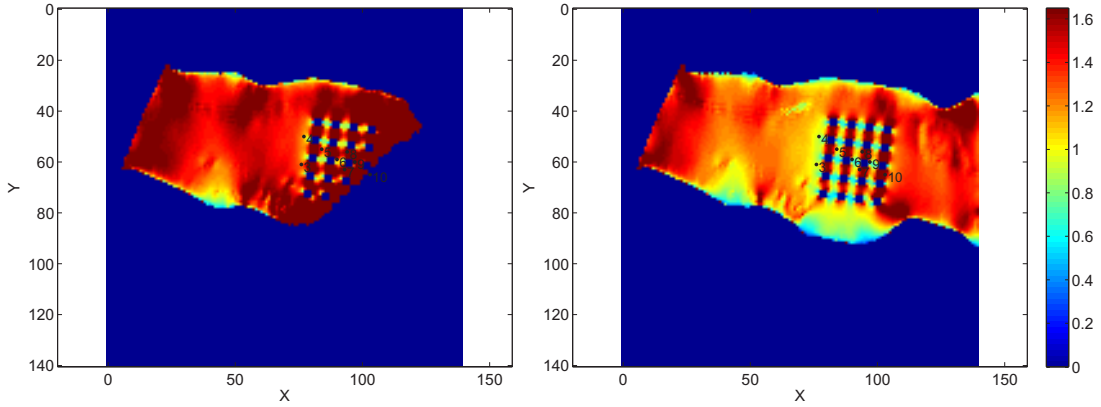

Figure 5.32: Froude number after 9 s (left) and 15 s (right); simulation with roughness value of 0.0162 $m^{1/3}s$, aligned buildings configuration and medium hydrograph

also by Soares Frazão et al. (2008) and Sanders et al. (2008) when using fully dynamic SWE. The authors hypothesized that the time shift is probably due to the difficult definition of the upstream boundary condition (see Section 5.4.2). Wave front celerity could also be influenced by grid resolution, especially over dry bed; Yu and Lane (2006a) and Dottori and Todini (2011) observed a faster propagation of the wave front with coarse grids, due to the approximated discretization of the model partial differential equations over the computation grid.

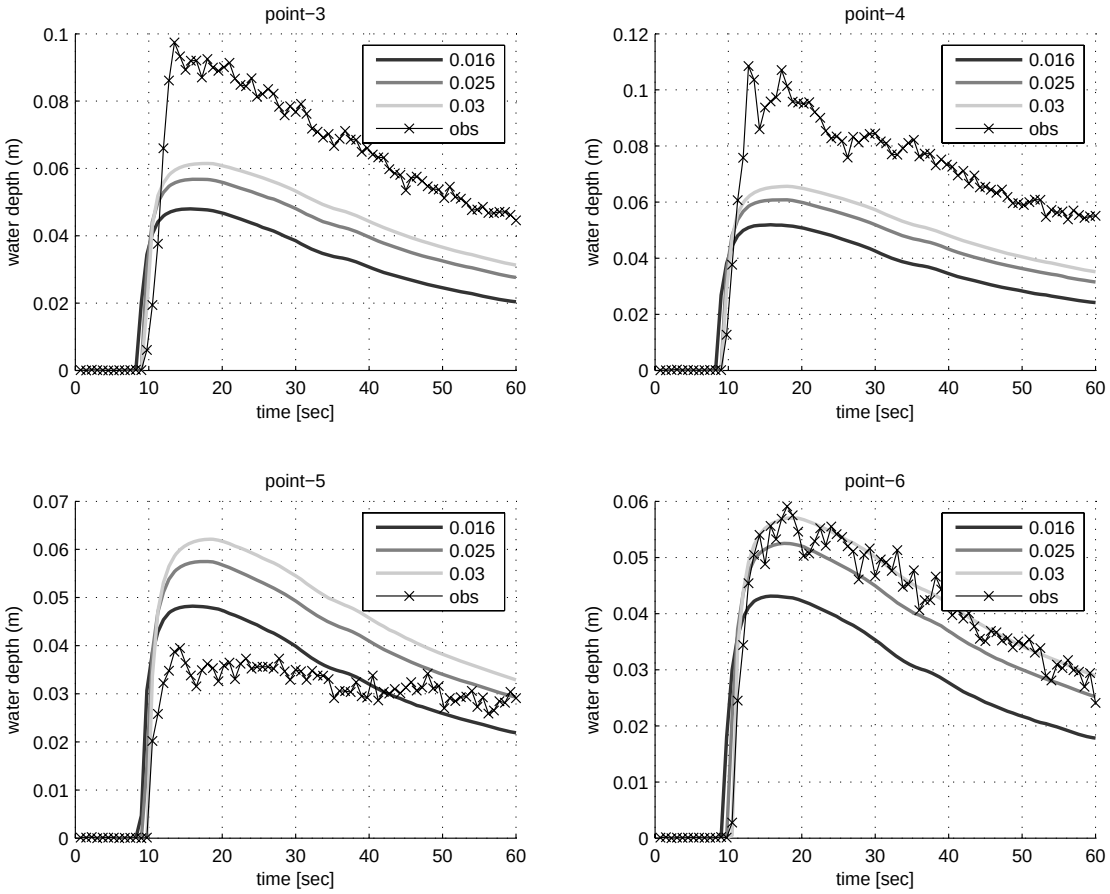

Figure 5.33: comparison of computed and observed water depths with different roughness values in gauge points from 3 to 6 (aligned buildings configuration and medium hydrograph).

The model performance improves as the flow progresses downstream inside the urban area, where the flow condition is more uniform: for points 6, 7, 8, 9 the average error is below 20% for a roughness value of 0.025 $m^{1/3}s$. Finally, downstream conditions in point 10 are quite well reproduced with low roughness values. It is also interesting to note how the computed Froude number agreed with observed processes, indicating a transition to subcritical flow upstream of the urban district (Figure 5.35).

It is interesting to note how changes in roughness coefficient modify the simulation of the flow processes within the model: as roughness is increased model results for points 3

and 4 improves, while the opposite occurs for points 5 and 10. In particular, the use of a roughness value between 0.025 and 0.03 $m^{1/3}s$ improves the model performance in terms of overall error.

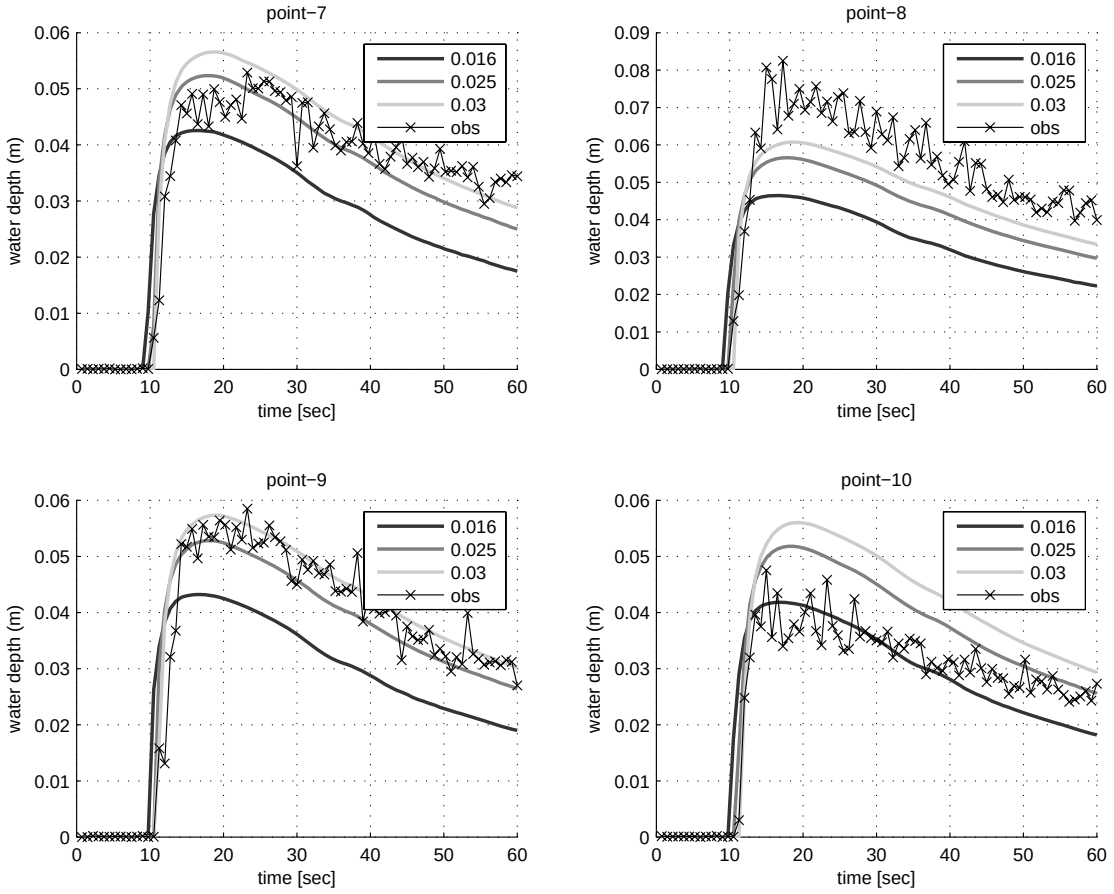

Figure 5.34: comparison of computed and observed water depths with different roughness values in gauge points from 7 to 10 (aligned buildings configuration and medium hydrograph).

It should be noted that the Froude number decreases with the increase of roughness coefficient; for values greater than 0.025 $m^{1/3}s$, the model indicates a subcritical flow in all the area upstream of the urban district, contrary to the physical model (Figure 5.35). However, since the diffusive equations are not able to reproduce sharp flow transitions, changes in model results are gradual.

Finally, it is worth noting that the magnitude of hydrograph does not affect significantly the model performance, as normalized RMSE are similar both for low and medium hydrograph (Table 5.3) with the exceptions of point 5 and 10, where higher errors are computed by the model if the medium hydrograph is used. This is probably due to the fact that flow processes were similar in both the experiments.

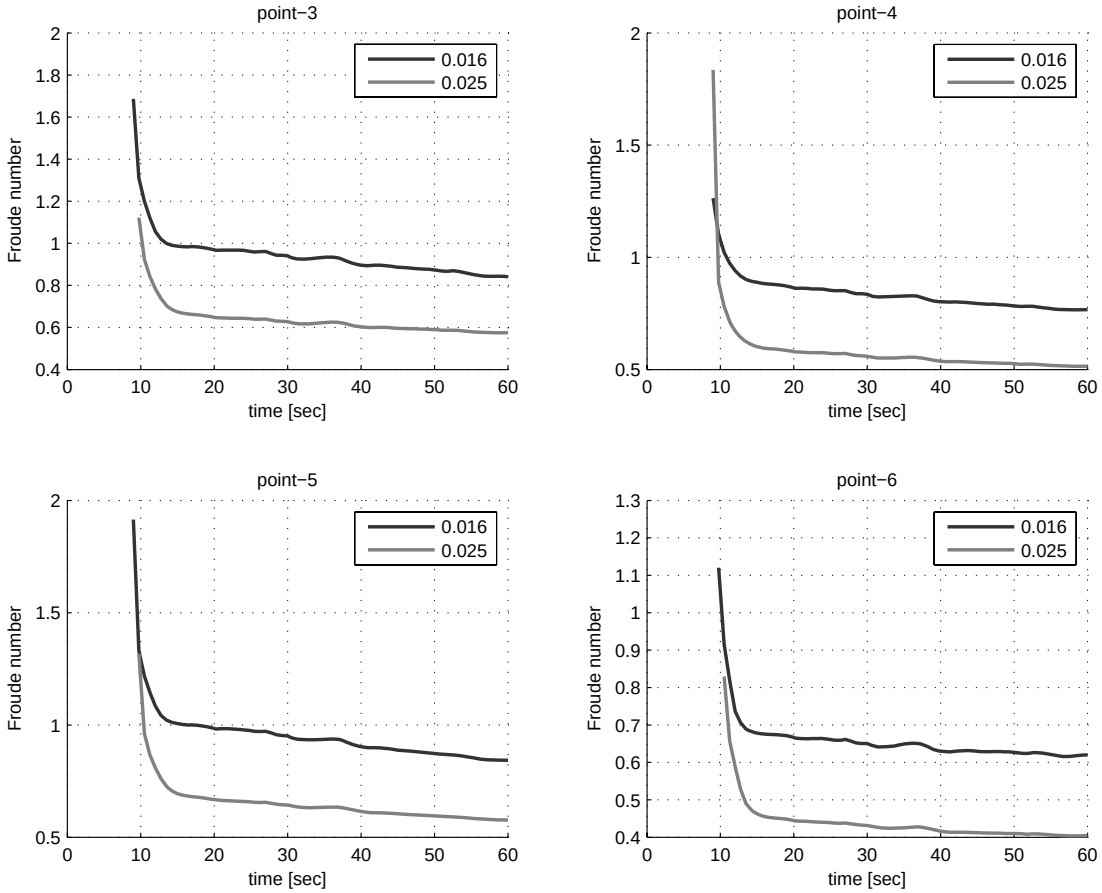

Figure 5.35: Froude number for roughness values of 0.016 and 0.025 $m^{1/3}s$, in gauge points from 3 to 6 (aligned buildings configuration and medium hydrograph).

	Low hydrograph					**Medium hydrograph**				
rough.	***0.016***	***0.025***	***0.03***	***0.035***	***0.04***	***0.016***	***0.025***	***0.03***	***0.035***	***0.04***
p3	0.029	0.021	0.017	0.014	0.011	0.032	0.024	0.020	0.023	0.019
p4	0.034	0.026	0.022	0.019	0.016	0.035	0.027	0.023	0.024	0.021
p5	0.006	0.007	0.008	0.010	0.013	0.008	0.013	0.016	0.015	0.018
p6	0.010	0.007	0.004	0.004	0.005	0.012	0.005	0.003	0.004	0.004
p7	0.011	0.008	0.005	0.003	0.004	0.011	0.005	0.005	0.005	0.006
p8	0.019	0.014	0.011	0.008	0.006	0.021	0.013	0.010	0.011	0.008
p9	0.012	0.007	0.005	0.004	0.006	0.012	0.005	0.004	0.005	0.005
p10	0.003	0.004	0.005	0.007	0.010	0.006	0.008	0.011	0.008	0.012
average	**0.015**	**0.012**	**0.010**	**0.009**	**0.009**	**0.017**	**0.013**	**0.012**	**0.012**	**0.011**

Table 5.2: RMSE (m) for simulations with the aligned buildings configuration (roughness in $m^{1/3}s$).

	Low hydrograph					**Medium hydrograph**				
rough.	***0.016***	***0.025***	***0.03***	***0.035***	***0.04***	***0.016***	***0.025***	***0.03***	***0.035***	***0.04***
p3	47.0%	38.0%	31.6%	25.9%	20.6%	45.9%	34.3%	28.3%	25.7%	20.5%
p4	44.2%	40.6%	35.3%	30.5%	25.9%	45.3%	34.9%	29.3%	26.4%	21.5%
p5	18.5%	21.0%	26.4%	33.2%	40.5%	23.5%	39.2%	49.5%	55.1%	64.8%
p6	28.8%	17.6%	10.7%	10.6%	16.1%	27.8%	11.0%	7.5%	9.6%	16.0%
p7	27.2%	22.1%	14.5%	10.2%	11.6%	27.4%	13.2%	12.6%	14.4%	20.1%
p8	32.4%	30.4%	24.1%	18.5%	13.4%	36.1%	22.1%	15.6%	12.9%	8.4%
p9	24.0%	17.9%	12.1%	11.8%	16.6%	25.8%	9.9%	9.2%	11.0%	17.4%
p10	12.7%	13.8%	17.0%	24.9%	33.7%	14.7%	22.4%	32.9%	34.6%	46.1%
average	**29.8%**	**25.2%**	**21.5%**	**20.7%**	**22.3%**	**30.8%**	**23.4%**	**23.1%**	**23.7%**	**26.9%**

Table 5.3: normalized RMSE (% with respect to observed values) for simulations with aligned buildings configuration (roughness in $m^{1/3}s$).

5.4.4 Results: simulations with staggered buildings

The overall results obtained with this buildings configuration are comparable with those described in Section 5.4.3. The use of the suggested roughness coefficient of 0.0162 $m^{1/3}s$ provides poor results, therefore more simulations were carried out using roughness values ranging from 0.02 to 0.04 $m^{1/3}s$. The graphs of Figures 5.36 and 5.37 illustrate the comparison between observed and simulated water stages, while Tables **??** and **??** contain RMSE values.

The comparison with observed water levels provides results similar to the aligned configuration, except for points 5 and 6, due to their different relative position. The model is not able to reproduce the hydraulic jump upstream of the urban district, as well as the subsequent transition to supercritical flow and the blocking effect of buildings, while the performance improves inside the urban area and downstream. The overall level of errors however are slightly higher than for aligned configuration, probably because of the greater resistance given by the staggered layout. For this grid configuration, the use of roughness

values between 0.03 and 0.04 $m^{1/3}s$ provide the best results. Finally, simulations with low and medium hydrograph provide similar levels of errors in all the gauge points.

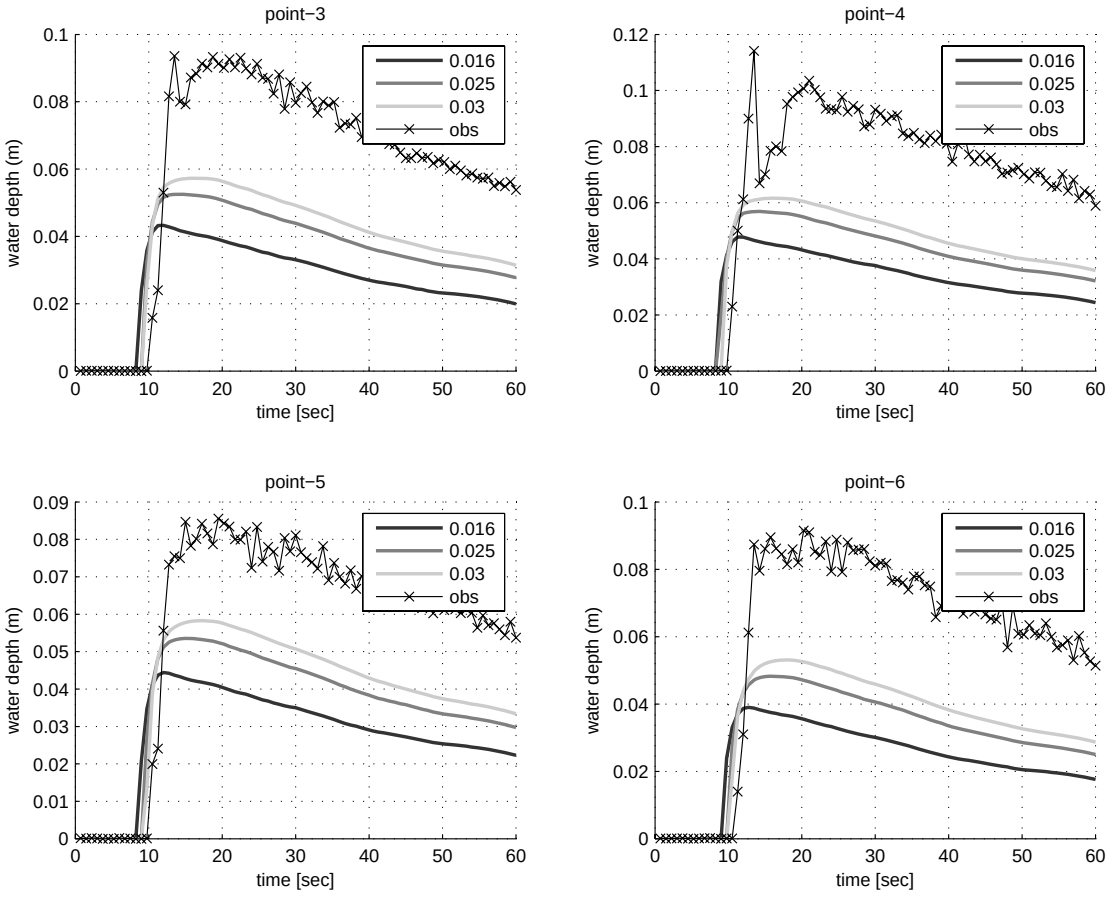

Figure 5.36: comparison of computed and observed water depths with different roughness values in gauge points from 3 to 6 (staggered buildings configuration and medium hydrograph).

	Low hydrograph				**Medium hydrograph**				
rough.	***0.025***	***0.03***	***0.035***	***0.04***	***0.016***	***0.025***	***0.03***	***0.035***	***0.04***
p3	0.023	0.019	0.016	0.013	0.037	0.032	0.027	0.023	0.020
p4	0.028	0.025	0.022	0.019	0.040	0.035	0.030	0.026	0.023
p5	0.020	0.016	0.013	0.011	0.032	0.026	0.022	0.018	0.015
p6	0.025	0.021	0.018	0.016	0.039	0.034	0.029	0.026	0.022
p7	0.009	0.006	0.004	0.004	0.015	0.010	0.007	0.006	0.006
p8	0.021	0.017	0.014	0.011	0.032	0.026	0.022	0.018	0.015
p9	0.009	0.006	0.004	0.004	0.015	0.010	0.007	0.005	0.005
p10	0.009	0.010	0.012	0.014	0.013	0.012	0.012	0.012	0.014
average	**0.018**	**0.015**	**0.013**	**0.011**	**0.028**	**0.023**	**0.020**	**0.017**	**0.015**

Table 5.4: RMSE (m) for simulations with the aligned buildings configuration (roughness in $m^{1/3}s$).

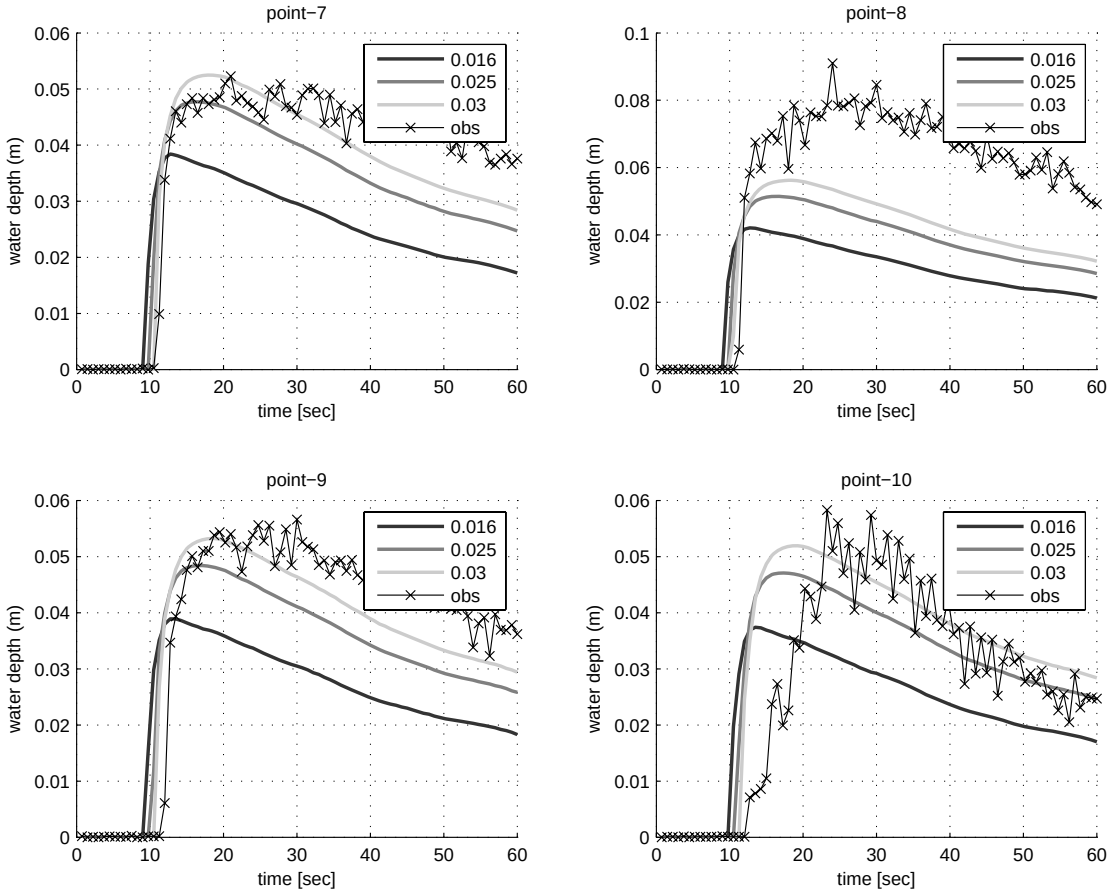

Figure 5.37: comparison of computed and observed water depths with different roughness values in gauge points from 7 to 10 (staggered buildings configuration and medium hydrograph).

	Low hydrograph				**Medium hydrograph**				
rough.	***0.025***	***0.03***	***0.035***	***0.04***	***0.016***	***0.025***	***0.03***	***0.035***	***0.04***
p3	41.7%	35.8%	30.3%	25.2%	50.3%	43.3%	38.1%	33.2%	28.7%
p4	44.3%	39.3%	34.7%	30.3%	49.9%	43.3%	38.4%	33.9%	29.6%
p5	37.4%	31.4%	25.8%	20.6%	46.7%	38.8%	33.3%	28.2%	23.3%
p6	45.4%	39.4%	33.7%	28.4%	53.2%	45.4%	39.9%	34.8%	30.0%
p7	25.3%	17.7%	12.3%	11.1%	32.6%	21.5%	15.0%	11.9%	13.4%
p8	37.8%	31.6%	26.0%	21.0%	46.3%	37.7%	31.8%	26.6%	21.8%
p9	22.7%	15.2%	10.2%	10.2%	31.0%	20.1%	12.8%	8.6%	9.9%
p10	10.4%	15.8%	23.2%	30.6%	23.9%	22.6%	26.6%	33.0%	40.2%
average	**33.1%**	**28.3%**	**24.5%**	**22.2%**	41.7%	**34.1%**	**29.5%**	**26.3%**	**24.6%**

Table 5.5: normalized RMSE (% with respect to observed values) for simulations with the staggered buildings configuration (roughness in $m^{1/3}s$).

5.4.5 Results: grid configurations

All the results previously described were obtained using a 4 direction grid configuration. Figures 5.38 and 5.39 compare respectively water depths and velocities computed using 4- and 8-direction grids in two representative simulations. As can be seen, the 8–dir. grid computes lower water depths and velocities, which in this case produces a higher error in respect to observed values. Wave celerity is almost equal for both the configurations, contrary to the results of case 6 (Section 4.4).

5.4.6 Discussion

The results previously described highlight important limitations of the CA model in this test case. As expected, the absence of inertial terms and shock capturing schemes in model equations means that several flow processes cannot be represented. Localized flow conditions are smoothed out, unlike the previous works by Guinot and Soares-Frazão (2006); Soares Frazão et al. (2008); Sanders et al. (2008) where fully dynamic SWE models were used. Consequently, the model has a low sensitivity in respect to the layout of buildings, as can be seen clearly in Figure 5.40.

Of course, such conclusions are valid for the physical experiments analyzed here, which indeed represent a severe test for a diffusive model. On this topic, Aricó et al. (2011) suggested that differences between diffusive and fully dynamic models should be relevant for Froude numbers around 1, which is indeed the case. It is likely that model performance would improve under less severe conditions, as suggested by the results of Prestininzi (2008) and Hunter et al. (2008).

Dottori and Todini (2012) integrated these results by applying simplified representations of urban area, based on porosity and upscaled roughness approaches (Yu and Lane, 2006a; McMillan and Brasington , 2007; Yu and Lane, 2011). The authors pointed out that the model performance with these methods were comparable or even better than results obtained by explicitly reproducing buildings and roads. Thus, the model could take little practical

advantage from detailed description of urban area, because of low sensitivity of diffusive equations to small scale features (Hunter et al., 2007; Aricó et al., 2011). On the other hand, the introduction of additional parameters like urban roughness allowed to partially overcome the model limitations.

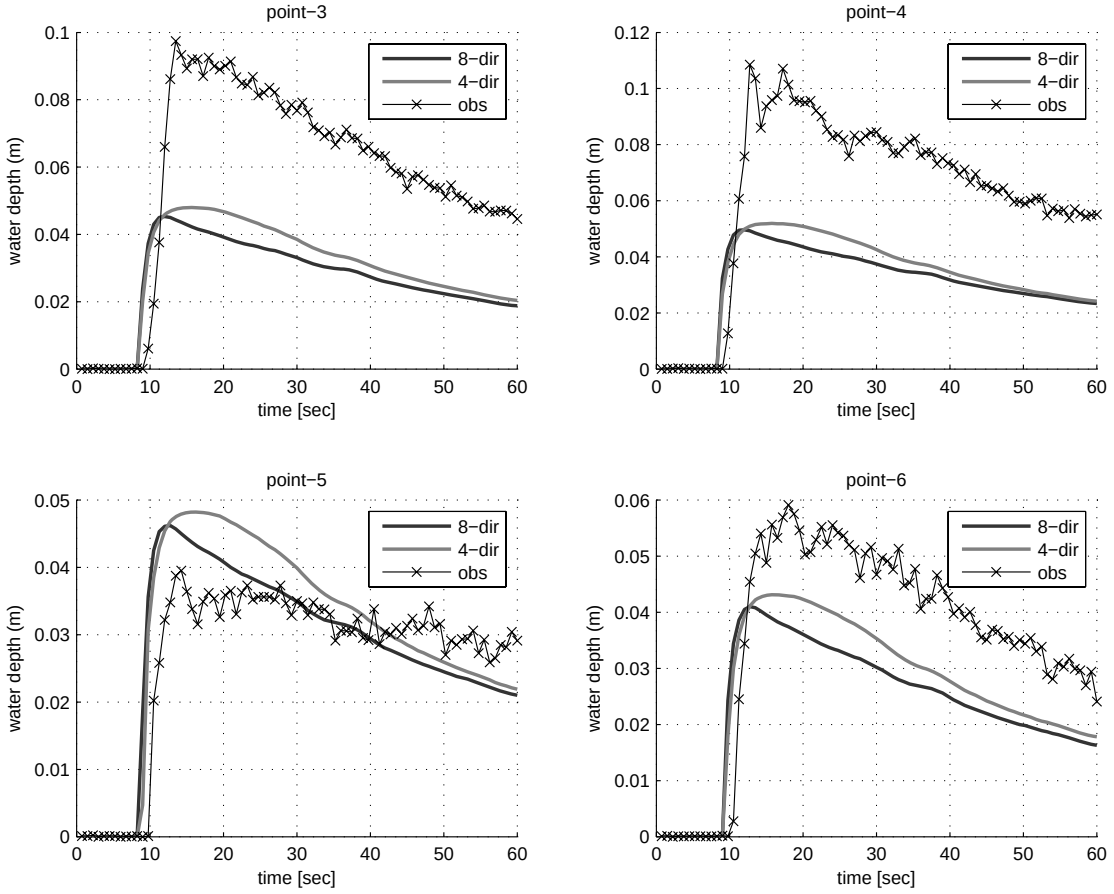

Figure 5.38: comparison of computed water depths using 4 and 8 direction link networks in gauge points from 3 to 6 (roughness 0.016 $m^{1/3}s$, aligned buildings configuration and medium hydrograph).

The improvement in the model performance with a calibration of the overall roughness coefficient (Sections 5.4.3 and 5.4.4) may be a further confirmation of this hypothesis. Such results are consistent with existing literature, since according to different authors (Romanowicz and Beven, 2003; Pappenberger et al., 2005; Di Baldassarre et al., 2009b) roughness cannot be considered an independent variable, being influenced by floodplain and channel geometry, grid resolution and model structure. When a 2D model is used, the roughness parameter must account for momentum losses not explicitly modelled, like local head losses (Soares Frazão et al., 2008), turbulence effects and dispersion processes resulting from the integration of the fully 3D Navier-Stokes equations (Yu and Lane, 2006a). This is true both for 2D models based on the complete SWE and for zero-inertia (or diffusive) 2D mod-

els(Soares Frazão et al., 2008); for the latter, higher values of roughness are needed to offset the absence of energy loss mechanisms due to inertial effects (Di Baldassarre et al., 2010b).

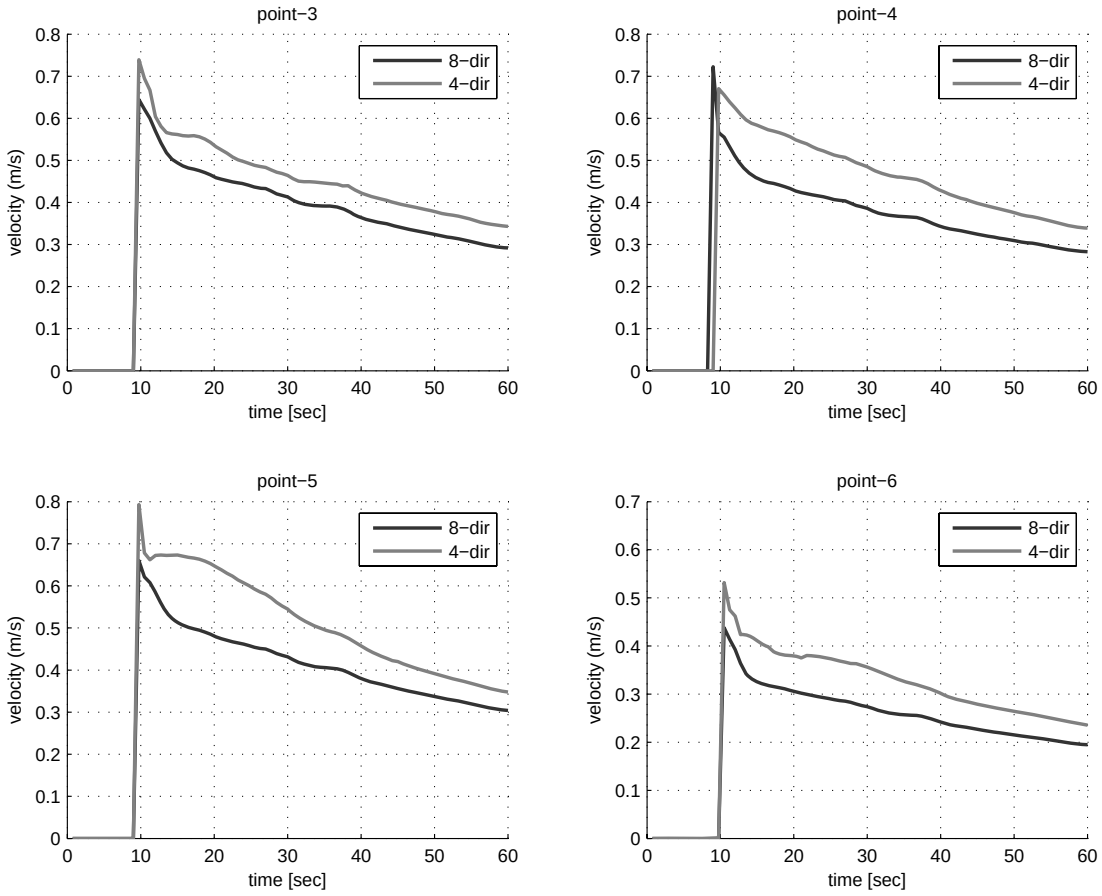

Figure 5.39: comparison of computed velocities using 4 and 8 direction link networks in gauge points from 3 to 6 (roughness 0.025 $m^{1/3}s$, aligned buildings configuration and medium hydrograph).

As a conclusion, roughness coefficient can lose its physical meaning and become more a conceptual calibration parameter. Moreover, roughness represents also topographic features that are smoothed out by grid coarsening (Yu and Lane, 2006a). Finally, Prestininzi (2008) stated that steep slopes (like those characterising the physical model of the IMPACT project) should be considered in model equations by modifying the friction term to account both for lateral and longitudinal slopes. Also, lateral friction in the urban district could be significant.

5.5 Conclusions

The overall results of the CA2D model in simulating the described flood events and scenarios can be considered very satisfactory. First of all, the model proved to be robust, providing stable and meaningful results in all the test cases both in terms of water depth and velocity. In particular, the model could handle different grid resolutions, from coarse to extremely

fine (up to 5cm in the urban flood scenario described in Section 5.4); mixed 1D and 2D flow processes both on mild and steep slopes; test sites with complex topography, including large obstacles like embankments and levees, and localized obstacles like buildings.

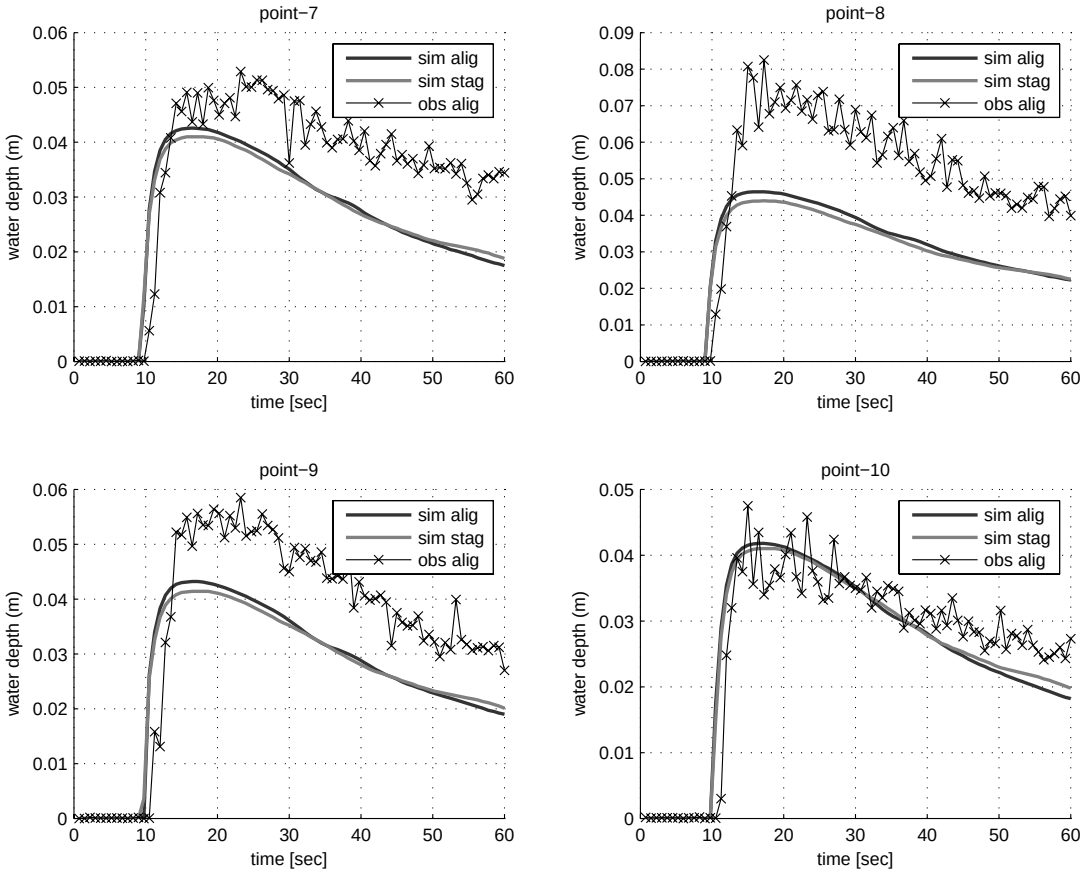

Figure 5.40: Comparison of computed water depths for aligned and staggered layouts, and observations with aligned layout in gauge points from 7 to 10 (experiment with medium hydrograph).

The model reproduced well flood events characterized by slow 1D and 2D flow processes, like those occurred in rivers Reno and Po (Sections 5.1, 5.2). Good results were obtained also in the application to the River Ubaye (Section 5.3), characterized by high resolution grids and steep slopes. In all these applications,the accuracy of model results was adequate to large scale analysis, and compatible with the uncertainty of available data for model construction and validation. Sensitivity analyses were carried out to investigate the effect of roughness calibration; the resulting values were physically meaningful and comparable with usual values for 2D hydraulic models.

The application to urban flood scenario experiments gave less satisfactory results (Section 5.4). The model was able to simulate the overall flow processes, but it could not capture the details of the complex processes produced by the interaction of buildings with the flow, such as hydraulic jumps and wake effects. However such results were expected, due to the

severity of the test case and the approximations in model equations. Under less severe flow conditions and when localized flow conditions are not of interest, the performances of diffusive 2D models are likely to be acceptable.

Chapter 6

Conclusions

The main objective of the described research work was to develop reliable models for large scale analysis of flood inundation events and scenarios. Two different models, CA2D and IFD-GGA, were developed, adopting a partially integrated approach and testing different configurations. Overall results highlighted relevant differences between the performance of the two models.

The performances of the CA2D model were very satisfactory. The model proved to be fast and robust, providing stable and consistent results in all the test cases, both in terms of water level and velocity. The model could reproduce mixed 1D and 2D flow processes and it could handle complex topographic features, including steep slopes, large obstacles like embankments and levees, and localized obstacles like buildings. Finally, the simple model structure and the use of methods to increase model stability enabled reduced computation times, which were faster or comparable to established 2D hydraulic models.

The model reproduced well test cases characterized by slow 1D and 2D flow processes. In these applications, the accuracy of model results was adequate to large scale analysis, and the magnitude of observed errors was below the typical uncertainty of data and observations in actual flood events, e.g. topography and inundation extent maps. The model performance was less satisfactory in test cases characterized by complex flow processes, such as flow transitions and interaction with obstacles. In these cases relevant local errors were observed, due to the diffusive form of the governing equations, which can not capture inertial effects and shock waves. However, local conditions did not compromise the ability of the model to correctly simulate overall flow processes, and in most cases the error was limited.

In conclusion, the results suggest that the CA model can be a valuable tool for the simulation of a wide range of flood event types.

On the contrary, the results of the IFD-GGA model in the considered numerical cases were not satisfactory. Except for simple 1D and 2D numerical cases, the different model versions showed serious problems and the poor performance of model algorithms prevented further applications. Therefore the work on the IFD-GGA model was interrupted and its development is now being reconsidered. A possible solution could be the use of the fully dynamic SWE as governing equations, while maintaining the existing model structure to preserve the integration with CA2D. This would enable a coupled application of the two

models: for instance, IFD-GGA could be applied where localized complex flow conditions are expected, while using CA2D in the rest of the study area. However, model development in this sense has not been undertaken yet.

6.1 Further developments of the model codes

So far, the CA2D model has been primarily used to reproduce flow routing and associated lowland flood events. However, numerical and practical applications (e.g. case 2, Section 4.2) demonstrated that the model is able to reproduce overland and concentrated flow and manage wetting and drying effects over wide areas (from hillslope up to small basin scale). Therefore the model could be used to simulate the surface runoff produced by intense rainfall events, including the formation of flash floodss and the analysis of related risk. However, the CA2D model should undergo adequate calibration tests before being applied in similar studies.

Within this framework, the model structure could be expanded to include more hydrological processes. For instance, the simulation of infiltration could be improved by implementing more complex methods like Horton and Green-Ampt. Accordingly, subsurface flow and soil moisture can be introduced without substantial modifications of model structure, improving the capacity of CA2D to reproduce event-based hydrological processes on small basins or hillslopes. Finally, soil erosion and sediment transport associated to overland flow could also be implemented within the model.

Besides these additions, further research would be needed to exploit the flexible structure of the model. The results described in Chapters 4 and 5 suggest that the diffusive and inertial formulations could be proficiently integrated and used alternatively, depending on flow conditions. However, more research to establish empirical or numerical criteria is needed. Similar criteria should be investigated to allow the integrated use of 8 directions and 4 directions link networks. Finally, additional functions are currently being implemented and tested in the model codes, to expand the basic versions described in Chapter 3. For instance, subgrid parameterizations can be used to characterize the geometry of grid elements (cells and connections), to simulate more accurately 1D open channel flows or to represent microtopography over coarse grids (Yu and Lane, 2006a; McMillan and Brasington , 2007; Yu and Lane, 2011; Dottori and Todini, 2012).

6.2 Future applications of the models

As mentioned in Section 3.5, the CA2D model is currently being integrated in the information system of the Civil Protection Agency. The first objective is to use CA2D to analyze flood scenarios caused by dyke breach and dyke overtopping along the main rivers of the Emilia-Romagna district. A further objective should be to integrate CA2D in the existing flood modelling system composed by meteorological, hydrological and 1D hydraulic models. This would allow more accurate flood risk analysis, including real-time forecasting of flood events.

To this end, the parallelisation of the model code on distributed multiprocessor machines and GPU cards has also been planned (Section 3.5).

Besides these specific applications, diffusive reduced complexity models like CA2D could be used to perform flood analysis at very large scale (even continental scale), exploiting the new remote sensing and freely available data sources that should be available in a few years (Di Baldassarre and Ulhenbrook, 2012). This would allow to produce reliable flood maps in countries where either scarce or no information of flood risk is available, thus providing a considerable contribute both to research works and flood risk management in developing countries. Actually, the CA2D model has already been used in a similar framework to develop probabilistic flood mapping of a large part of Italy, for insurance porpuses. Existing databases of past flood events and freely available remote sensing data were used for model construction and validation, with good results.

Finally, the developed models could be released as free, open source softwares. Nowadays a number of established flood inundation models are available as free softwares and can be downloaded from the website of respective developing institutions or companies (e.g. LISFLOOD-FP (*www.bris.ac.uk/geography/research/hydrology/models/lisflood*), and the CCHE2D model (*www.ncche.olemiss.edu*). On the other hand other model codes are available as open source software, for instance TELEMAC-2D (*www.opentelemac.org*) and XBEACH (*http://oss.deltares.nl/web/xbeach*). The availability of reliable free and open source flood inundation models can extremely useful especially (but not only) in developing countries, to increase the know-how of technicians and practitioners and to enable adequate flood risk analyses. Moreover, open source models are particulary suited for didactical and research purposes, allowing to learn how a model code can be developed, modified and expanded.

Indeed, this would probably be an excellent way to spread the results of the research work described in this thesis. Hopefully, this thesis will also be a small contribute to improve current and future flood risk management and mitigation strategies.

Bibliography

Alcrudo, F., 2004. Mathematical Modelling Techniques for Flood Propagation in Urban Areas. IMPACT Project technical report ($www.impact-project.net$).

Anselmo, V., Galeati, G., Palmieri, S., Rossi, U., Todini, E., 1996. Flood risk assessment using an integrated hydrological-hydraulic modelling approach: a case study, J. Hydrol. 175, 533-554.

Aricó, C.,Sinagra, M., Begnudelli, L., Tucciarelli, T., 2011. MAST-2D diffusive model for flood prediction on domains with triangular Delaunay unstructured meshes. Adv. Water Res. 34,1427-1449.

Aronica, G., Hankinb B., Beven, K., 1998.Uncertainty and equifinality in calibrating distributed roughness coefficients in a flood propagation model with limited data. Adv. Water Res. 22 (4), 349–365.

Avolio, M.V., Crisci, G.M., Di Gregorio, S., Rongo, R., William Spataro, W., D'Ambrosio, D., 2006. Pyroclastic flows modelling using cellular automata. Computers & Geosciences 32, 897-911.

Bagarello, V., Ferro, V., 2006. Erosion and soil conservation (in Italian), McGraw-Hill, Milano.

Bateman, A., Medina, V., Velasco, V., 2010. Soil infiltration effect in flat areas floods simulation. In: J. Carrera (Ed.) XVIII International Conference on Water Resources CMWR 2010, Barcelona (Spain).

Bates, P.D., de Roo, A.P.J., 2000. A simple Raster-Based Model For Flood Inundation Simulation. J. Hydrol. 236, 54-77.

Bates, P.D., 2004. Remote sensing and flood inundation modelling. Hydrol. Proces. 18, 2593–2597.

Bates, P.D., Wilson, M.D., Horritt, M.S., Mason, D.C., Holden, N., Currie, A., 2006. Reach scale floodplain inundation dynamics observed using airborne synthetic aperture radar imagery: Data analysis and modelling. J. Hydrol. 328, 306-318

Bates, P.D., Horritt, M.S., Fewtrell, T.J., 2010. A simple inertial formulation of the shallow water equations for efficient two-dimensional flood inundation modelling. J. Hydrol. 387, 33-45.

Bradbrook, K.F., Lane, S.N., Waller, S.G., Bates, P.D., 2004. Two dimensional diffusion wave modelling of flood inundation using a simplified channel representation. International Journal of River Basin Management 3, 1–13.

Casulli, V., 1990. Semi-implicit Finite Difference Methods for the Two- Dimensional Shallow Water Equations. Journal of Computational Physics, 86, 56-74.

Casulli, V., Stelling, G.S., 2010. Semi-implicit subgrid modelling of three-dimensional free surface flows, Int. Jour. for Numer. Meth. Fluids, DOI: 10.1002/fld2361.

Castellarin, A., Domeneghetti, A., and Brath, A. (2011). Identifying robust large-scale flood risk miti gation strategies: a quasi-2D hydraulic model as a tool for the Po river, Phys. Chem. Earth, 36, 299-308.

Chopard, B., Masselot, A., 1999. Cellular automata and lattice Boltzmann methods: a new approach to computational fluid dynamics and particle transport. Future Generation Computer Systems 16, 249-257.

Chow, V.T., 1959. Open-Channel Hydraulics. MCGraw-Hill, New York.

Cockburn, B., Shu, C.W., 2001. RungeKutta Discontinuous Galerkin Methods for Convection-Dominated Problems. Journal of Scientific Computing 16-3, 173-261.

Commission of the European Community, 1996. AFORISM, a Comprehensive Forecasting System for Flood risk Mitigation and Control, Final Report.

Commission of the European Community, 2007. Directive 2007/60/EC on the assessment and management of flood risks. Official Journal of the European Union.

Cremonini, 1994. Autopsy of a fluvial breach (in Italian), Il Carrobbio 20, 339-362, 1994.

Crossley, A.J., Wright, N.G., Chris D. Whitlow, C.D., 2003. Local Time Stepping for Modeling Open Channel Flows. J. Hydraul. Eng. 129(6), 455-462.

Cunge, J.A., 2003. Of data and models. J. Hydroinf. 5(2), 75-98.

D'Ambrosio, D., Di Gregorio, S., Iovine, G., 2003. Simulating debris flows through a hexagonal cellular automata model: SCIDDICA S3-hex. Natural Hazards and Earth System Sciences 3, 545–559.

Danish Hydraulic Institute (DHI) Water and Environment, 2000. Mike21, Danish Hydraulic Institute, Horsholm, Denmark.

Di Baldassarre, G., Castellarin, A., Brath, A., 2009a. Analysis on the effects of levee heightening on flood propagation: some thoughts on the River Po. Hydrol. Sci. J. 54(6),1007–17.

Di Baldassarre, G., Schumann, G.J.-P., Bates, P.D., 2009b. Near real time satellite imagery to support and verify timely flood modelling. Hydrol Process, 23, 799–803.

Di Baldassarre, G., Montanari, A., Lins, H., Koutsoyiannis, D., Brandimarte, L., Blschl, G., 2010. Flood fatalities in Africa: From diagnosis to mitigation, Geophys. Res. Lett., 37, L22402, doi:10.1029/2010GL045467.

Di Baldassarre, G., Schumann, G., Bates, P.D., Freer, J.E., Beven, K.J., 2010. Floodplain mapping: a critical discussion of deterministic and probabilistic approaches. Hydrol. Sci. J. 55(3), 364–376.

Di Baldassarre, G., and Ulhenbrook, S., 2012. Is the current flood of data enough? A treatise on research needs for the improvement of flood modelling. Hydrol. Process. 26, 153–158.

Di Giammarco, P., Todini, E., Lamberti, P., 1996. A conservative finite elements approach to overland flow: the control volume finite element formulation. J. Hydrol. 175 (1-4), 267–291.

Dottori, F., Todini, E., 2010a. A 2D flood inundation model based on an implicit parallelizable scheme. In: J. Carrera (Ed.), XVIII International Conference on Water Resources CMWR 2010, Barcelona (Spain).

Dottori, F., Todini, E., 2010b. A 2D flood inundation model based on cellular atomata approach. In: J. Carrera (Ed.), XVIII International Conference on Water Resources CMWR 2010, Barcelona (Spain).

Dottori, F., Todini, E., 2011. Developments of a flood inundation model based on the cellular atomata approach: testing different methods to improve model performance. Phys. Chem. Earth 36 (2011) 266-280.

Dottori, F., Alfonso, L., Di Baldassarre, G., 2011. The value of urban flood mapping: application to the case study of Barcelonnette (France). EGU 2011 Leonardo Conference, Bratislava.

Dottori, F., Todini, E., 2012. Testing a simple 2D hydraulic model in an urban ood experiment. Hydrol.l Proces. under review.

El Kadi Abderrezzak, K., Paquier, A., Mignot, E., 2009. Modelling flash flood propagation in urban areas using a two-dimensional numerical model. Nat. Hazards 50, 433–460.

Emergency Events Database 2011. OFDA/CRED International Disaster Database, Universite Catholique de Louvain, Brussels, *http* : *//www.cred.be/emdat*.

Ern, A., Piperno, S., Djadel, K., 2008. A well-balanced RungeKutta Discontinuous Galerkin method for the Shallow-Water Equations with flooding and drying. Int. J. Numer. Meth. Fluids. 58(1), 1–25.

U.S. Federal Emergency Management Agency. Numerical Models Meeting the Minimum Requirements of the National Flood Insurance Program. 11-Aug-2010 12:08 UTC (cited 2012 Feb 24). Available from: $http://www.fema.gov/plan/prevent/fhm/en\_modl.shtm$

Ferro, V., 2006. Management of river basins (in Italian), McGraw-Hill, Milano.

Fewtrell, T.J., Bates, P.D., Horritt, M.S., Trigg, M.A., 2007. The effect of temporal and spatial coarsening on storage cell predictions of urban flood inundation., 32nd Congress of the International Association for Hydraulic Engineering and Research, Venice, Italy, 1, 37-47, ISBN: 8889405066.

Fewtrell, T.J., Bates, P.D., Horritt, M.S., Hunter, N.M., 2008. Evaluating the effect of scale in flood inundation modelling in urban environments. Hydrol. Proc. 22, 5107-5118

Fewtrell, T.J., Duncan, A., Sampson, C.C., Neal, J.C., Bates, P.D., 2011. Benchmarking urban flood models of varying complexity and scale using high resolution terrestrial LiDAR data. Phys. Chem. Earth 36 (2011).

FLO-2D Software Inc., 2007. FLO-2D Users Manual (2007).

Gallegos, H.A., Schubert, J.E., Sanders, B.F., 2009. Two-dimensional, high-resolution modeling of urban dam-break flooding: a case study of Baldwin Hills, California. Adv. Water Res. 32, 1323–1335.

Götzinger J, Bárdossy A. 2008. Generic error model for calibration and uncertainty estimation of hydrological models. Water Resources Research W00B07: DOI:10.1029/2007WR006691.

Guinot, V., Soares-Frazão, S., 2006. Flux and source term discretization in two-dimensional shallow water models with porosity on unstructured grids. Int. J. Numer. Meth. Fluids 50, 309–345.

Guinot, V., Cappeleare, B., 2009. Sensitivity analysis of 2D steady-state shallow water flow. Application to free surface model calibration. Adv. Water. Res. 32, 540–60.

Guy, B.T., Rudra, R.P., Dickinson, W.T., 1992. Process-oriented research on soil erosion and overland flow. In Parsons, J., Abrahams, A.D. (eds.) Overland Flow, 225–242.

Hartanto, I.M., Beevers, L., Popescu, I., Wright, N.G., 2011. Application of a coastal modelling code in fluvial environments. Environmental Modelling & Software 26, 1685–1695.

Hydraulic Engineering Centre (HEC), 2001. HEC RAS Hydraulic Reference Manual, U.S. Army Corps of Engineers, Davis, California, USA, 377 pp.

Hervouet, J.M., 2000. A high resolution 2-D dam-break model using parallelization. Hydrol. Process. 13, 2211-2230.

Hervouet, J.M.,Van Haren, L., 1996. Recent advances in numerical methods for fluid flows. In Floodplain Processes, Anderson M.G., Walling D.E., Bates P.D. (eds). Wiley: Chichester; 183–214.

Horritt, M.S., 2002. Evaluating wetting and drying algorithms for finite element models of shallow water flow. Int. J. Numer. Meth. Eng., 55, 835–851.

Horritt., Bates, P.D., 2002. Evaluation of 1D and 2D numerical models for predicting river flood inundation. J. Hydrol. 268, 87–99

Horritt, M.S., Di Baldassarre, G., Bates, P.D, Brath, A., 2007. Comparing the performance of a 2-D finite element and a 2-D finite volume model of floodplain inundation using airborne SAR imagery. Hydrol. Process. 21, 2745–2759.

Horton, R.E., 1945. Erosion development in streams and their drainage basins; hydrophysical approach to quantitative geomorphology. Bull Geol. Soc. Am., 3,3 340–349.

Hunter, N.M., Bates, P.D., Horritt, M.S., De Roo, A.P.J., Werner, M.G.F., 2005a. Utility of different data types for calibrating flood inundation models within a GLUE framework. Hydrol. Earth Syst. Sci. 9 (4), 412–430.

Hunter, N.M., Horritt, M.S., Bates, P.D., Wilson, M.D., Werner, M.G.F., 2005b. An adaptive time step solution for raster-based storage cell modelling of floodplain inundation. Adv. Water Res. 28 (9), 975-991.

Hunter, N.M., Bates, P.D., Horritt, M.S., Wilson, M.D., 2007. Simple spatially-distributed models for predicting flood inundation: a review. Geomorphology 90, 208–225.

Hunter, N.M., Bates, P.D., Neelz, S., Pender, G., Villanueva, I., Wright, N.G., Liang, D., Falconer, R.A., Lin, B., Waller, S., Crossley, A.J., Mason, D.C., 2008. Benchmarking 2D hydraulic models for urban flooding. Water Management 161, 13–30.

Braca, G., Busettini, M., Dessi, B., Lastoria, B., Monacelli, G., Spizzichino, D., 2009. Towards, the implementation of the EU Diretctive 2007/60: analysis of current situation of flood risk planning and management and proposal for derogations from art. 13, ISPRA (Istituto Superiore per la Protezione e la Ricerca Ambientale), in Italian.

Jia, Y.F., Wang, S.S.Y., 2001. CCHE2D: Two-dimensional Hydrodynamic and Sediment Transport Model for Unsteady Open Channel Flow Over Loose Bed. NCCHE Technical Report. NCCHE-TR-2001-01.

Kalyanapu, A.J., Shankar, S., Pardyjak, E.R., Judi D.R., Burian S.J., 2011. Assessment of GPU computational enhancement to a 2D flood model. Environmental Modelling & Software 26, 1009-1016

Kelley, C. T., 1995. Iterative Methods for Linear and Nonlinear Equations. SIAM, Philadelphia.

Kleb, W.L., Batina, J.T., 1992. Temporal adaptive Euler/Navier-Stokes algorithm involving unstructured dynamic meshes. AIAA J. 30(8), 1980–1985.

Lamb, R., Crossley, A.,Waller, S., 2009. A fast 2D floodplain inundation model. Water Management (Proceedings of the Institution of Civil Engineers) 162.

Liang, D., Lin, B., Falconer, R. A., 2007. Simulation of rapidly varying flow using an efficient TVD-MacCormack scheme. International Journal for Numerical Methods in Fluids, 53(5), No. 3, 811–826.

Lin, B., Wicks, J., Falconer, R., Adams, K., 2006. Integrating 1D and 2D hydrodynamic models for flood simulation. Water Manage. 159 (1), 19–25.

Luenberger, D. G., 2003. Linear and nonlinear programming. Kluwer Academic Publishers, (2nd Ed.).

McMillan, H.K., Brasington, J., 2007. Reduced complexity strategies for modelling urban floodplain inundation. Geomorphology 90, 226–243.

Mignot, E., Paquier, A., Haider, S., 2006. Modeling floods in dense urban areas using 2D shallow water equations. J. Hydrol. 327, 186–199.

Muller, S., Stiriba, Y., 2007. Fully adaptive multiscale schemes for conservation laws employing locally varying time stepping. J. Sci. Comput. 30 (3), 493–531.

Neal, J.C., Bates, P.D., Fewtrell, T.J., Hunter, N.M., Wilson, M.D., Horritt, M.S., 2009a. Distributed whole city water level measurements from the Carlisle 2005 urban flood event and comparison with hydraulic model simulations. J. Hydrol.368, 42–55.

Neal, J.C., Fewtrell, T.J., Trigg, M.,. 2009b. Parallelisation of storage cell flood models using OpenMP. Environmental Modelling & Software 24, 872–877.

Neal, J.C., Fewtrell, T.J., Bates, P.D., Wright., N.G., 2010. A comparison of three parallelisation methods for 2D flood inundation models. Environmental Modelling & Software 25, 398–411.

Neelz, S., Pender, G., 2007. Sub-grid scale parameterisation of 2D hydrodynamic models of inundation in the urban area. Acta Geophysica 55(1), 65-72. DOI 10.2478/s11600-006-0039-2

Neelz, S. Pender, G., 2010, Benchmarking of 2D Hydraulic Modelling Packages. SC080035/SR2 Environment Agency, ISBN 978-1-84911-190-4.

Osher, S., Sanders, R. (1983). Numerical approximations to nonlinear conservation laws with local varying time and space grids. Mathematics of Computation 41(164), 321–336.

Pappenberger, F., Beven, K., Horritt, M., Blazkova, S., 2005. Uncertainty in the calibration of effective roughness parameters in HEC-RAS using inundation and downstream level observations. Journal of Hydrology, 302, 46–69.

Parsons, J.A., Fonstand, M.A., 2007. A cellular automata model of surface water flow. Hydrol. Process. 21, 2189–2195.

Ponce, V.M., 1978. Applicability of kinematic and diffusion models. Journal of The Hydraulics Division 104, 353.

Prestininzi, P., 2008. Suitability of the diffusive model for dam break simulation: Application to a CADAM experiment. J. Hydrol. 361, 172–185.

Prestininzi, P. , Di Baldassarre, G., Schumann G., Bates, P.D., 2011. Selecting the appropriate hydraulic model structure using low-resolution satellite imagery. Adv. Water Res. 34, 38–46.

Rao, P., 2005. A parallel RMA2 model for simulating large-scale free surface flows. Environmental Modelling & Software 20 (1), 47–53.

Romanowicz, R., Beven, K., 2003. Estimation of flood inundation probabilities as conditioned on event inundation maps. Water Resources Research 39 (3), 1073–1085.

Sanders, B.F., Schubert, J.E., Gallegos, H.A., 2008. Integral formulation of shallow-water equations with anisotropic porosity for urban flood modeling. J. Hydrol. 362, 19–38.

Sanders, B.F., 2008. Integration of a shallow water model with a local time step. J. Hydraul. Res. 46(4),466–475.

Schubert, J.E., Sanders, B.F., Smith, M.J., Wright, N.G., 2008. Unstructured mesh generation and landcover-based resistance for hydrodynamic modeling of urban flooding. Adv. Water Res. 31, 1603–1621.

Schumann, G., Di Baldassarre, G., Alsdorf, D., Bates, P.D., 2010. Near real time flood wave approximation on large rivers from space: application to the River Po, Italy. Water Resources Res., 46.

Smith, M.B., 2006. Comment on 'Analysis and modelling of flooding in urban drainage systems'. J. Hydrol. 317, 355–363.

Soares-Frazão, S., Lhomme, J., Guinot, V., Zech Y., 2008.Two-Dimensional Shallow-Water Model With Porosity For Urban Flood Modeling. Journal of Hydraulic Research 46-1, 45–64.

Soares-Frazão, S., Zech, Y., 2008. Dam-break flow through an idealized city. J. Hydraul. Eng., 46(5), 648–658.

Syme, W.J., 2001, TUFLOW Two & one-dimensional Unsteady FLOW Software for Rivers, Estuaries and Coastal Waters, IEAust 2D Seminar, Sydney, Feb 2001.

Tayfur, G., Levent Kavvas, M., Govindaraju, R.S., 1993. Applicability of St. Venant Equations for two-dimensional overland flows over rough infiltrating surfaces. J. Hydraul. Eng., 1, 51–63.

Testa, G., Zuccala, D., Alcrudo, F., Mulet, J., Soares-Frazão, S., 2007. Flash flood flow experiment in a simplified urban district. J. Hydraul. Res. 45, 37–44.

Todini, E., Pilati, S., 1988. A gradient algorithm for the analylis of pipe networks, in B. Colulbeck and C.H.Orr (eds), Computer Applications in Water Supply, Vol.1: System Analysis and Simulation, John Wiley & Sons, London,1–20.

Toro, E.F., 1992. Riemann Problems and the WAF Method for Solving the Two-Dimensional Shallow Water Equations. Philosophical Transactions: Physical Sciences and Engineering 338, No. 1649, 43–68.

UN International Strategy for Disaster Reduction, 2009. Reducing Disaster Risks through Science: Issues and Actions, The full report of the ISDR Scientific and Technical Committee 2009, available at *http* : *//www.unisdr.org/preventionweb/files/*11543*STCReportlibrary.pdf*

Villanueva, I.,Wright, N.G., 2006. Linking Riemann and storage cell models for flood prediction. ICE J. Water Manage. 159 (1), 27–33.

Werner, M., Blazkova, S., Petr J., 2005. Spatially distributed observations in constraining inundation modelling uncertainties. Hydrol. Process. 19, 3081–3096.

Wikipedia contributors. Cellular automaton. Wikipedia, The Free Encyclopedia. 13-Feb-2012 11:15 UTC (cited 2012 Feb 23). Available from: *http* : *//en.wikipedia.org/wiki/Cellular_automaton*

Wood, D.J., Charles, C. O. A., 1972. Hydraulic network analysis using linear theory, Journal of the Hydraulics Division, ASCE, 98, HY7, Paper 9031, 1157–1170.

Wright, N. G., Villanueva, I., Bates, P.D., Mason, D.C., Wilson, M. D., Pender, G., Neelz, S., 2008. Case Study of the Use of Remotely Sensed Data for Modeling Flood Inundation on the River Severn, UK. J. Hydraul. Eng. 134 (5), 533–540.

Xanthopoulos, T., Koutitas, C., 1976. Numerical simulation of a two-dimensional flood propagation due to dam-failure. J. Hydraul. Res. 14 (4), 321–331.

Yu, D., Lane, S.N., 2006a. Urban fluvial flood modelling using a two-dimensional diffusion-wave treatment, part 1: mesh resolution effects. Hydrol. Proc. 20 (7), 1541–1565.

Yu, D., Lane, S.N., 2006b. Urban fluvial flood modelling using a two-dimensional diffusion-wave treatment, part 2: development of a sub-grid-scale treatment. Hydrol. Proc. 20 (7), 1567–1583.

Yu, D., 2010. Parallelization of a two-dimensional flood inundation model based on domain decomposition. Environmental Modelling & Software 25, 935–945.

Yu, D., Lane, S.N., 2011. Interactions between subgrid-scale resolution, feature representation and grid-scale resolution in flood inundation modelling. Hydrol. Proc. 25, 36–53.

Zanobetti, D., Longeré, H., Preissmann, A., Cunge, J.A., 1970. Mekong Delta mathematical model program construction. Journal of the Waterways and Harbors Division 96 (WW2), 181–199.

Zhang, X. D., Trepanier, J.Y., Reggio, M., Camarero, R., 1994. Time-accurate local time stepping method based on flux updating. AIAA J. 32(9), 1926–1929.

Appendix A

List of symbols

The following list include the symbols extensively used in the thesis; other specific symbols are described together with the related equations.

- A : cross section wetted area $[m^2]$;
- B : width of the cross section $[m]$;
- c : wave celerity $[ms^{-1}]$;
- g : gravity acceleration $[ms^{-2}]$;
- H : water level $[m]$;
- h : water depth $[m]$;
- J : head loss [-];
- n : Manning roughness coefficient $[m^{1/3}s]$;
- Q : discharge $[m^3s^{-1}]$;
- q : discharge per unit width $[m^2s^{-1}]$;
- R : hydraulic radius $[m]$;
- S_0 : bed slope [-];
- t : time $[s]$;
- u : velocity in x direction $[ms^{-1}]$;
- v : velocity in y direction $[ms^{-1}]$;
- V : water volume $[m^3]$;
- Z : elevation $[m]$;
- Δx : lenght of the connection $[m]$;
- Ω : surface area of a grid element (cell) $[m^2]$;

Appendix B

Software codes and programs

All the software codes developed within the thesis work have been written in Fortra language. The development of the CA2D and IFD-GGA codes has been mainly devoted to write fast and efficient computation algorithms, in particular the implementation of governing equations and solution schemes. Therefore , the development of other aspects of the programs has been limited; for example the model softwares do not have a Graphical user interface (GUI) or a dedicated GIS environment to visualize the results. However, the structure of model codes has been designed to be as simple as possible, to allow an easy application to any flood event of interest. To this end, a suite of preprocessing programs has been developed to process input data, and both auxiliary and main programs include straightforward textual interfaces. In addition, the structure of input and output files is simple and flexible and it is compatible with different established softwares, like ArcGIS, Matlab and Excel.

In this appendix, just a general description of auxiliary programs and input and output file structure is provided; for a complete description the reader should refer to the technical notes prepared for the models.

B.1 Auxiliary preprocessing programs

In order to facilitate the use of the IFD-GGA and CA2D models, the model softwares have been integrated with a number of common preprocessing software codes. These auxiliary programs read the topographic data, extract from them the structure of the computation grid, and provide the main program with the input files describing the grid elements (cells ad connections). The auxiliary programs are designed to minimize the need of manual preparation of input files.

Topographic data may be provided using either the standard ASCII raster format, or an XYZ format (list of points); the latter may be used either for regular or irregular grids. To produce irregular meshes, topographic data can be processed using the AMESH program (developed by the Earth Sciences Division of the US Lawrence Berkeley National Laboratory, $http://esd.lbl.gov/research/projects/tough/software/processors.html$), which creates polygonal meshes using Voronoi tessellation. In addition to the digital elevation model, the user has to provide information about terrain roughness, boundary conditions, internal

special conditions (e.g. drainage network), and initial conditions. Most of this information can be provided within the preprocessors.

B.2 Structure of input and output files

Input files of the main models codes are in standard *txt* format, and can be modified using any text editor. The computation grid is described by two separate files, describing respectively the cells and the connections. Both the two files contain a list with geometry settings for each grid element, and this allows to easily describe regular and irregular grids within the same file structure. Separate files describe the initial conditions, the boundary conditions (stage or discharge hydrographs, or rainfall hyetographs), and the simulation settings. If special internal conditions are present in the simulation, further separate input files need to be used. Most of these files are automatically generated by the preprocessing programs.

Output files can be produced in different data format, like ASCII and *csv* (comma separated values), according to user's specifications. Hence, the results can be easily visualized in any GIS environment, or using visualization functions of programs such as MatLab and Excel.